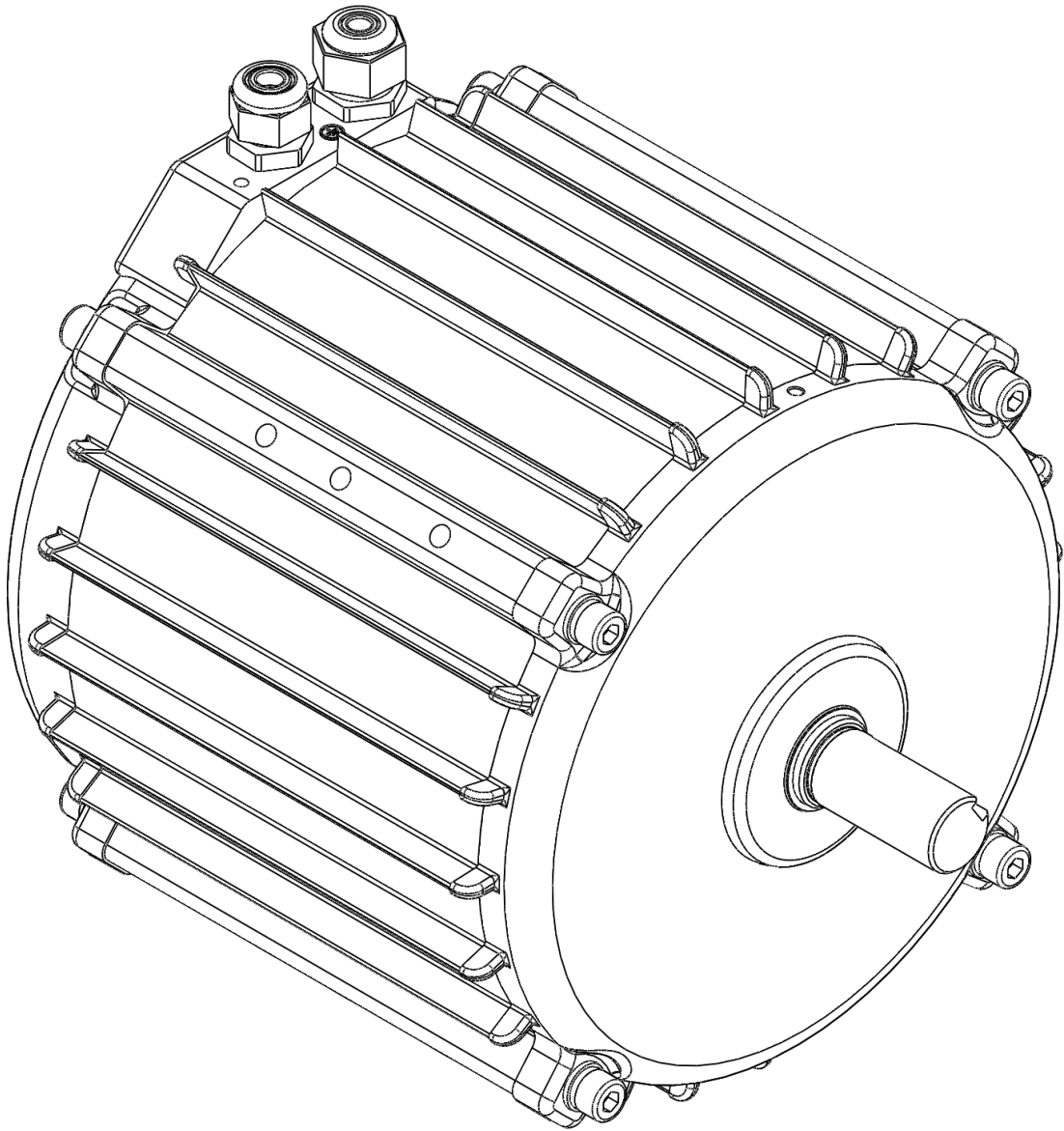# Redesign of Induction Machine

Ejner Daniel Baltasar Møgelbjerg
Niels Pihlkjær Kellmer Hjortshøj

Master's Thesis
Aalborg University
Department of Materials And Production
Denmark
May 30, 2024

AALBORG UNIVERSITY
STUDENT REPORT

Title:
Redesign of Induction Machine

Theme:
Induction machines

Project Period:
Autumn semester 2023 and spring semester 2024

Project Group:
Group EN

Participants:
Ejner Daniel Baltasar Møgelbjerg
Niels Pihlkjær Kellmer Hjortshøj

Supervisor:
Peter Omand Rasmussen

Page Numbers: 104
Appendix pages 62

Date of Completion:
May 31, 2024

Summary

This project investigates the task of redesigning the UMP-3C3-210-25-4 squirrel cage induction machine to develop a more compact fan pack solution for Multi-Wing. The primary objective is to reduce the machine's length while maintaining its performance and cost-effectiveness.

To achieve this, the study begins with a detailed examination of induction machine operations and the application of an equivalent circuit model for steady-state condition representation. Equivalent circuit parameters for two induction machines are determined and compared against machine ratings from datasheets and load tests to validate the modelling approach.

The software MotorCAD is then used to model these two induction machines. The equivalent circuit results are then utilised to validate MotorCAD, as this software relies on geometrical inputs rather than empirical testing to determine equivalent circuit parameters. This validation demonstrates MotorCAD's capability to predict machine behaviour without physical prototypes.

MotorCAD is subsequently employed to model the UMP-3C3-210-25-4. The MotorCAD model of the UMP-3C3-210-25-4 is validated against real-world data and used as a baseline for further design improvements.

Various methods to reduce the length of the UMP-3C3-210-25-4 are explored using the validated MotorCAD model. These methods consider parts already available from the manufacturer to ensure feasibility and cost-effectiveness. The investigation covers several potential strategies for length reduction, including changing the winding configuration, scaling stator and rotor diameters, and redesigning the machine housing.
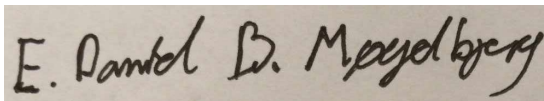
Preface

This master's project spanned from September 2023 to May 2024 and was carried out by Electro-Mechanical Systems Design students from Aalborg University. The project was supervised by Professor Peter Omand Rasmussen, and made in cooperation with the company Multi-Wing. The authors express their gratitude to the representatives of Multi-Wing for their assistance in making this project possible.

The report uses source references to the bibliography placed at the end. In the report, a source is referred to as (Last name; Year) passively and Last name (Year) actively. In the bibliography, books are specified with the author, title, edition and publisher, while web sources are specified with the author, title, address, year and last visit.
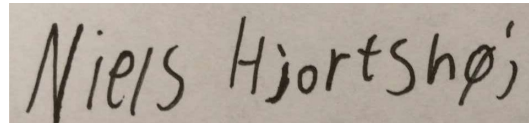
Figures and tables are numbered according to chapter, which means that the first figure in chapter four, has number 4.1, the second 4.2 and so on. Captions to tables are found above the given table and text to figures are found below. Chapters in the appendices are enumerated using letters.

The nomenclature lists each symbol and abbreviation used throughout the paper. If available the unit of measurement and subscript is also given.

The main paper can be read independently of the attached appendices.

Ejner Daniel Baltasar Møgelbjerg	Niels Pihlkjær Kellmer Hjortshøj

Nomenclature

Abbreviations

AC   Alternating current

FEM   Finite Element Method

IEC   International Electrotechnical Commission

NEMA National Electrical Manufacturers Association

OD   Outer diameter

PMSM Permanent Magnet Synchronous Machine

Symbols

α	Angle between slots	[rad]
ε	Absolute error	[-]
η	Efficiency	[-]
$\eta_{internal}$	Internal efficiency	[-]
η_{rated}	Rated efficiency	[-]
γ	Angular reduction of the pitch	[rad]
γ	Correlation coefficient	[-]
ω_s	Characteristic velocity of stribeck curve	[rad/s]
ω_{mech}	Mechanical speed	[rad/s]
ω_{sync}	Synchronous mechanical speed	[rad/s]
Φ_p	Flux per pole	[Wb]
Φ_{eq}	Equivalent phase angle	[rad]
τ	Torque	[Nm]
τ_C	Coulomb friction torque	[Nm]
τ_{fric}	Frictional torque	[Nm]
τ_{mech}	Output torque	[A]
τ_s	Static friction torque	[Nm]
θ	Angle	[rad]
A	Linear gradient	[-]
A_{cu}	Total area of copper	[m^2]
$A_{insulation}$	Total insulation area	[m^2]
A_{slot}	Total slot area	[m^2]

$A_{surface,MCAD}$ surface area of MotorCAD model $\qquad$ [m^2]

$A_{surface,real}$ Real surface area $\qquad$ [m^2]

$A_{surface}$ Surface area $\qquad$ [m^2]

A_{wedge} Total wedge area $\qquad$ [m^2]

A_{wire} Total wire area $\qquad$ [m^2]

B $\qquad$ Linear offset $\qquad$ [-]

B_v $\qquad$ Viscous friction coefficient $\qquad$ [Nm/s]

cp_{mean} Mean coil pitch $\qquad$ [mm]

$D_{stator,FAB}$ Diameter of stator in FAB112M-4 $\qquad$ [mm]

$D_{stator,UMP}$ Diameter of stator in UMP-3C3-210-25-4 $\qquad$ [mm]

D_{stator} Diameter of stator $\qquad$ [mm]

D_{wire} Diameter of wire $\qquad$ [mm]

E_1 $\qquad$ Per-phase induced voltage in the stator $\qquad$ [V]

E_2 $\qquad$ Per-phase induced voltage in the rotor at line frequency f_2 $\qquad$ [Hz]

E_{rms} Induced voltage $\qquad$ [V]

Ext_F Front end winding extension $\qquad$ [mm]

Ext_R Rear end winding extension $\qquad$ [mm]

f $\qquad$ Electrical frequency $\qquad$ [Hz]

f_1 $\qquad$ Line frequency in stator $\qquad$ [rpm]

f_2 $\qquad$ Line frequency in rotor $\qquad$ [rpm]

F_{LR} Electrical frequency during locked rotor test $\qquad$ [Hz]

ff_{cu} Copper fill factor $\qquad$ [-]

ff_{slot} Slot fill factor $\qquad$ [-]

G_{fe} Iron loss conductance $\qquad$ [1/Ω]

H $\qquad$ Heat transfer coefficient $\qquad$ [W/m^2]

h $\qquad$ Harmonic order $\qquad$ [-]

H_{factor} Heat transfer coefficient multiplication factor $\qquad$ [-]

I $\qquad$ Current $\qquad$ [A]

I_2 $\qquad$ Rotor current $\qquad$ [A]

I_2' $\qquad$ Referred rotor current $\qquad$ [A]

i_a $\qquad$ Current of phase a $\qquad$ [A]

i_b $\qquad$ Current of phase b $\qquad$ [A]

I_{cl1} Current of loop 1 $\qquad$ [A]

I_{cl2} Current of loop 2 $\qquad$ [A]

I_{cl3}	Current of loop 3	[A]
i_c	Current of phase c	[A]
I_{fe}	Current across R_{fe}	[A]
I_{LR}	Per-phase RMS current during locked rotor test	[A]
I_m	Current across X_m	[A]
$I_{NL,LL}$	Line to line RMS current during no load test	[A]
I_{NL}	Per-phase RMS current during no load test	[A]
I_{peak}	Peak current	[A]
$I_{rated,LL}$	Line to line rated current	[A]
K_d	Distribution factor	[]
K_p	Pitch factor	[]
K_w	Winding factor	[]
k_θ	Correction factor	[-]
K_{sqv}	Skew factor	[]
N	Number of turns	[-]
n	Rotational speed	[rpm]
n_s	Synchronous rotational speed	[rpm]
N_{ph}	Number of series turns per phase	[-]
N_{sppb}	Number of slots per phase belt	[]
$N_{strands}$	Number strands in hand	[m^2]
N_{turns}	Number of turns	[-]
$Ohang_F$	Front end winding overhang	[mm]
$Ohang_R$	Rear end winding overhang	[mm]
p	Number of poles	[-]
P_r	Rotor conducting loss	[W]
P_s	Stator conducting loss	[W]
P_{ag}	Air gap power	[W]
P_{Cu}	Average power loss for a single phase	[W]
P_C	Constant losses	[W]
P_{eddy}	Eddy current loss	[W]
P_{fe}	Iron loss	[W]
$P_{hysteresis}$	Hysteresis loss	[W]
$P_{in,\theta}$	Corrected input power	[W]
P_{in}	Input power	[W]

P_{LL}	Additional load loss	[W]
P_{LR}	Total real power drawn during locked rotor test	[W]
P_{Lr}	Residual loss	[W]
P_{mech}	Mechanical power	[W]
P_{NL}	Total real power drawn during no load test	[W]
$P_{r,\theta}$	Corrected rotor conducting losses	[W]
$P_{rated,in}$	Rated input power	[W]
$P_{rated,LL}$	Rated additional load loss	[W]
$P_{rated,mech}$	Rated output power	[W]
P_{rcl}	Rotor conducting losses	[W]
$P_{s,\theta}$	Corrected stator conducting losses	[W]
P_T	Total loss	[W]
$P_{WF,s}$	Friction and windage losses corrected for slip	[W]
P_{WF}	Windage and friction losses	[W]
PF	Power factor	[-]
PF_{eq}	Equivalent power factor	[-]
Q_{LR}	Reactive power during locked rotor test	[W]
Q_{NL}	Reactive power during no load test	[W]
R_1	Per phase stator winding resistance	[Ω]
R_2	Per-phase rotor circuit resistance	[Ω]
R_2'	Referred rotor resistance	[Ω]
$R_{1_{LR}}$	Per-phase stator resistance during locked rotor test	[Ω]
$R_{1_{NL,LL}}$	Line to line stator resistance during no load test	[Ω]
$R_{1_{NL}}$	Per-phase stator resistance during no load test	[Ω]
$R_{1_{rated,LL}}$	Line to line rated winding resistance	[Ω]
$R_{2_{LR}}$	Uncorrected rotor resistance from locked rotor test	[Ω]
$R_{2_{LR}}'$	Corrected rotor resistance from locked rotor test	[Ω]
R_{eq}	Equivalent resistance	[Ω]
R_{fe}	Per-phase iron loss resistance	[Ω]
$R_{thermal}$	Thermal resistance	[K/W]
$R_{1_{DC,LL}}$	Measured line to line stator resistance	[ω]
$R_{1_{DC}}$	Measured per-phase stator resistance	[ω]
s	Slip	[-]
s_θ	Corrected slip	[-]

x

Contents

Chapter 1

Introduction

Industrial electrical machines are typically manufactured in standard housing sizes. These housing sizes are defined by standards conceived and approved by councils such as the International Electrotechnical Commission (IEC) or the National Electrical Manufacturers Association (NEMA). Such standards simplify the design process and facilitate the seamless replacement of products from different manufacturers. However, in some applications, customized size requirements must be met, and manufacturers are required to design these custom machines themselves.

The design of customised electric machines can be achieved by scaling existing standard machines and basing the new design on the standard machine's characteristics. Doing so allows for the reuse of parts and production methods from standard machines. Furthermore, predicting how the scaled machine performs before it is put into production is essential to avoid wasting time, money, and materials. Thus, knowledge regarding prediction, modelling, general behaviour, design, and development is needed to create a customised electrical machine.

In recent years, much of the research and development has been focused on the Permanent Magnet Synchronous Machine (PMSM). This is due to the increasing market share, driven by the PMSM's combination of high performance, efficiency, smooth torque delivery, and low noise. However, controlling a PMSM requires using an inverter drive to manage the applied currents. While this approach offers benefits, it also introduces potential drawbacks, such as increased initial costs and the risk of inverter failure. Therefore, operating a machine directly online (DOL) is often simpler and preferred by some companies due to its simplicity.

Additionally, PMSMs often use samarium–cobalt (SmCo) or neodymium (NdFeB) magnets, which contain rare-earth elements. This reliance on rare-earth materials increases the environmental impact and cost, while also limiting the supply chain primarily to China. Consequently, PMSMs are susceptible to supply chain issues due to global political factors.(Haque et al.; 2014)

In those cases, it is more appropriate to use other types of electrical machines, such as induction machines, that do not use permanent magnets and can operate DOL.

An example of a situation where standard-sized frames may not fit, and an inverter is unavailable, is the design of industrial fan solutions, such as those produced by Multi-Wing. Based in Vedbæk, Denmark, Multi-Wing has been producing axial impellers since 1958. The company has its own internal machine and drive competence centre, where they develop customised induction and PM machines. Although Multi-Wing typically uses standard IEC-size electrical machines, they seek an alternative form factor that can fit into narrower spaces. This new form factor must maintain the efficiency and performance characteristics of a standard-sized electrical machine, presenting the following problem statement:

"What are the considerations and requirements, when redesigning an induction machine to fit narrow spaces?"

Chapter 2

Problem Analysis

To address the initial problem statement, this problem analysis aims to provide a deeper understanding of the problem and the potential solutions. Furthermore, it investigates what requirements must be met, as the case is subject to both company-specific challenges and regulations that must be adhered to.

2.1   Resizing Challenge

When Multi-Wing is designing industrial fan pack solutions, it is often relevant to consider the total length and height of the fan and machine assembly, as this determines the space they occupy. One obvious option to achieve a more compact solution is to reduce the machine volume. However, another approach is to maintain the machine's volume but reduce its length by increasing its diameter. While this also reduces the overall space occupied by the fan and machine assembly, it might decrease fan performance due to increased airflow resistance. These different approaches are illustrated in Figure 2.1.
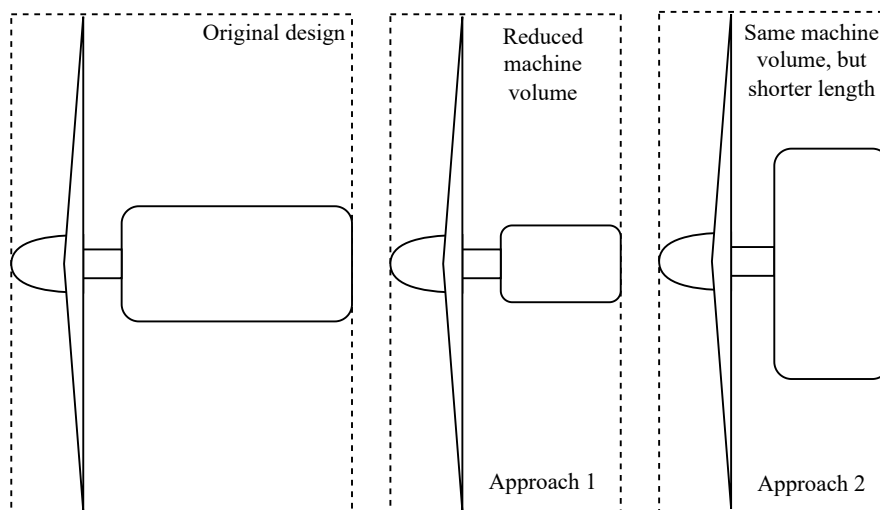
Figure 2.1: Possible solutions to reduce the size of a fan pack with the outer dimensions marked by the dashed line

A fundamental challenge with the first approach is the requirement for higher torque density. Achieving higher torque density necessitates higher magnetic loading (average flux density), which results in increased losses and, consequently, reduced efficiency. To mitigate these losses, modifications such as higher-quality materials can be used. However, this can be very costly, as such materials may be more expensive or difficult to work with.

A fundamental challenge with the first approach is the requirement for higher torque density. Achieving higher torque density necessitates higher magnetic loading (average flux density), which results in increased losses and, consequently, reduced efficiency. To mitigate these losses, modifications such as using higher-quality materials can be made. However, this can be very costly, as such materials may be more expensive or difficult to work with. (Tapani Jokinen; 2013)

In practice, if the machine is to be made shorter while maintaining efficiency, the diameter of the machine should also be expected to increase. Therefore, changing the aspect ratio of the machine, as seen in approach 2 in Figure 2.1, is potentially a good design strategy to allow for a more compact fan pack, provided the diameter increase does not significantly interfere with airflow.

2.2   Company Case

Multi-Wing has recognised a market demand for fan pack solutions utilising a 4 kW induction machine that fits in narrow spaces. Typically, Multi-Wing would use its own 4 kW induction machine in a standard housing, designated as the FAB112M-4. The performance characteristics of this machine are detailed in Table 2.1, and the full datasheet is available in Appendix A.

However, the standard frame housing of this machine is too long to meet customer requirements, necessitating the development of a new machine.

Table 2.1: Performance characteristics of FAB112M-4 induction machine

Characteristics	Units	Performance values		
Freq.	[Hz]	50.0	60.0	60.0
Rated torque	[Nm]	26.2	25.1	25.0
Rated voltage Δ/Y	[V]	230/400	[-]/440	[-]/480
Rated current Δ/Y	[A]	14.5/8.42	[-]/7.97	[-]/7.54
Rated power	[kW]	4.00	4.60	4.60
Power factor (cos(Φ))	[-]	0.82	0.85	0.82
Poles	[-]		4.00	
Speed	[1/min]	1456	1750	1759
Efficiency	[-]	88.6%	89.1%	89.5%
IE class	[-]	IE3	IE2	IE2
IEC frame size	[-]		112M	
Insulation class	[-]		H	
Duty type	[-]		S1	
Ambient temperature	[°C]		$-35\,°C$ to $90\,°C$	
Cooling type	[-]		IC418	

To create a shorter fan pack solution, Multi-Wing outsourced the development of a shorter induction machine to their supplier in China. The performance characteristics of the outsourced shortened machine were set to be similar to the FAB112M-4. The supplier from China then produced the UMP-3C3-210-25-4 as a proposed solution to the problem. Performance characteristics of the UMP-3C3-210-25-4 induction machine can be seen in Table 2.2, with the datasheet available in Appendix B.

The total length, including the shaft, of the UMP-3C3-210-25-4 is 330 mm, while the length of the FAB112M-4 is 350 mm. However, this reduction in length comes at the cost of an increased diameter; the FAB112M-4 has an outer diameter (OD) of 215 mm, while the UMP-3C3-210-25-4 has an OD of 254 mm. When considering the cylindrical shape defined by the length and diameter of the machines, the total volume is 12.1 L for the UMP-3C3-210-25-4 and 16.7 L for the FAB112M-4. As a result, the UMP-3C3-210-25-4 exhibits a lower torque density compared to the FAB112M-4. Consequently, Multi-Wing believes that the UMP-3C3-210-25-4 has potential for improvement and could be designed to be shorter.

Table 2.2: Performance characteristics of the UMP-3C3-210-25-4 induction machine

Characteristics	Units	Performance values
Freq.	[Hz]	50.0
Rated torque	[Nm]	25.5
Rated voltage Δ/Y	[V]	400/690
Rated current Δ/Y	[A]	7.86/4.55
Rated power	[kW]	4.00
Power factor (cos(Φ))	[-]	0.83
Poles	[-]	4
Speed	[1/min]	1462
Efficiency	[-]	88,6%
IE class	[-]	IE3
Frame size	[-]	UMP 210
Insulation class	[-]	H
Duty type	[-]	S1
Ambient temperature	[°C]	−20 °C to 45 °C
Cooling type	[-]	IC418

2.3 Requirements and Standards for Induction Machines

Multi-Wing is an international company, thus requiring compliance with international regulations. When complying with these international regulations, it is important to recognise that within the many international regulations, the European Union (EU) has established some of the world's most demanding regulations. Many companies, including Multi-Wing, often refer to EU regulations as a benchmark, since compliance with these often facilitates sales, both within and outside Europe.

Most of the requirements in the EU relating to rotating electrical machines, including induction machines, are found in the IEC 60034 standard series.

2.3.1 Ratings and Tolerances

Rated nameplate data on squirrel cage induction machines in the EU must follow the IEC 60034-1. In the IEC 60034-1, an induction machine can obtain ratings at different duty types. Different duty types specified by the 60034-1 can be seen in Table 2.3.

Table 2.3: Duty types according to IEC 60034-1 (2010)

Duty type	Description
S1	Continuous running duty
S2	Short-time duty
S3	Intermittent periodic duty
S4	Intermittent periodic duty with starting
S5	Intermittent periodic duty with electric braking
S6	Continuous operation periodic duty
S7	Continuous operation periodic duty with electric braking
S8	Continuous operation periodic duty with related load/speed changes
S9	Duty with non-periodic load and speed variations
S10	Duty with discrete constant loads and speeds

When rating an induction machine, one selects the mechanical load point (P_{mech}) at which it shall be

rated. Subsequently, the voltage (U), electrical frequency (f), and configuration for the machine's operation are determined, followed by the selection of the duty type. The machine can then be operated under the chosen duty type at its rated mechanical power, voltage, electrical frequency, and configuration. During this operation, efficiency (η), power factor (PF), and slip (s) are measured as specified in IEC 60034-2-1:2014 (2014). From these specified values, additional ratings such as current (I) and torque (τ) can be derived, as demonstrated in (2.1) and (2.2) where p is the number of poles.

$$I = \frac{P_{mech} \cdot \sqrt{3}}{3 \cdot \eta \cdot PF \cdot U} \tag{2.1}$$

$$\tau = \frac{P_{mech} \cdot p}{4 \cdot (1-s) \cdot f \cdot \pi} \tag{2.2}$$

IEC 60034-30-1:2014 (2014) includes tolerances on efficiency, power factor and slip as shown in Table 2.4. Similarly to the ratings, the upper and lower tolerances for parameters such as current and torque can be derived, based on upper or lower limits of the power factor, slip, or efficiency. .

Table 2.4: Nameplate tolerances according to IEC 60034-1 (2010)

Quantity	Tolerance description
Efficiency (η)	$-15\% \cdot (1-\eta)$
Power factor (PF)	$-1/6 \cdot (1-PF)$
Slip (s) at full load and working temperature.	$\pm 20\% \cdot s$

Some tolerances in Table 2.4 are seen only to have a negative calculation value, indicating a limitation in only one direction. In IEC 60034-30-1:2014 (2014) it is stated that if a tolerance only is given in one direction, the value is not limited in the other direction. Thus, nameplate ratings, supplied by datasheets, are not necessarily expected operating values.

2.3.2 Efficiency Requirements

In 2019 a new EU commission regulation laid down eco-design requirements for electric machines and variable speed drives, setting new requirements for the energy efficiency of three phase machines among other things. Since July 1st 2021 three phase machines with a rated output between 0.75 kW and 1000 kW, with 2, 4, 6 or 8 poles are required to have IE3 efficiency or above. (Council of European Union; 2019)

The IE efficiency classes for line-operated induction machines are defined in IEC 60034-30-1:2014 (2014). An induction machine is almost always more efficient at 60 Hz compared to 50 Hz because the increase in losses due to higher frequency does not exceed the corresponding increase in power. This higher efficiency at 60 Hz is also reflected in the IE class requirements, as detailed in Appendix C.

Efficiency and losses used in the IE class identification is to be acquired in accordance with the preferred methodology for the individual machine given in IEC 60034-2-1:2014 (2014).

2.3.3 Frame Sizes

Despite the new machine design, being a non standard length, it is still relevant to partly meet the standard sizes found in IEC 60072-1:2022. This standard specifies the fixing dimensions, shaft extension dimensions and the assignment of output powers and frame sizes.

Standard dimensions of shafts, mounting flanges etc. remain important to consider. As it ensures a degree of compatibility with existing infrastructures and industry practices.

2.3.4   Product Safety Certification

Multi-Wings electric machines are certified by Underwriters Laboratories (UL), which means they must meet the UL 1004-1 (2020). This standard establishes essential safety and performance requirements for rotating electrical machines to ensure they operate safely and reliably in various applications.

It is therefore important, that any new machine design is still able to be UL certified.

2.3.5   Thermal Requirements

Another important set of rules that must be considered is related to cooling and temperatures. IEC 60085:2007 ED4 (2007) establishes the criteria for evaluating the thermal endurance of either electrical insulating materials or electrical insulation systems. It also establishes the procedure for assigning thermal classes, which is used when designing induction machines. The FAB112M-4 and UMP-3C3-210-4 are class H machines, meaning that the maximum continuous operating temperature of the machine is 180 °C.

The maximum temperatures of the machines are measured when they hit thermal equilibrium during their rated duty cycle, at the maximum rated ambient temperature. While the FAB112M-4 has a rated ambient temperature range of −35 °C to 90 °C, the UMP-3C3-210-4's datasheet states a rated ambient temperature range of −20 °C to 45 °C. However, these ratings may not reflect the actual temperature range, as the supplied datasheet for the UMP-3C3-210-4 is tailored for a specific customer. Multi-Wing has requested that the ambient temperature range be set to −50 °C to 100 °C. Additionally, the machine should be capable of operating at 60 Hz, and temperatures should be measured when the machine is running continuously with a load of 4.6 kW.

Additionally, both machines have a cooling type of IC418, as defined in IEC 60034-6:1991 (1991). This indicates that they are totally enclosed machines with an air stream moving over them, generated by the fan to which the machine is attached. Therefore, it is crucial to consider the fan's operation and the volume of air being pushed over the machine.

Determining the exact fan load point is challenging because it depends on various environmental factors such as ambient temperature and surrounding air pressure. Generally, the fan load is not expected to reach 4 kW and tends to decrease as the temperature rises. This trend is illustrated in Table 2.5, which shows data supplied by Multi-Wing of the same fan being operated at different ambient temperatures.

Table 2.5: Operating point description of fan as supplied by Multi-Wing

Ambient temperature	°C	20	85
Airflow	[m^3/s]	7.47	7.2
Static pressure	[Pa]	226	211
Total efficiency	[%]	70.6	70.4
Dynamic pressure	[Pa]	141	107
Power	[kW]	3.878	3.253
Total pressure	[Pa]	368	318

Multi-Wing has already tested the UMP-3C3-210-4's ability to stay cool in the required environments. Therefore, the cooling performance of a new design can be compared to that of the UMP-3C3-210-4 to determine if it is satisfactory.

2.4 Design Limitations

To reduce the cost and development time of a new design, standard parts that are readily available are preferred. This means that laminate qualities, winding configurations, laminate geometries etc. should be kept to what is already being produced, readily available, or easily adjustable at the fabrication site. Naturally, if a non-standard part is found to shorten the length of the machine by a significant magnitude, the non-standard part is considered a solution.

The housings for standard-size stator laminates are available as extrusion profiles, meaning that producing a shorter housing does not require any new equipment.

As the UMP-3C3-210-25-4 is Multi-Wing's previous attempt at creating a shortened induction machine, it is used as an initial design basis for this project.

Chapter 3

Problem Statement

The problem analysis investigated how Multi-Wing identified a demand for a 4 kW induction machine suitable for narrow spaces where their standard frame size machine, the FAB112M-4, cannot be used.

To address this need, Multi-Wing outsourced the design of a new machine to their Chinese supplier. The supplier designed an induction machine with a larger diameter but shorter length, named the UMP-3C3-210-25-4, to fit Multi-Wing's requirements.

However, the UMP-3C3-210-25-4 has a larger volume than the FAB112M-4, resulting in a lower torque density. Consequently, Multi-Wing believes that a redesign of the UMP-3C3-210-25-4 could potentially lead to a further reduction in the machine's length.

This leads to the following problem statement:

> *"What redesign strategies can Multi-Wing employ to shorten the UMP-3C3-210-25-4 induction machine, while maintaining its performance characteristics and ensuring the redesign remains cost-effective?"*

To provide an overview of how the problem statement is addressed in this project, the following sections are described: requirements, solution strategy, methodology, delimitations, and limitations of the project.

3.1 Requirements

When addressing redesign strategies for the UMP-3C3-210-25-4 induction machine, the established standards, regulations, and certifications, identified throughout Chapter 2, should be adhered to. Additionally, the redesigned machine should retain the characteristics of the UMP-3C3-210-25-4 to ensure compatibility with the existing fan pack solution. This includes maintaining the same load point, duty cycle, thermal class, etc.

In Table 3.1 specified requirements derived from Chapter 2 are presented, based on adherence to regulations and maintenance of characteristics.

Table 3.1: Requirements used in the redesign process of the UMP-3C3-210-25-4

Parameter	Unit	Requirement
Duty type	[-]	S1
Load point (P_{mech})	[kW]	4.00
Operating voltage (U)	[V]	400
Electrical frequency (f)	[Hz]	50.0
Number of poles (p)	[-]	4
Efficiency (η)	[-]	86.9% - 100%
Power factor (PF)	[-]	0.80 - 1.00
Slip (s)	[-]	2.02% - 3.04%
Operating temperature	[°C]	$\leq$180
Ambient temperature	[°C]	-50 - 100
Total length	[mm]	$\leq$330

3.2   Solution Strategy

Being able to predict how changes in the design of the UMP-3C3-210-25-4 impact performance, it is essential to estimate which design modifications have the potential to reduce the length without compromising the performance of the UMP-3C3-210-25-4.

To achieve this, equivalent circuit models are obtained and validated through experiments on multiple 4 kW, 4-pole, induction machines. This validation method ensures the reliability of equivalent circuit models, allowing for comparisons of equivalent circuit parameters across different machines with similar characteristics.

To predict how changing the design of the UMP-3C3-210-25-4 impacts the machine characteristics, numerical tools and simulation methods is employed. To ensure the validity of these tools, verification is carried out by comparing simulated model parameters with measured model parameters for all tested machines.

With the models and simulation tools verified, potential redesigns of the UMP-3C3-210-25-4 are investigated. The goal is to identify what modification proposals provide a feasible reduction in length.

Once the modification proposals have been analysed, a prototype machine will be constructed. This prototype enables a final evaluation of whether the new design maintains the desired performance characteristics.

3.3   Delimitations and Limitations

To establish the boundaries and scope of this project, delimitations are made. The delimitations of this project are presented below:

- Only components readily available by Multi-Wing's supplier is considered.
- Only the characteristics specified in the datasheet of the UMP-3C3-210-25-4 is maintained during the redesign.
- Housing geometry is only changed in length.

Furthermore, the project is also subject to the limitations, listed below:

- The induction machines and their technical specifications and geometries, are supplied by Multi-Wing and therefore limited to what information Multi-Wing can provide.

- Laboratory work is performed at Aalborg University's facilities, and therefore the project is limited to what facilities the university is capable of providing.
- The equipment used in this project is limited to what is already available at Aalborg University or what can be ordered through Multi-Wing.
- Exact prices are unavailable, and therefore price estimations for different solutions cannot be presented. Only material use and production time are considered, as part of this project.

3.4 Methods

The induction machine equivalent circuit model used in this project is based on the industry standard models used in IEC 60034-2-1:2014 (2014) and IEEE std 112 - 2017 (2017) standards.

To validate the accuracy of this model, the parameters are estimated for the UMP-3C3-210-25-4, FAB112M-4, and another standard size 4 kW, 4-pole machine provided by Multi-Wing. This additional machine called the Y3PE112M4, is produced by the company MOLL, and has characteristics similar to the FAB112M-4, a datasheet is provided in Appendix D. The equivalent circuit parameters of these machines are estimated using methods described in the IEC 60034-2-1:2014 (2014) and IEEE std 112 - 2017 (2017). These methods involve performing locked rotor and no-load testing.

To determine the efficiencies of the machines, test methods presented by the IEC 60034-2-1:2014 (2014) are used.

To predict the performance of new designs, Finite Element Methods (FEM) are used alongside analytical methods. Specifically, ANSYS MotorCAD software is employed to simulate induction machine designs. To obtain inputs for the software, the machines are dismantled to measure geometry and observe winding configurations. Validation of the software is then carried out, by simulating the performance of the machines and comparing it with test measurement data.

Once the models and software are validated, various design changes to the UMP-3C3-210-25-4 are simulated using MotorCAD. This helps identify which modifications provide a feasible reduction in length.

A prototype machine based on the most promising design changes is then constructed. This allows for a final validation of the design proposal.

Chapter 4

Introduction to Induction Machines

To achieve a better understanding of the design task at hand, this chapter focuses on the general construction and working principle of an induction machine. A simplified example induction machine layout can be seen in Figure 4.1.
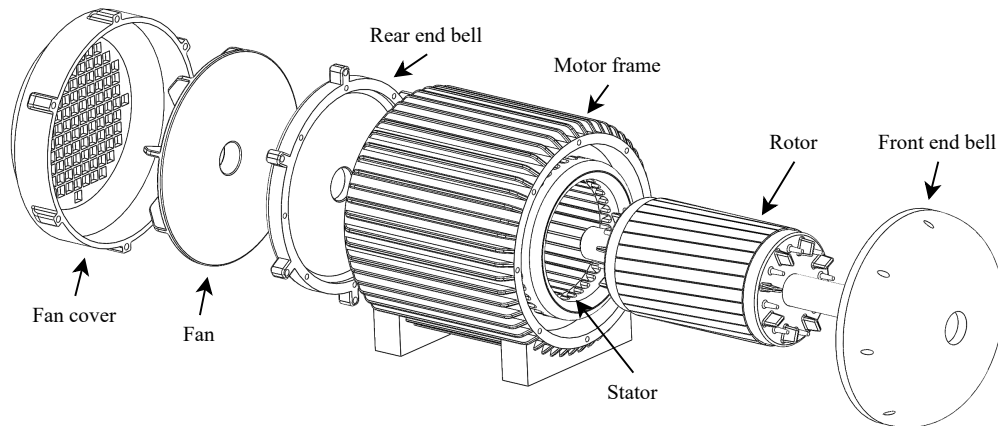
Figure 4.1: Exploded view of a 3-phase induction machine

As the name suggests the induction machine works on the principle of induction. When a 3-phased power is applied to the stator windings of the machine, a rotating magnetic field is established within the machine's air gap. This rotating magnetic field, in turn, induces a voltage in the rotor conductors, leading to the generation of a secondary current within the rotor. Consequently, the rotor establishes its own magnetic field, that tries to synchronise with the magnetic field of the stator, thereby generating a torque that drives the rotor's rotation.

4.1 Stator Construction

The stator of an induction machine consists of a stator core with slots filled by windings. The windings consist of three phases, that can generate a rotating magnetic field when connected to a three phase power supply.

4.1.1 Stator Core

The stator core itself is made from thin laminates stacked together to form the complete core as seen in Figure 4.2. Thin sheets of laminates are used, as they decrease the amount of eddy currents appearing in the core. Which are circulating currents in the core, that do not contribute to anything, thus decreasing efficiency.

The magnetic steel laminates used, also known as electrical steel, contain silicon as a key alloying element. The addition of silicon enhances the material's electrical and magnetic properties, further reducing eddy current and hysteresis losses.
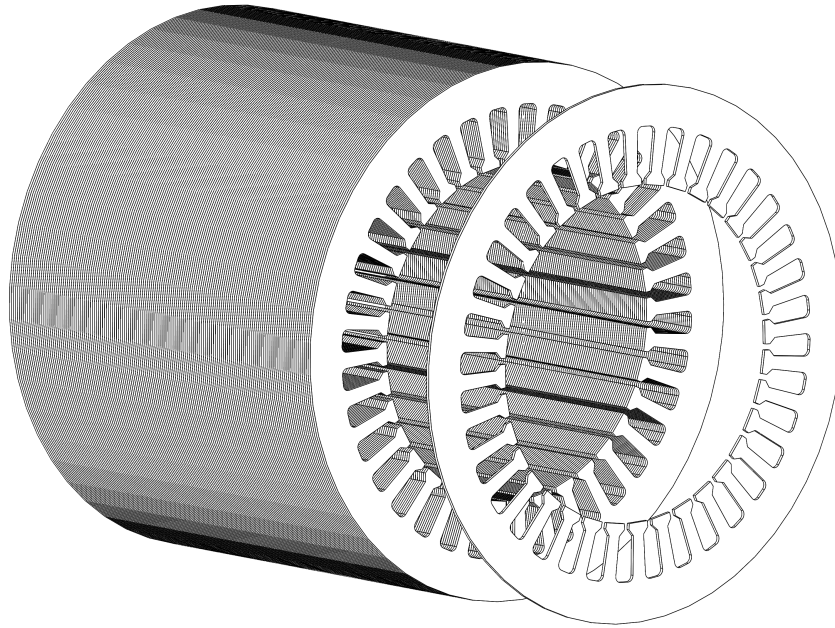
Figure 4.2: Laminate stacks used to construct the stator core

The laminates of the stator core feature slots for the windings, as illustrated in Figure 4.3 where a quarter section of the laminate is shown.
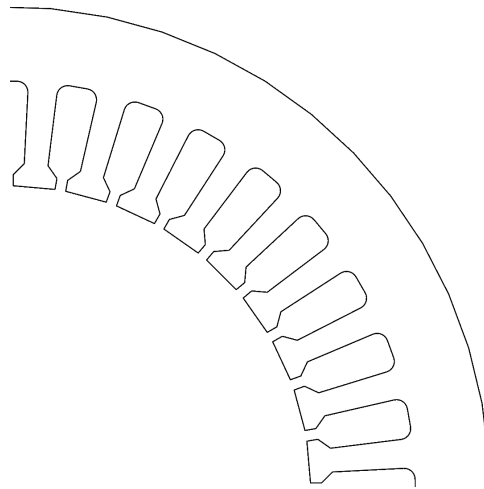
Figure 4.3: Quarter section of a stator laminate

The choice of slot geometry is a compromise between being able to fit as many winding turns as possible and increasing the magnetic field strength while avoiding saturation in the teeth. Furthermore, the slot opening is chosen such that the reluctance is high enough to minimise flux leakage between adjacent teeth while maintaining a good magnetic coupling between the stator and rotor.

To reduce the risk of damage to the winding insulation, the slots are fitted with an insulation liner that lies between the windings and core laminate. This liner must therefore be considered when fitting the coils inside the slot, as it occupies some of the space.

4.1.2 Stator Windings

Stators can be wound in different ways, to achieve certain behaviours of an induction machine.

Figure 4.4 shows a simplified sketch of a two-pole stator with three phases, where dots are wires coming out and + are wires going in.
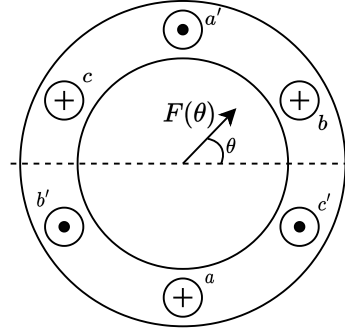
Figure 4.4: Concentrated windings of a simplified 3-phase AC machine

In each slot, there might be multiple turns, and the magnetomotive force (MMF) $\mathscr{F}$ along a path defined by the angle θ is calculated as (4.1).

$$\mathscr{F}(\theta) = N \cdot I \tag{4.1}$$

Where N is the number of turns and I is the current.

If the depicted windings are considered sinusoidally distributed along the stator, and a 50 Hz current in the phases are described by (4.2) to (4.4).

$$i_a(t) = I_{peak} \cdot \cos(2 \cdot \pi \cdot 50\,\text{Hz} \cdot t) \tag{4.2}$$

$$i_b(t) = I_{peak} \cdot \cos\left(2 \cdot \pi \cdot 50\,\text{Hz} \cdot t - \frac{2 \cdot \pi}{3}\right) \tag{4.3}$$

$$i_c(t) = I_{peak} \cdot \cos\left(2 \cdot \pi \cdot 50\,\text{Hz} \cdot t + \frac{2 \cdot \pi}{3}\right) \tag{4.4}$$

The MMF component of each phase can be written as (4.5), (4.6) and (4.7):

$$\mathscr{F}_a(\theta,s) = \mathscr{F}_{max} \cdot \sin(\theta) \cdot \cos(50\,\text{Hz} \cdot 2 \cdot \pi \cdot t) \tag{4.5}$$

$$\mathscr{F}_b(\theta,s) = \mathscr{F}_{max} \cdot \sin(\theta - \pi/3) \cdot \cos(2 \cdot \pi \cdot 50\,\text{Hz} \cdot t - \pi/3) \tag{4.6}$$

$$\mathscr{F}_c(\theta,s) = \mathscr{F}_{max} \sin(\theta + \pi/3) \cdot \cos(2 \cdot \pi \cdot 50\,\text{Hz} \cdot t + \pi/3) \tag{4.7}$$

The total MMF is the sum of all three components, as depicted in Figures 4.5 and 4.6 for $t = 0$ and $t = 3.33\,\text{ms}$ respectively.
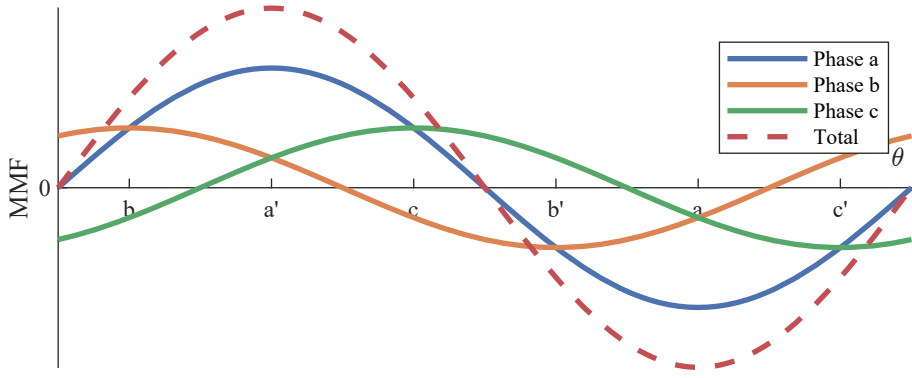
Figure 4.5: Total MMF for $t = 0$
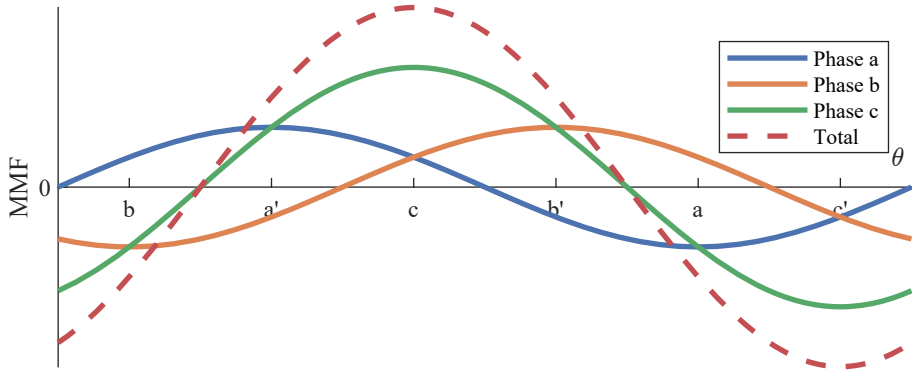
Figure 4.6: Total MMF for $t = 3.33\,\text{ms}$

Distributed Windings

In reality, it is not realisable to have a perfectly sinusoidal distribution of windings across a stator, instead, they are distributed across a number of slots. If the windings in Figure 4.4 are considered as concentrated meaning that they are placed in a single slot, the MMF at $t = 0$ is instead distributed as shown in Figure 4.7.
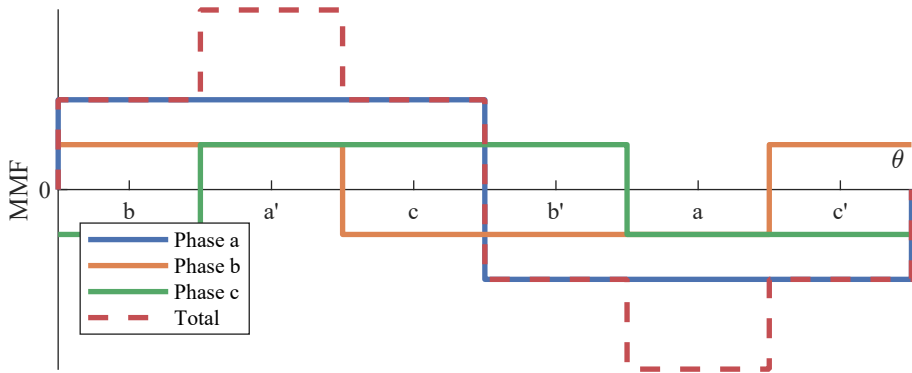
Figure 4.7: MMF distribution with concentrated windings

Since the MMF of the concentrated windings, is not a perfectly sinusoidal wave it contains harmonics that can be calculated using a Fourier transform as shown in (4.8).

$$\mathscr{F}(\theta) = \sum_{h=1,3,5,\dots} \mathscr{F}_{max} \cdot \frac{2 + \cos\left(\frac{h \cdot \pi}{3}\right) - \cos\left(\frac{2 \cdot h \cdot \pi}{3}\right) - \cos\left(\frac{4 \cdot h \cdot \pi}{3}\right) + \cos\left(\frac{5 \cdot h \cdot \pi}{3}\right)}{3 \cdot \pi \cdot h} \cdot \sin(h \cdot \theta) \qquad (4.8)$$

The size of the harmonic orders with concentrated windings is shown in Figure 4.8, where the amplitude is normalised to the first order. Low-order harmonics are unwanted in a stator's MMF
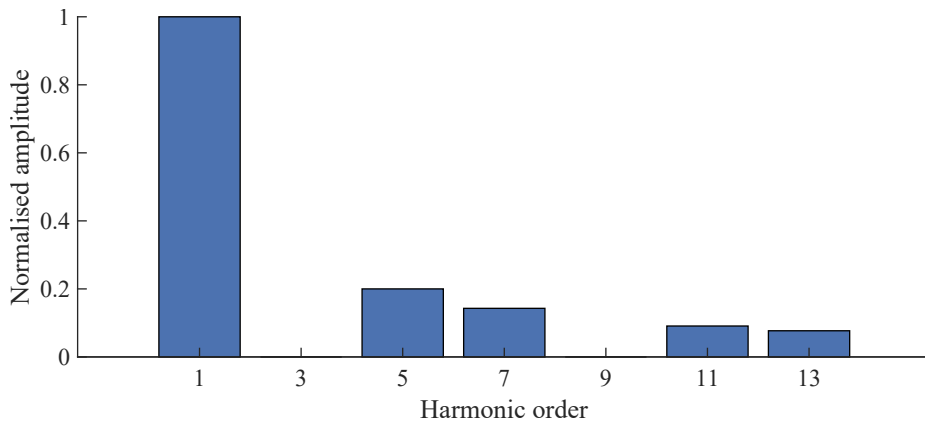
Figure 4.8: Harmonic orders 1-13 of MMF in stator with concentrated windings

because they can lead to undesirable effects such as increased losses, torque ripple, and noise in the machine. Liang and Luy (2006)

To reduce the lower-order harmonics in the stator MMF, the windings can be distributed over several slots instead, as shown in Figure 4.9, where the windings are distributed across three slots.
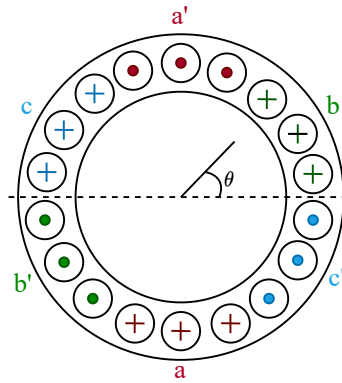
Figure 4.9: Stator with distributed windings

With the distributed windings used in Figure 4.9, the MMF instead look like Figure 4.10.
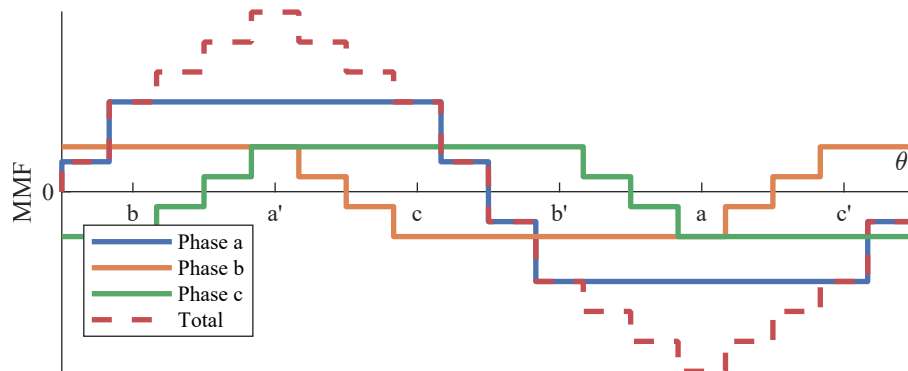
Figure 4.10: MMF with windings distributed across 3 slots

17

And the harmonics can likewise be calculated using a Fourier transform resulting in the harmonics shown in Figure 4.11.
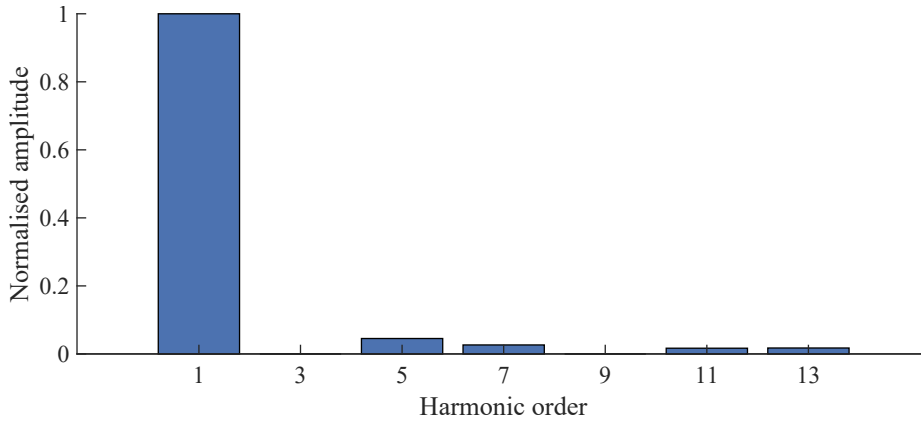
Figure 4.11: Harmonic orders 1-13 of MMF in stator with distributed windings

Short Pitching

The end turn of the stator windings has a copper loss associated with them, which should be as small as possible. To alleviate this problem, short pitching of the stator windings is commonly found in induction machines. Short pitching means that the coil span is reduced, as illustrated in Figure 4.12.

(a) Full pitch
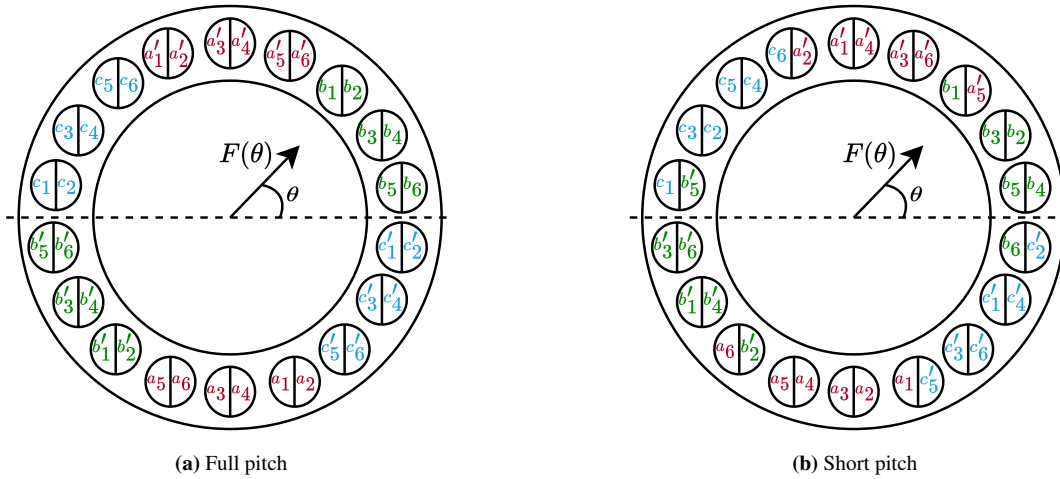
(b) Short pitch

Figure 4.12: Illustration of full and short-pitched stator windings

As seen in the figure, each slot contains two phase bands, this kind of slot packaging is called double layer windings. Double layer windings are not necessary to perform short pitching, but short pitching is usually present when using double layered winding.

Apart from shorter coil length and therefore reduced losses, the overlapping phase belts shown in Figure 4.12 also change the MMF distribution as seen in Figure 4.13, and a decrease in harmonics as seen in Figure 4.14.
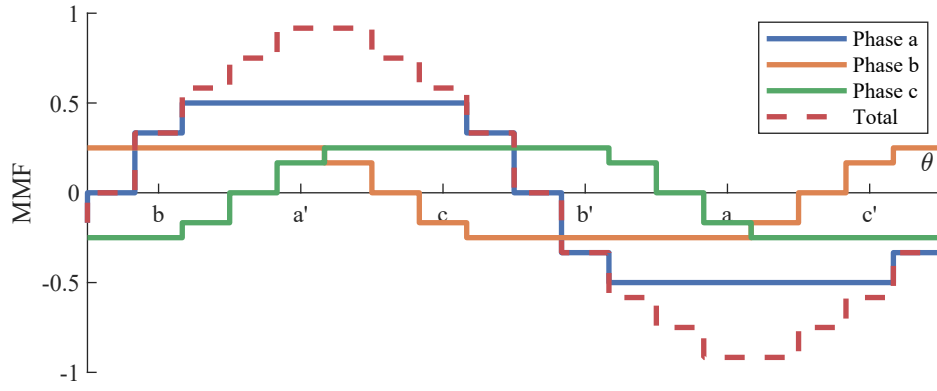
Figure 4.13: MMF with windings short pitched
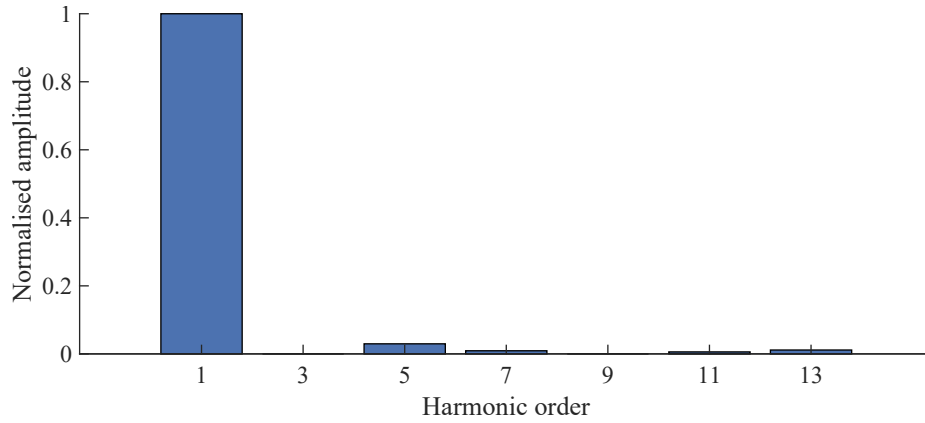
Figure 4.14: Harmonic orders 1-13 of MMF in stator with short pitch windings

Winding Factor

While distributing the windings and having a short pitched coil is advantageous from a harmonics point of view, it decreases the amplitude of the magnetic field and thus also the voltage is induced in the stator. To calculate the voltage induced in the stator, a simplified equation can be made by introducing a winding factor K_w, as seen in (4.9).

$$E_{rms} = \frac{2 \cdot \pi}{\sqrt{2}} \cdot f \cdot N_{ph} \cdot \Phi_p \cdot K_w \tag{4.9}$$

Where N_{ph} is the total number of series turns per phase and Φ_p is the flux per pole.

The winding factor consists of a distribution factor and a pitch factor as in (4.10).

$$K_w = K_d \cdot K_p \tag{4.10}$$

The distribution factor, K_d is calculated using (4.11).

$$K_d = \frac{\sin\left(\frac{N_{sppb} \cdot \alpha}{2}\right)}{N_{sppb} \cdot \sin\left(\frac{\alpha}{2}\right)} \tag{4.11}$$

Where N_{sppb} is the slots per phase belt and α is the angle between slots. The pitch factor K_p is calculated using (4.12).

$$K_p = \cos\left(\frac{\gamma}{2}\right) \tag{4.12}$$

Where γ is the angular reduction of the pitch.

4.2 Rotor Construction

The rotor in an induction machine can take two main forms: a wound rotor or a squirrel cage rotor. Wound rotors are typically wound with copper or aluminium wires, and they incorporate slip rings to facilitate connection to a variable load, enabling control over the rotor current. However, more commonly used are squirrel cage rotors, exemplified by the design illustrated in Figure 4.15.
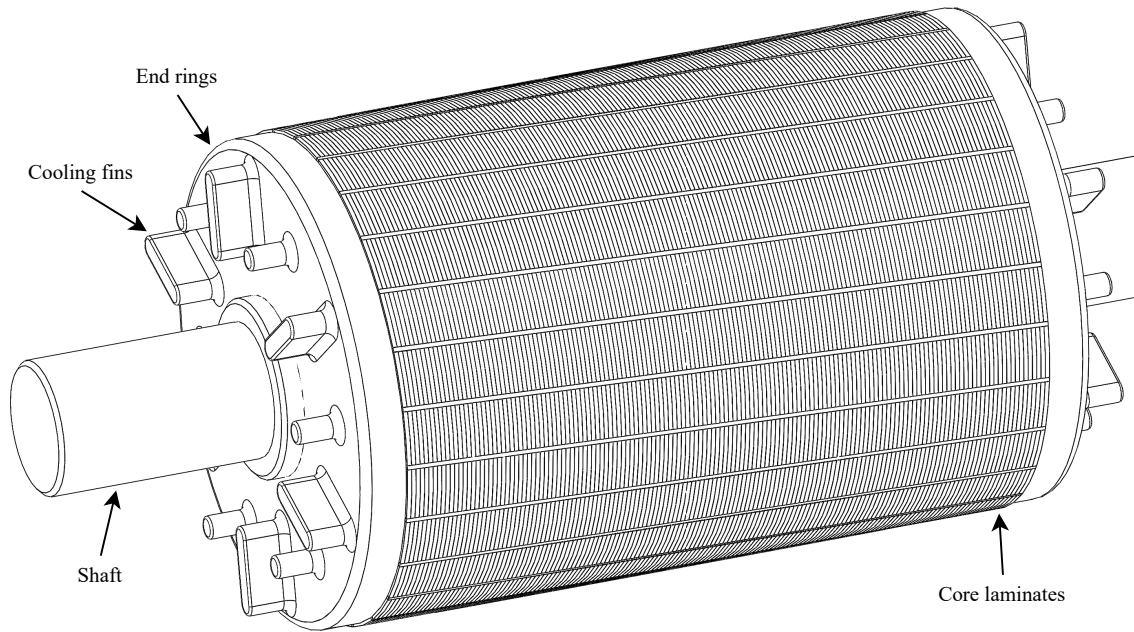
Figure 4.15: Illustration of squirrel cage rotor

Squirrel cage rotors feature a laminate core, to reduce the eddy currents in the same way as the stator. Electrically conducting bars run through slots in the core and are shorted by end rings forming the "squirrel cage" as illustrated in Figure 4.16.
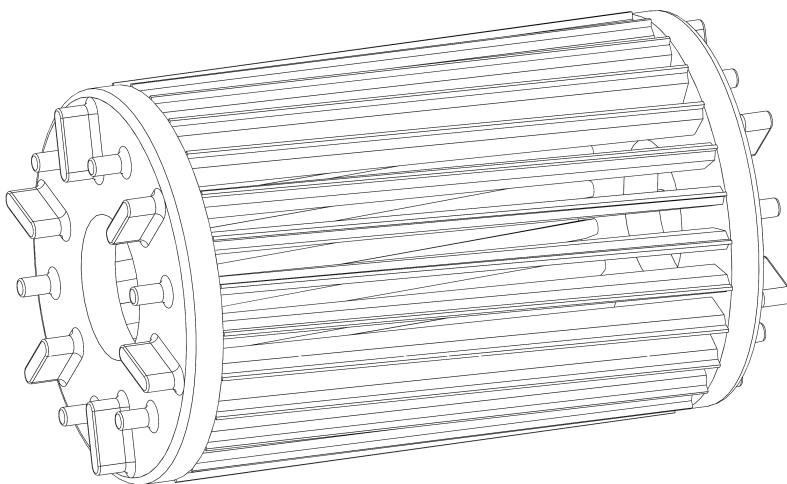
Figure 4.16: Illustration of rotor bars in a squirrel cage rotor

The rotor bars and end ring can be brazed or soldered together but are often cast as a single piece by

using the core as the cast form. On the end rings straight fins are found that helps cool down the end windings on the stator. Adjacent to these fans, extrusions are sometimes incorporated to balance the rotor before installation. Typically, rotor bars and end rings are crafted from either aluminium or copper. While copper is the preferred choice from a conductivity standpoint, aluminium is often a suitable option as it is easy to cast.

The bars in the rotor are intentionally skewed at an angle. This ensures that the same fraction of the rotor bar is under each of the stator slots, thus reducing air gap harmonics. This also reduces the induction effect between rotor bars and the stator field compared to a straight rotor bar. Both of these effects can be accounted for by the use of the skewing factor, which can be calculated as seen in (4.13) for the *h*'th harmonic.

$$K_{sqv} = \frac{\sin\left(h\alpha/2\right)}{h\alpha/2} \tag{4.13}$$

Where h is the harmonic order, and α is the skew angle defined as shown in Figure 4.17. The skewing
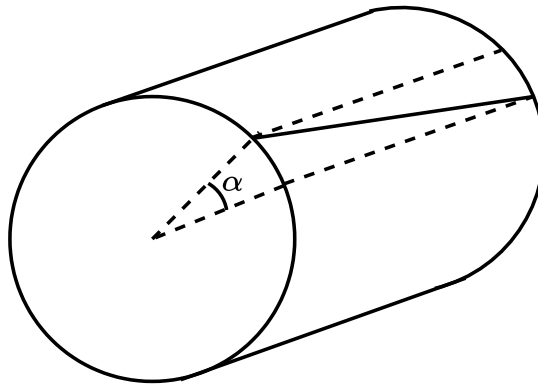
Figure 4.17: Definition of skew angle

angle α in induction machines is usually the same as a single stator slot pitch (Tapani Jokinen; 2013).

The winding factor is then multiplied by the skew factor, to account for the drop in induced voltage. The mutual magnetic flux is also reduced by the same factor.

The geometry of rotor slots can vary significantly depending on factors such as the desired speed-torque curve. Standards like ANSI/NEMA MG 1-2021 (2021) or IEC 60034-12:2016 (2016) are employed to classify the speed-torque characteristics of induction machines. In Figure 4.19, typical NEMA class A, B, C, and D speed-torque curves can be observed, while Figure 4.18 shows examples of geometry used for the NEMA design classes.

Class A   Class B   Class C   Class D
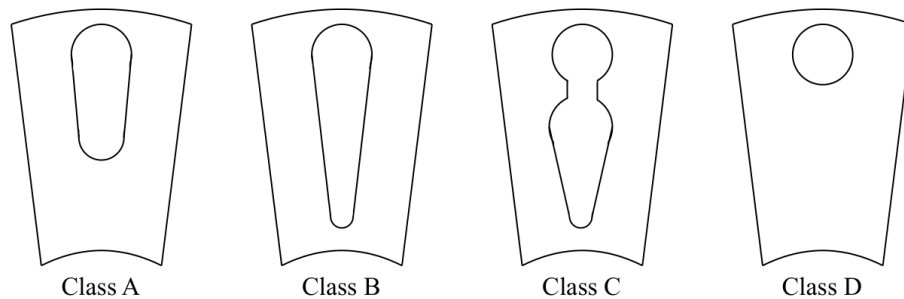
Figure 4.18: Examples of different rotor geometries according to their NEMA design class
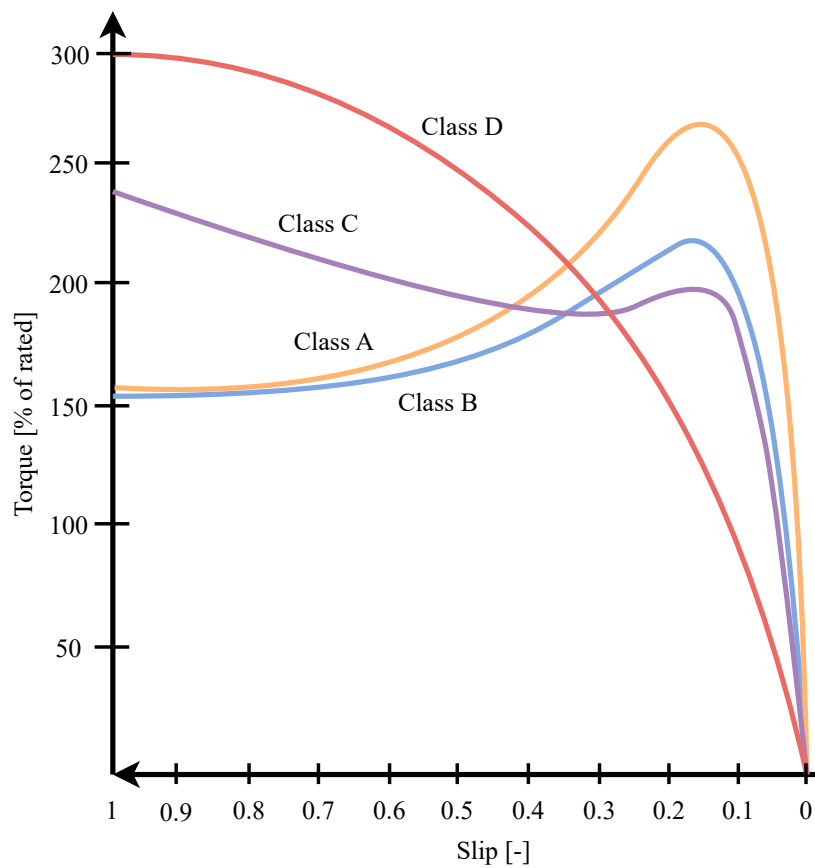
Figure 4.19: Torque-speed curves for different NEMA design classes

4.3   Housing Construction

Induction machine housings are made in many different ways, depending on the application. Some of the considerations when designing housing can be seen in Figure 4.20.
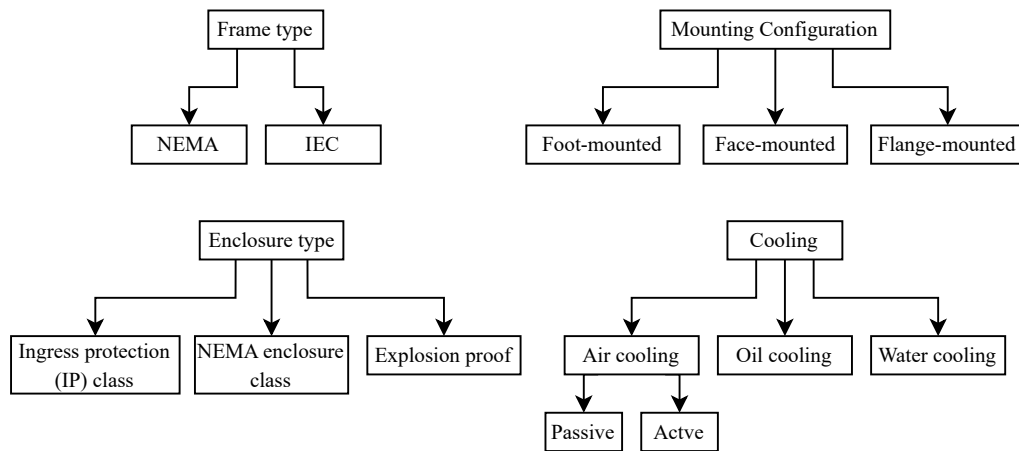
Figure 4.20: Overview of housing considerations

The design requirements for machine housings are governed by either IEC or NEMA standards, depending on the target market. Once a standard is chosen, one must consider the mounting configuration, cooling method, and enclosure type. machine mounting can be done in different ways, such as foot-mounted, face-mounted, or flange-mounted, sometimes a combination of these methods. Cooling is crucial due to heat generation, with options like oil, water, or the most common choice, air cooling (active with a fan or passive). Lastly, enclosure type refers to protecting the internal components from environmental factors, such as water, debris or dust.

Air cooling, whether active or passive is the most common cooling option. Induction machines commonly feature external cooling ribs designed to efficiently dissipate the generated heat. Consequently, the machine housing is typically cast or extruded to allow for the complicated geometry. Aluminium or steel are typically used as materials, due to their relatively high thermal conductivity compared to the price.

Chapter 5

Steady State Model of Induction Machine

An important aspect when designing induction machines is being able to predict certain performance characteristics of the machine. The most important characteristics of a machine are the torque- and current profiles, power factor and efficiency. To understand what parameters influence these characteristics, a steady state model of the induction machine is described. The equivalent circuit model presented in the following section is based on the equivalent circuit model used in IEEE std 112 - 2017 (2017) and IEC 60034-2-1:2014 (2014). With derivations based on Sen (2013) and Boldea and Nasar (2001).

5.1   Equivalent Circuit

To reduce the equation complexity for an induction machine, it is convenient to first define the slip s as shown in (5.1).

$$s = \frac{n_s - n}{n_s} \tag{5.1}$$

Where n is the mechanical speed of the induction machine in rpm, and n_s is the synchronous speed of the induction machine calculated in rpm as (5.2).

$$n_s = \frac{120 \cdot f}{p} \tag{5.2}$$

Where f is the electrical frequency, and p is the number of poles.

For a squirrel-cage induction machine, the per-phase equivalent circuit diagram of the windings in the stator can be represented as shown in Figure 5.1, Where the symbols are:

- U_1: Per-phase terminal voltage
- R_1: Per-phase stator winding resistance
- X_1: Per-phase stator leakage reactance
- R_{fe}: Per-phase iron loss resistance
- X_m: Per-phase magnetising reactance
- E_1: Per-phase induced voltage in the stator

The equivalent circuit diagram of the stator windings is identical to the primary side of a transformer.

To simplify determining the parameters in Figure 5.1, the R_{fe} resistance can be removed from the equivalent circuit diagram. In this case, it is maintained, as it allows for easier comparison with MotorCAD once parameters have been estimated because MotorCAD also includes R_{fe} in the equivalent circuit.

Looking at the rotor windings it can be modelled as seen in Figure 5.2a where:

- R_2: Per-phase rotor circuit resistance
- X_2: Per-phase rotor leakage reactance
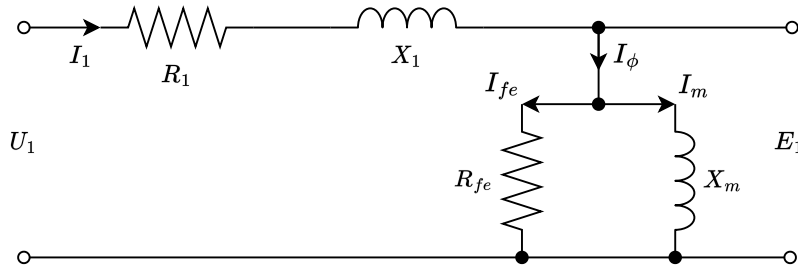
Figure 5.1: Stator winding equivalent circuit

(a)   (b)
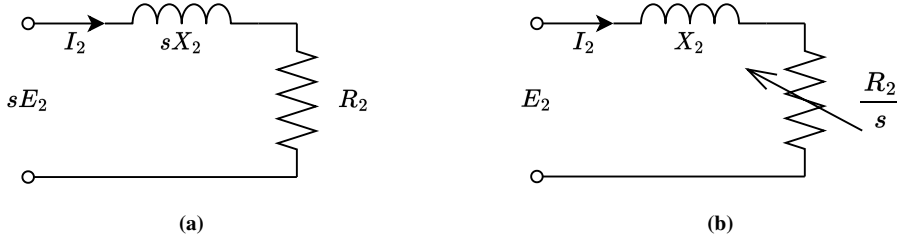
Figure 5.2: Rotor winding equivalent circuit

- E_2: Per-phase induced voltage in the rotor, at line frequency f_1

The equivalent circuit in Figure 5.2a have a frequency different to that of the stator, therefore the current I_2 at slip frequency f_2 can be calculated as (5.3).

$$I_2(s) = \frac{sE_2}{R_2 + jsX_2} \Rightarrow \frac{E_2}{\frac{R_2}{s} + jX_2} \tag{5.3}$$

This suggests that if the rotor current is viewed at line frequency f_1, the resistance should be R_2/s. Looking at power per phase at slip frequency f_2, it is possible to describe the conducting losses in the rotor P_{rcl} as in (5.4).

$$P_{rcl}(s) = I_2(s)^2 R_2 \tag{5.4}$$

When looking at the power per phase at line frequency f_1, it instead describes the total power crossing the air gap between the rotor and stator P_{ag} as (5.5) and the equivalent circuit diagram seen from the stator is as seen in Figure 5.2b.

$$P_{ag}(s) = I_2(s)^2 \frac{R_2}{s} \tag{5.5}$$

The varying resistance used in (5.5) can also be split into two components as shown in (5.6).

$$\frac{R_2}{s} \Rightarrow R_2 + \frac{R_2}{s}(1-s) \tag{5.6}$$

From this R_2 is recognised from (5.4) as the rotor conducting losses, and $R_2(1-s)/s$ is an expression for the mechanical power developed by the machine as seen in (5.7).

$$P_{mech}(s) = I_2(s)^2 \frac{R_2}{s}(1-s) \tag{5.7}$$

Much like a single phase transformer circuit, the frequency of the two equivalent circuit diagrams in Figure 5.1 and 5.2b are the same. Meaning that they can be combined into a single equivalent circuit diagram. However, the difference in turns in the stator and rotor windings must be accounted for,

leading to the combined equivalent circuit diagram seen in Figure 5.3, where $'$ denotes parameters seen from the stator side. (Sen; 2013)
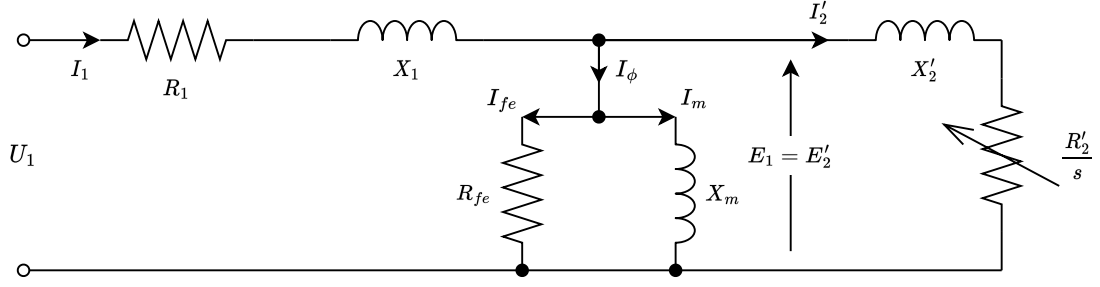
Figure 5.3: Combined induction machine equivalent circuit diagram

Using Figure 5.3 as the steady state model equivalent circuit, Kirchhoff voltage law and an equivalent impedance, can then be used to calculate the currents in the circuit.

5.1.1   Current Loops

For the steady state equivalent circuit, three current loops are defined as shown in Figure 5.4.
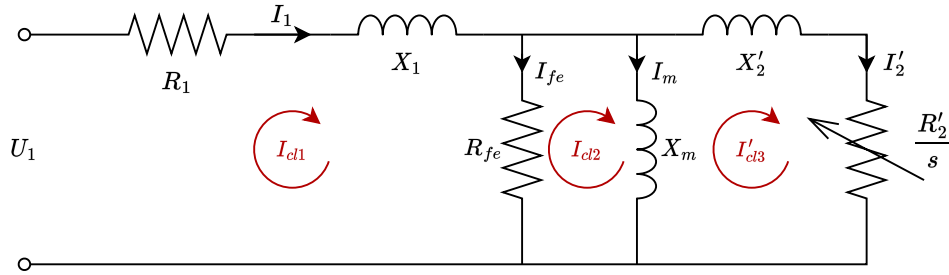
Figure 5.4: Current loops of the steady state equivalent circuit diagram

To calculate the current I_{cl1} the equivalent impedance Z_{eq} is defined as:

$$Z_{eq}(s) = R_1 + jX_1 + \left(\frac{1}{R_{fe}} + \frac{1}{jX_m} + \frac{1}{R'_2/s + jX'_2} \right)^{-1} \tag{5.8}$$

The current I_{cl1} is then calculated:

$$I_{cl1}(s) = \frac{U_1}{Z_{eq}(s)} \tag{5.9}$$

Using the closed loops of $I_{cl1}(s)$ and $I_{cl2}(s)$, the voltages across them should be zero according to Kirchhoff's voltage law, and the following two equations are found:

$$0 = U_1 - R_1 I_{cl1}(s) - jX_1 I_{cl1}(s) - R_{fe}(I_{cl1}(s) - I_{cl2}(s)) \tag{5.10}$$

$$0 = -R_{fe}(I_{cl2}(s) - I_{cl1}(s)) - jX_m(I_{cl2}(s) - I_{cl3}(s)) \tag{5.11}$$

Solving two equations with two unknowns, the solutions for $I_{cl2}(s)$ and $I_{cl3}(s)$ are found.

$$I_{cl2}(s) = U_1 \frac{jX_1 + R_1 + R_{fe} - Z_{eq}(s)}{R_{fe} Z_{eq}(s)} \tag{5.12}$$

$$I_{cl3}(s) = U_1 \frac{(X1 + X_m + jZ_{eq}(s) - jR_1)R_{fe} + (jX_1 + R_1 - Z_{eq}(s))X_m}{R_{fe}Z_{eq}(s)X_m} \tag{5.13}$$

Returning to the notations used in Figure 5.3, the currents are:

$$I_1(s) = \frac{U_1}{Z_{eq}(s)} \tag{5.14}$$

$$I_{fe}(s) = I_{cl1}(s) - I_{cl2}(s) = \frac{R_{fe}(U_1 - 1) - jU_1X_1 - R_1 + Z_{eq}(s)}{R_{fe}Z_{eq}(s)} \tag{5.15}$$

$$I_m(s) = I_{cl2}(s) - I_{cl3}(s) = \frac{R_{fe}(U_1(jR_1 - jZ_{eq}(s) - X_1 - X_m) + X_m) + jX_1X_m(U_1 - 1)}{R_{fe}Z_{eq}(s)X_m} \tag{5.16}$$

$$I_2'(s) = I_{cl3}(s) = U_1 \frac{(X1 + X_m + jZ_{eq}(s) - jR_1)R_{fe} + (jX_1 + R_1 - Z_{eq}(s))X_m}{R_{fe}Z_{eq}(s)X_m} \tag{5.17}$$

$$I_\phi(s) = I_{fe}(s) - I_m(s) = U_1 \frac{R_{fe}(jR_1 - jZ_{eq}(s) - X_1) - (jX_1 + R1 - Z_{eq}(s))X_m}{R_{fe}Z_{eq}(s)X_m} \tag{5.18}$$

5.2   Characteristics and Performance

Using the equivalent circuit and current loops from Section 5.1, general characteristics and performance of an induction machine can be described. The figures presented in this section are all based on a 4kW machine used in Helonde and Mankar (2019), which has the ratings shown in Table 5.1, and the parameters shown in Table 5.2.

Table 5.1: Ratings of example machine (Helonde and Mankar; 2019)

Specification	Unit	Value
Power	[kW]	4
Poles	[-]	4
Voltage	[V]	380
Curretn	[A]	8.6
Speed	[rpm]	1432
Power factor	[-]	0.85
Efficiency	[-]	83%
Rated torque	[Nm]	26.8

Table 5.2: Example machine parameters used for plotting (Helonde and Mankar; 2019)

Parameter	Unit	Value
X_1	[Ω]	3.9
X_2	[Ω]	6.6
X_M	[Ω]	136.5
R_1	[Ω]	3.9
R_2'	[Ω]	4.2
R_{fe}	[Ω]	1382.0

5.2.1 Current Characteristics

An important characteristic of an induction machine is how much current it draws. Using the steady state model equivalent circuit from Figure 5.3, the drawn current from the power supply is seen equal to $I_1(s)$.

Looking at (5.9) it can be seen that $I_1(s)$ is dependant on $Z_{eq}(s)$ which is slip dependant. This indicates the magnitude of the current drawn from the power supply increases with slip, as illustrated in Figure 5.5 where the current also is shown for different R_2 values.
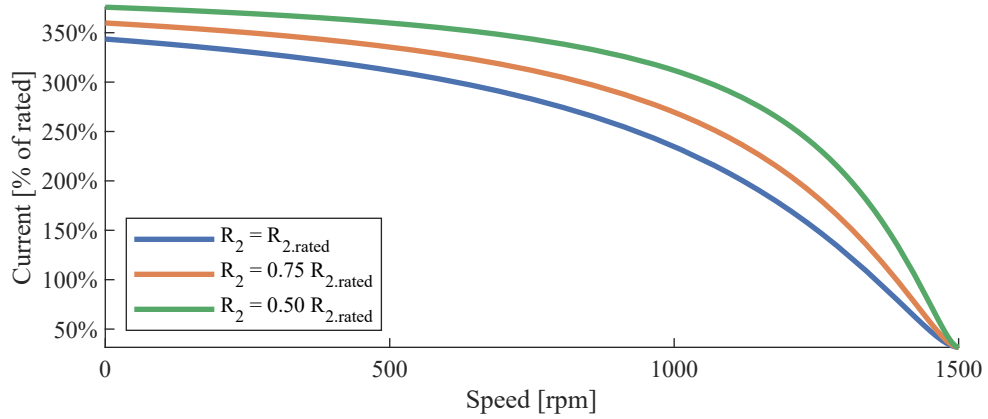
Figure 5.5: $I_1(s)$ as a function of speed

As it can be seen, the stator current $I_1(s)$ increases with slip, meaning that the current is at it's maximum at a slip of 1, where the machine is at a standstill. For induction machines the starting current is typically 5 to 8 times larger than the rated current. (Sen; 2013)

5.2.2 Power Factor

From the impedance $Z_{eq}(s)$ it is also a possibility to calculate the power factor defined as (5.21), by remembering the impedance can be divide into a real part and an imaginary part as shown in (5.19).

$$Z_{eq}(s) = R_{eq}(s) + jX_{eq}(s) \tag{5.19}$$

$$\Phi_{eq}(s) = \arctan\left(\frac{X_{eq}(s)}{R_{eq}(s)}\right) \tag{5.20}$$

$$PF_{eq}(s) = \cos(\Phi_{eq}(s)) \tag{5.21}$$

Where $\Phi_{eq}(s)$ is the phase angle between voltage U_1 and the current $I_1(s)$, which is the same as the phase angle calculated from the impedance in (5.20). As $Z_{eq}(s)$ is slip dependant this angle also varies with speed, as seen in Figure 5.6.

The power factor is a way to describe the ratio of the active and reactive power, whose vector sum is equal to the apparent power. The apparent power dictates how much current the machine draws, hence a higher apparent power requires larger equipment and infrastructure to handle. Since the induction machine uses active power to generate mechanical power, it is always beneficial to have most of the apparent power be active power. Having a power factor close to one indicates a high amount of active power compared to reactive power. The power factor typically increases for larger induction machines.
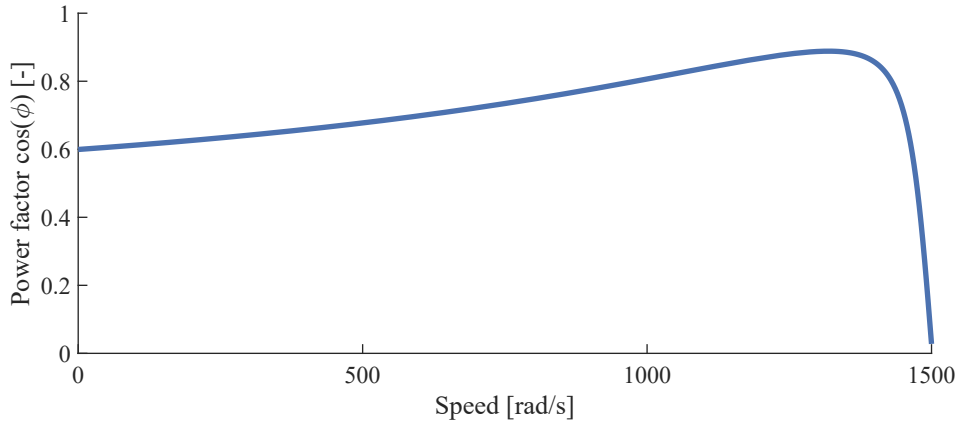
Figure 5.6: Power factor as a function of speed

5.2.3 Torque Profile

The mechanical torque developed by the induction machine can be found by looking at the developed mechanical power of the machine written per-phase as (5.22).

$$P_{mech}(s) = \tau_{mech}(s)\omega_{mech}(s) = I_2'(s)^2 \frac{R_2}{s}(1-s) \tag{5.22}$$

Since the mechanical speed, is related to the synchronous speed as in (5.23). The torque of the induction machine can be written as (5.24).

$$\omega_{mech}(s) = (1-s)\omega_{sync} \tag{5.23}$$

$$\tau_{mech}(s) = \frac{1}{\omega_{sync}}I_2'(s)^2 \frac{R_2}{s} = \frac{1}{\omega_{sync}}I_2'(s)^2 \frac{R_2'}{s} \tag{5.24}$$

From these equations, it can be seen, that the developed torque depends on the slip *s* of the induction machine, as it can be seen in the example curve in Figure 5.7 where the torque curve is also shown at different voltages.
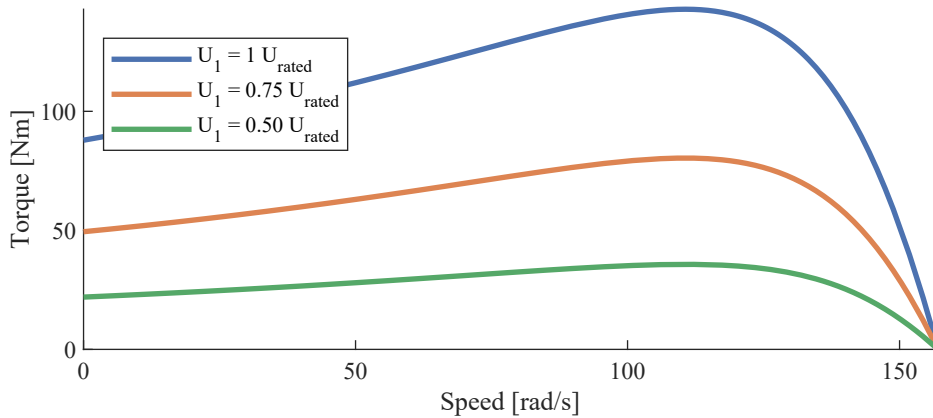
Figure 5.7: Torque curves at different voltages as a function of speed

The torque profile also changes depending on the rotor resistance R_2 as seen in Figure 5.8.

Decreasing the rotor resistance does not change the peak torque but increases the output power as more torque is being delivered at higher speeds. However, a smaller starting torque is achieved. It also results in less copper loss as described in (5.4), further increasing the overall efficiency.
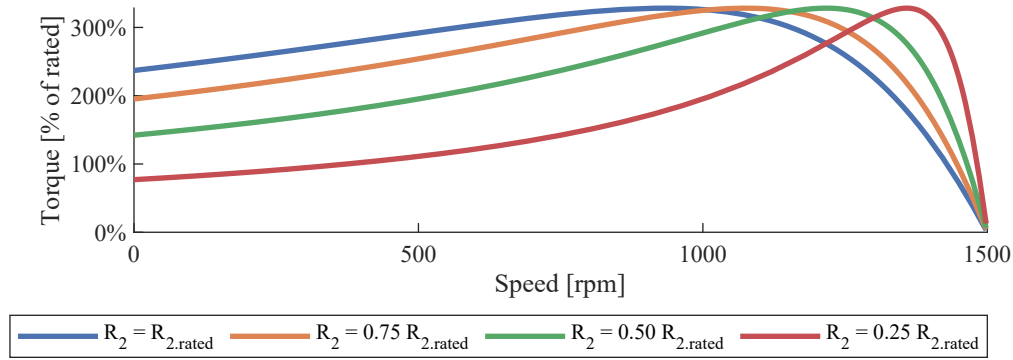
Figure 5.8: Torque curves at different R_2 values as a function of speed

5.2.4 Efficiency

To describe the efficiency of an induction machine, the individual losses must be identified. These losses are illustrated in Figure 5.9 which shows the power flow in an induction machine.
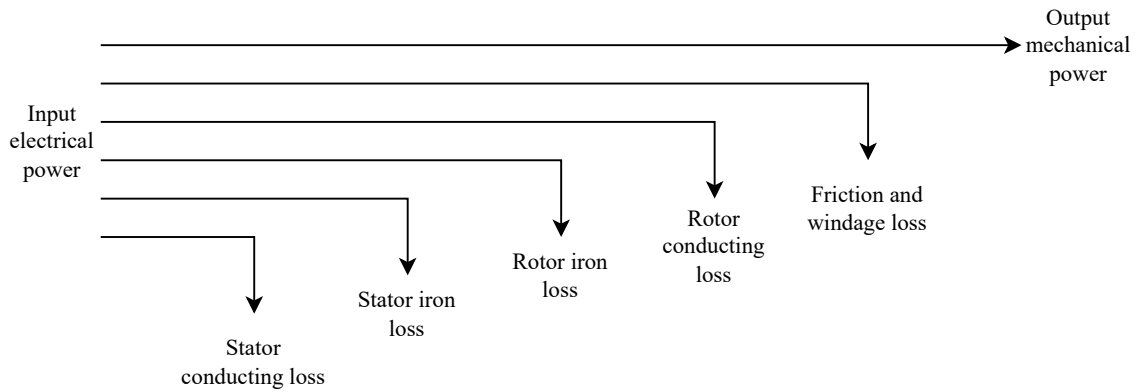
Figure 5.9: Power flow in an induction machine

Iron Losses

Iron losses in both the stator and rotor can be divided into three components: magnetic hysteresis losses, eddy current losses and excess losses.

Magnetic hysteresis is a phenomenon observed in magnetic materials, wherein the material retains some magnetisation even after the removal of an external magnetic field. This retention, known as magnetic reminiscence, occurs due to incomplete realignment of magnetic domains within the material when subjected to a magnetic field. Not all domains return to their original random orientations when the field is removed, resulting in residual magnetism.

The concept of magnetic hysteresis is encapsulated by the lagging of magnetic effects behind the forces causing them. In practical terms, this is represented by a hysteresis loop, a graphical depiction of the relationship between magnetic induction (B) and magnetising force (H). This loop illustrates the material's response to varying magnetic fields, showcasing both the magnetisation and demagnetisation processes. Induction machines are subjected to an alternating magnetic field, thus hysteresis losses occurs.

A commonly used method for calculating hysteresis losses is equation (5.25) presented by Steinmetz

(1892), which can be used to approximate the loss for sinusoidal signals.

$$P_{hysteresis} \approx K_h f^a B_m^b V \tag{5.25}$$

In this equation f is the frequency, V is the core volume and B_m is the maximum flux density. k_h, a and b are material parameters known as Steinmetz coefficients, which must be determined experimentally.

Eddy currents are circular currents induced in a conductor when it is exposed to a changing magnetic field. They are a result of electromagnetic induction. Eddy currents create their own magnetic fields, which oppose the original magnetic field that induced them, leading to energy loss in the form of heat.

Eddy current loss can be approximated using (5.26) if skin effects are ignored. (Fiorillo; 2010)

$$P_{eddy} \approx \frac{V \pi^2 B_m^2 d^2 f^2}{6\rho} \tag{5.26}$$

Where d is the sheet thickness, ρ is the resistivity of the material and D is the material density.

In the equivalent circuit model, the iron losses are calculated as in (5.27).

$$P_{fe}(s) = I_c(s)^2 R_{fe} \tag{5.27}$$

Noticeably, the resistance R_{fe} is not a slip-dependant parameter, despite representing eddy currents and hysteresis loss which both vary with frequency. To ensure precision in calculations, R_{fe} values are typically estimated at the rated slip value. At this operating point, iron losses within the rotor are practically insignificant due to the low electrical frequency in the rotor. Consequently, in practical scenarios, iron losses are often determined through no-load testing of the machine, as these losses exhibit minimal variation from no-load to rated load.

Conducting Losses

The conducting losses in both the rotor and stator, are the result of resistance in the windings. The conducting losses in the rotor are calculated as (5.28), and the stator conducting losses are calculated using (5.29).

$$P_r(s) = 3I_2'(s)^2 R_2 \tag{5.28}$$

$$P_s(s) = 3I_1(s)^2 R_1 \tag{5.29}$$

Ideal Efficiency

To describe the upper limits of the efficiency of an induction machine, the machine internal efficiency can be considered. The internal efficiency of the induction machine, is defined as (5.30).

$$\eta_{internal}(s) = \frac{P_{mech}(s)}{P_{ag}(s)} = 1 - s \tag{5.30}$$

The internal losses are considered the ideal efficiency, as it sets an upper limit of the efficiency depending on the slip. From the equation, it is easily seen that the upper limit of the efficiency is highest when the slip is 0. It is therefore beneficial from an efficiency point of view, to design induction machines to operate with a low slip value. This is visualised in Figure 5.10, where the ideal efficiency line is drawn along with the actual efficiency ($\eta(s)$), assuming a constant voltage supply and full

loading. The actual efficiency is defined as (5.31), where the electrical input power ($P_{in}(s)$) is defined as (5.32).

$$\eta(s) = \frac{P_{mech}(s)}{P_{in}(s)} \tag{5.31}$$

$$P_{in}(s) = U_1 \cdot I_1(s) \cdot PF_{eq}(s) \tag{5.32}$$
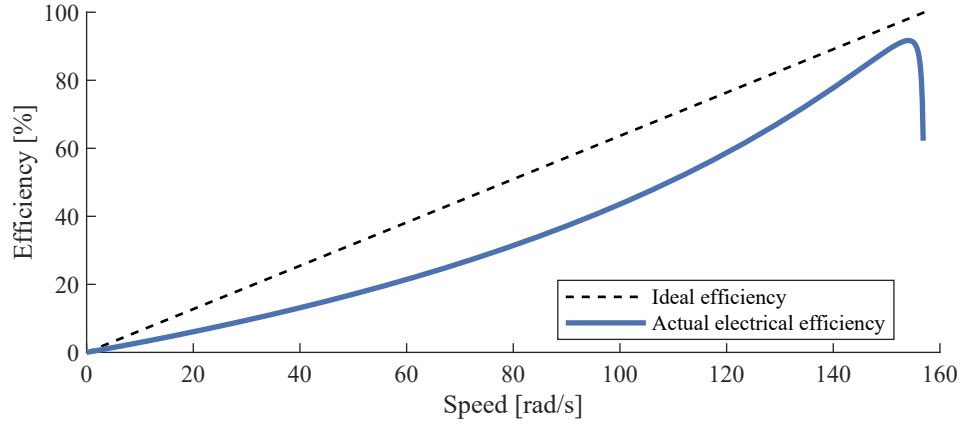
Figure 5.10: Efficiency of example machine, as a function of slip

Friction and Windage Losses

The frictional losses are often modelled using a combination of static, coulomb, and viscous friction components as seen in (5.33).

$$\tau_{fric}(s) = \begin{cases} \tau_s & \omega_{mech}(s) = 0 \\ \tau_C + B_v \omega_{mech}(s) & \omega_{mech}(s) > 0 \end{cases} \tag{5.33}$$

τ_s is the static friction, τ_C is the Coulomb friction and B_v is the viscous friction coefficient.

A Stribeck friction curve should be used instead for a more accurate representation of friction. To model a Stribeck friction curve Hess and Soom (1990), has proposed a simple model shown in (5.34).

$$\tau_{fric}(s) = \tau_C + \frac{\tau_s - \tau_C}{1 + \left(\frac{\omega_{mech}(s)}{\omega_s} \right)^2} + B_v \omega_{mech}(s) \tag{5.34}$$

Where ω_s is the characteristic velocity of the Stribeck curve. An illustrative comparison of the frictional torque using the two models presented in (5.33) and (5.34) can be seen in Figure 5.11.

The losses associated with overcoming this friction are found by multiplying the speed and torque, as done in Figure 5.12.

As it can be seen in the figure, there is no significant difference between the two friction models as viscous and Coulomb friction dominates at lower slip values. The best way to reduce power loss due to friction losses are therefore to reduce the viscous friction and Coulomb friction components.

Windage losses are the result of air resistance acting on the rotor. The air resistance is mainly due to cooling wings on each end of the rotor, but a small part originates from the rotor surface itself. The windage losses are often much smaller than frictional losses. However, some machines are made with an internal fan, often leading to higher windage losses.
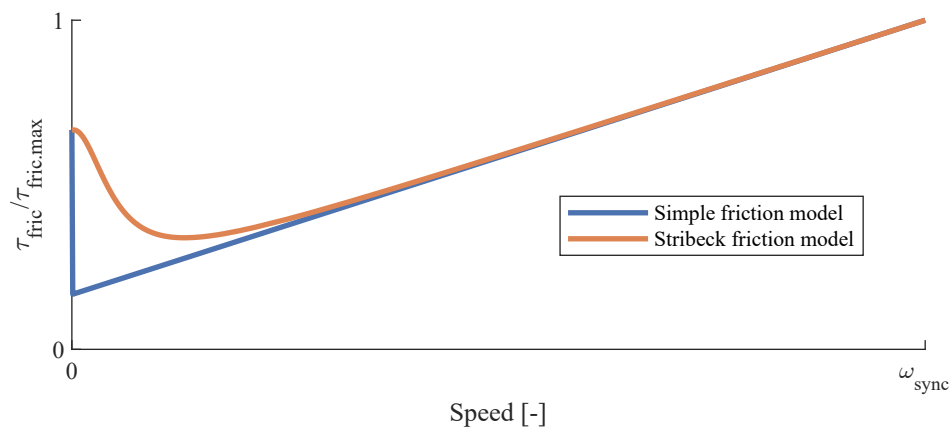
Figure 5.11: Frictional torque as a function of speed
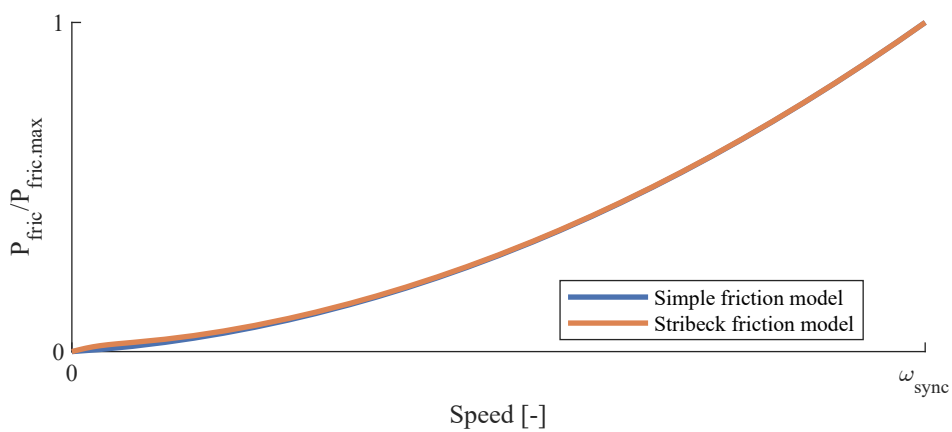
Figure 5.12: Frictional losses as a function of speed

Chapter 6

Steady State Model Parameter Estimation

To validate if the equivalent circuit model introduced in Chapter 5, accurately models induction machines, tests are performed to estimate the equivalent circuit parameters. The test and validation of the equivalent circuit model are performed on the FAB112M-4 and the Y3PE112M4. The testing and parameter calculation methods, are be presented in Section 6.1 and Section 6.2. These experiments and parameter calculation methods are inspired by the impedance test method 1, found in IEEE std 112 - 2017 (2017) and method 2-1-1H from IEC 60034-2-1:2014 (2014). The nameplate data for the FAB112M-4 and Y3PE112M4 are found in Table 6.1, and Table 6.2 respectively.

Table 6.1: Performance characteristics of FAB112M-4 induction machine

Characteristics	Units	Performance values		
Freq.	[Hz]	50.0	60.0	60.0
Rated torque	[Nm]	26.2	25.1	25.0
Rated voltage Δ/Y	[V]	230/400	[-]/440	[-]/480
Rated current Δ/Y	[A]	14.5/8.42	[-]/7.97	[-]/7.54
Rated power	[kW]	4.00	4.60	4.60
Power factor	[-]	0.82	0.85	0.82
Poles	[-]		4	
Speed	[1/min]	1456	1750	1759
Efficiency	[-]	88.6%	89.1%	89.5%
IE class	[-]	IE3	IE2	IE2
IEC frame size	[-]		112M	

Table 6.2: Performance characteristics of Y3PE112M induction machine

Characteristics	Units	Performance values	
Freq.	[Hz]	50.0	60.0
Rated torque	[Nm]	26.2	25.1
Rated voltage Δ/Y	[V]	400/690	460/795
Rated current Δ/Y	[A]	7.95/4.61	7.68/4.44
Rated power	[kW]	4.00	4.60
Power factor	[-]	0.82	[-]
Poles	[-]		4
Speed	[1/min]	1460	1752
Efficiency	[-]	88.7%	91.7%
IE class	[-]	IE3	[-]
IEC frame size	[-]		112M

As seen from the nameplate data in the tables, the machines are rated to operate at different line to line voltages at the same configuration. Hence to compare steady state models and estimated equivalent circuit parameters, both machines are operated at 400 V line to line. This means experimentation on the

Y3PE112M4 physically is made in a delta configuration, but during calculation, it is seen as a Y configuration.

6.1 Tests for Determination of Unknown Parameters

The steady state parameters which needs to be determined are: R_1, R_2', R_{fe}, X_m, X_1, and X_2'.

To determine these parameters three different tests are conducted: a DC resistance test, a no-load test, and a locked rotor test.

The DC test is used to determine the resistance across the stator windings R_1. This is done by using a multimeter for resistance measurement, and a thermostat to determine at what temperature this resistance was measured. The DC test description can be found in Appendix E, and the following values are obtained from it:

- $R_{1_{DC}}$: The stator resistance across a single phase.
- T_{DC}: The temperature of the stator windings during the resistance measurement.

The no load tests are made by operating the machine at the rated frequency without any load on its shaft. Without any mechanical load the rotor is assumed to be very close or equal to zero slip, hence only a negligible current is induced in the rotor. Using this assumption the power consumption equals windage, friction, stator iron, and stator copper losses. Multiple no load tests are then made at different % rated voltages to separate and determine the different losses. Thus the no load tests are made using a variable voltage transformer to vary the voltage. The no load test description is found in Appendix F and the values obtained are:

- U_{NL}: The per phase RMS voltage during a no load test.
- $U_{NL,LL}$: The line to line RMS voltage during a no load test.
- I_{NL}: The per phase RMS current during a no load test.
- $I_{NL,LL}$: The line to line RMS current during a no load test.
- P_{NL}: The total real power drawn during a no load test.
- $R_{1_{NL}}$: The per phase stator resistance during a no load test, measured with a multimeter right after the no load test.
- $R_{1_{NL,LL}}$: The line to line average stator resistance during a no load test, measured with a multimeter right after the no load test.

The locked rotor tests are made by locking the shaft of the machine and running it at the rated current. With the rotor locked, it can not rotate, hence the slip value is one. This means that the rotor has an electric frequency equal to that of the stator. Thus multiple locked rotor tests are made at different frequencies to eliminate influences such as skin effect by interpolation. Here it is recommended by both the IEEE std 112 - 2017 (2017) and IEC 60034-2-1:2014 (2014) to get at least one locked rotor test at under 25% rated frequency. The locked rotor test is made by using a variable frequency drive and adjusting it based on rated current. The locked rotor test is described in Appendix G, and the acquired values are:

- U_{LR}: The per phase RMS voltage during a locked rotor test.
- I_{LR}: The per phase RMS current during a locked rotor test.
- P_{LR}: The total real power drawn during a locked rotor test.
- $R_{1_{LR}}$: The per phase stator resistance during a locked rotor test, measured with a multimeter immediately after the locked rotor test.
- f_{LR}: The electrical frequency during the test.

6.2 Calculation Method for Parameter Estimations

Using the data from the tests as presented in Section 6.1, equivalent circuit parameters can be estimated. These estimations are based on IEEE std 112 - 2017 (2017) impedance test method 1 and IEC 60034-2-1:2014 (2014) method 2-1-1H, the calculation method is presented below.

First the reactive power for the no load test (Q_{NL}) and the locked rotor test (Q_{LR}) is calculated using (6.1) and (6.2). Where Q_{NL} only needs to be found for the no load test done at 100% rated voltage, while Q_{LR} needs to be found for all locked rotor frequencies tested at.

$$Q_{NL} = \sqrt{(3U_{NL}I_{NL})^2 - P_{NL}^2} \tag{6.1}$$

$$Q_{LR} = \sqrt{(3U_{LR}I_{LR})^2 - P_{LR}^2} \tag{6.2}$$

The reactances X_m and X_1 are then determined for each locked rotor frequency tested, by using the following procedure:

1. Assume a relationship between X_1 and X_2, if design details are available, use the calculated ratio X_1/X_2, otherwise use the relations shown in (6.3), (6.4) and (6.5), where each machine type is defined in ANSI/NEMA MG 1-2021 (2021).

$$\left(\frac{X_1}{X_2'}\right) = 1.00 \text{ for design A, design D and wound rotor machines} \tag{6.3}$$

$$\left(\frac{X_1}{X_2'}\right) = 0.67 \text{ for design B} \tag{6.4}$$

$$\left(\frac{X_1}{X_2'}\right) = 0.43 \text{ for design C} \tag{6.5}$$

2. Solve equation 6.6 for X_m, assuming a value of X_1/X_M and X_1

$$X_M = \frac{3U_{NL}^2}{Q_{NL} - 3I_{NL}^2 X_1} \cdot \frac{1}{(1 + \frac{X_1}{X_M})^2} \tag{6.6}$$

3. Solve equation 6.7 for X_{1LR}, using the same value of X_1/X_M as above

$$X_{1_{LR}} = \frac{Q_{LR}}{3I_{LR}^2 \cdot [1 + (\frac{X_1}{X_2'}) + \frac{X_1}{X_M}]} \cdot \left[\left(\frac{X_1}{X_2'}\right) + \frac{X_1}{X_M}\right] \tag{6.7}$$

4. Solve Equation 6.8 for X_1

$$X_1 = \frac{f_{NL}}{f_{LR}} \cdot X_{1_{LR}} \tag{6.8}$$

5. Then repeat step 2-4 by solving equation 6.6 for X_M, using X_1 from equation 6.8 and a ratio of X_1/X_M from equation 6.6 and Equation 6.8

6. Continue iterating solutions until stable values of X_1 and X_M are obtained within 0.10%

Then for each locked rotor frequency tested at, X_2' can be determined. X_2' is determined based on the relation between X_1 and X_2' and corrected to rated frequency, as shown in (6.9) and (6.10).

$$X_{2_{LR}}' = \frac{X_{1_{LR}}}{\left(\frac{X_1}{X_2'}\right)} \tag{6.9}$$

$$X_2' = \frac{f_{NL}}{f_{LR}} \cdot X_{2_{LR}}' \tag{6.10}$$

Then the power consumed during no load tests is divided into stator copper, stator iron, and windage and friction losses. This is done by first determining the total stator copper losses (P_s) at each no load test. In 6.11 and 6.12 equations are given to determine copper losses if a machine is in either Δ or Y configuration. Looking at these two equations they are seen equal by rewriting them into 6.13, hence the stator copper losses do not depend on the machine configuration.

Δ configured machine copper losses:

$$P_s = 3 \cdot \left(\frac{I_{NL,LL}}{\sqrt{3}}\right)^2 \cdot R_{1_{NL,LL}} \cdot \frac{3}{2} \tag{6.11}$$

Y configured machine copper losses:

$$P_s = 3 \cdot I_{NL,LL}^2 \cdot R_{1_{NL,LL}} \cdot \frac{1}{2} \tag{6.12}$$

Copper losses for a Δ or Y configured machine are seen equal and rewritten to:

$$P_s = 1.5 \cdot I_{NL,LL}^2 \cdot R_{1_{NL,LL}} \tag{6.13}$$

Having determined the stator copper losses, they are subtracted from the total power consumption for each no load test. The remaining losses are then the stator iron losses and the windage and friction losses. The remaining losses are historically known as constant losses, even though they depend on, e.g., frequency, current etc. hence the notation P_C is used in (6.14), when determining these.

$$P_C = P_{NL} - P_s \tag{6.14}$$

The windage and friction losses (P_{WF}) are then estimated by developing a curve of P_C plotted against $U_{NL,LL}^2$. The curve is made from no load tests between 60% rated voltage down to 10% rated voltage, or until further voltage reduction increases the current, at least 4 points are needed. Using the curve, extrapolate a straight line to zero voltage squared, determining where the line intercepts zero voltage squared, this is then equal to P_{WF}. If no current flows through the machine at zero voltage squared, it can be assumed that the iron loss is not present, hence the isolation of P_{WF}.

Having separated P_{WF} only P_{fe} is left to be found at the machine's operating point. This is done by developing another curve by plotting P_{fe} against $U_{NL,LL}^2$, this time for no load tests made between 60% rated voltage up to 125% rated voltage, again at least 4 points are needed. P_{fe} is found by subtracting P_{WF} from P_C as stated in 6.15. Then develop a straight line between the points, which intercepts with zero power at zero voltage squared. Using that straight line interpolate the iron loss at full load at U_i^2. The voltage U_i is the inner voltage which takes the resistive voltage drop in the primary winding into

account. It is calculated based on load testing at rated load or specifications from the technical datasheet. The equation for U_i for a machine in motor-mode is shown in 6.16, with $\cos(\phi)$ defined as shown in 6.17, $\sin(\phi)$ defined as shown in 6.18, and $P_{rated,in}$ defined as shown in 6.19

$$P_{fe} = P_C - P_{WF} \tag{6.15}$$

$$U_i = \sqrt{\left(U_{rated,LL} - \frac{\sqrt{3}}{2} \cdot I_{rated,LL} \cdot R_{1_{rated,LL}} \cdot \cos(\phi)\right)^2 + \left(\frac{\sqrt{3}}{2} \cdot I_{rated,LL} \cdot R_{1_{rated,LL}} \cdot \sin(\phi)\right)^2} \tag{6.16}$$

$$\cos(\phi) = \frac{P_{rated,in}}{\sqrt{3} \cdot U_{rated,LL} \cdot I_{rated,LL}} \tag{6.17}$$

$$\sin(\phi) = \sqrt{1 - \cos^2(\phi)} \tag{6.18}$$

$$P_{rated,in} = \frac{P_{rated,mech}}{\eta_{rated}} \tag{6.19}$$

Using the iron loss found at U_i^2, the iron loss conductance can be found using (6.20), which is then used to determine the iron loss resistance using (6.21).

$$G_{fe} = \frac{P_{fe}}{3U_{NL}^2} \cdot \left(1 + \frac{X_1}{X_M}\right)^2 \tag{6.20}$$

$$R_{fe} = \frac{1}{G_{fe}} \tag{6.21}$$

The uncorrected rotor resistance for each locked rotor frequency is then found using (6.22).

$$R_{2_{LR}} = \left(\frac{P_{LR}}{3I_{LR}^2} - R_{1_{LR}}\right) \cdot \left(1 + \frac{X_2}{X_M}\right)^2 - \left(\frac{X_2}{X_1}\right)^2 \cdot (X_{1LR}^2 \cdot G_{fe}) \tag{6.22}$$

The temperature during each locked rotor test is found using $R_{1_{DC}}$ which is measured at a known temperature (T_{DC}). Using the $R_{1_{LR}}$ and the DC value at a known temperature the relation shown in 6.23 can then be used to calculate the temperature for each locked rotor test made. This equation is based on the assumption that the windings are 100% IACS conductivity copper hence $k_{1_{Cu}}$ is a constant with the value 234.5 °C.

$$T_{LR} = R_{1_{LR}} \cdot \frac{T_{DC} + k_{1_{Cu}}}{R_{1_{DC}}} - k_{1_{Cu}} \tag{6.23}$$

Knowing the temperature for each locked rotor test performed, $R_{1_{LR}}$ and $R_{2_{LR}}$ can then be corrected to a temperature of 25 °C using (6.24) and (6.25) setting T_{cor} to 25 °C. Assuming windings in the stator are 100% IACS conductivity copper making $k_{1_{Cu}}$ a constant with a value of 234.5 °C. Assuming that rotor

windings are aluminium with a volume conductivity of 62% IACS conductivity copper making $k_{1_{Al}}$ a constant with a value of 225 °C, and a temperature equal to the stator windings.

$$R_1 = R_{1_{LR}} \cdot \frac{T_{cor} + k_{1_{Cu}}}{T_{LR} + k_{1_{Cu}}} \tag{6.24}$$

$$R'_{2_{LR}} = R_{2_{LR}} \cdot \frac{T_{cor} + k_{1_{Al}}}{T_{LR} + k_{1_{Al}}} \tag{6.25}$$

Then using the found $R'_{2_{LR}}$ for each locked rotor test, a curve can be made by plotting $R'_{2_{LR}}$ against the locked rotor frequency it was found at (f_{lr}). Using this curve R'_2 can be interpolated at the rated slip frequency for the rotor.

For the X_M, X_1, X_2', and R_{fe} found at different locked rotor testing frequencies an average is taken. They depend on applied current and saturation which may vary a bit from test to test, hence the averaging out.

6.3 Estimated Parameters for the FAB112M-4 and the Y3PE112M4

The parameter estimations are based on a DC, a no load, and a locked rotor test, as described earlier in Section 6.1. The DC test measurements for the FAB112M-4 are presented in Table 6.3, while Table 6.4 shows the no-load test measurements, and Table 6.5 contains the results of the locked rotor test. The test results from the Y3PE112M4 are found in Appendices H.1 to H.3.

Table 6.3: DC test measurement for the FAB112M-4 both line to line and per phase seen as Y configured

DC test data		
T_{DC} [°C]	$R_{1_{DC,LL}}$ [Ω]	$R_{1_{DC}}$ [Ω]
21.5	2.08	1.04

Table 6.4: No load test measurements for the FAB112M-4 both line to line and per phase seen as Y configured

No-load data						
$R_{1_{NL,LL}}$ [Ω]	$R_{1_{NL}}$ [Ω]	$U_{NL,LL}$ [V]	U_{NL} [V]	$I_{NL,LL} = I_{NL}$ [A]	P_{NL} [W]	f_{NL} [Hz]
2.24	1.12	447	258	5.35	369	50
2.24	1.12	400	231	3.92	276	50
2.24	1.12	300	173	2.46	170	50
2.24	1.12	240	139	1.88	128	50
2.24	1.12	200	115	1.54	107	50
2.24	1.12	160	92.4	1.22	89.5	50
2.24	1.12	120	69.3	0.96	75.1	50
2.24	1.12	80.2	46.3	0.77	65.1	50

Following the calculation method from Section 6.2, the parameters for both the FAB112M-4 and the Y3PE112M4 have been calculated. The determination curves for P_{WF}, P_{fe}, and R'_2 for the FAB112M-4 can be seen in Figure 6.1, Figure 6.2, and Figure 6.3 respectively. However, during testing, to perform measurements at a low frequency, two AC sources with a variable frequency drive was used. The first AC source delivered up to 8 A but only went down to 40 Hz. The second AC source went down to 15 Hz, but only delivered up to 4 A. Hence the locked rotor data below 40 Hz has not been taken at approximately rated current, so a difference in X_M, X_1, X_2', and R_{fe} around this point was found. The impact of the current drop between 40 Hz and 35 Hz on the parameters, as illustrated in Figure 6.4 for

Table 6.5: Locked rotor test measurements for the FAB112M-4 both line to line and per phase seen as Y configured

T_{LR}	$R_{1_{LR,LL}}$ [Ω]	$R_{1_{LR}}$ [Ω]	$U_{LR,LL}$ [V]	U_{LR} [V]	$I_{LR,LL} = I_{LR}$ [A]	P_{LR} [W]	f_{LR} [Hz]
			Locked rotor data				
24.5	2.10	1.05	16.7	9.62	3.81	85.0	15.0
25.4	2.11	1.06	19.4	11.2	3.86	89.4	20.0
29.4	2.14	1.07	22.1	12.8	3.83	90.8	25.0
30.4	2.15	1.08	25.1	14.5	3.85	94.1	30.0
30.9	2.16	1.08	28.1	16.2	3.86	97.2	35.0
34.3	2.18	1.09	66.2	38.3	8.41	478	40.0
40.2	2.23	1.12	72.9	42.1	8.44	497	45.0
47.6	2.29	1.15	76.7	44.3	8.09	477	50.0
56.5	2.36	1.18	78.0	45.0	7.55	451	55.0
57.4	2.37	1.19	83.5	48.2	7.49	439	60.0

R_{fe}. Hence only the tests above 40 Hz have been used for averaging these values, as the others have not been taken at rated current. The found parameters for both the FAB112M-4 and the Y3PE112M4 seen as Y configured can be seen in Table 6.6. The parameters are seen to be similar, which is to be expected due to both machines having similar ratings.
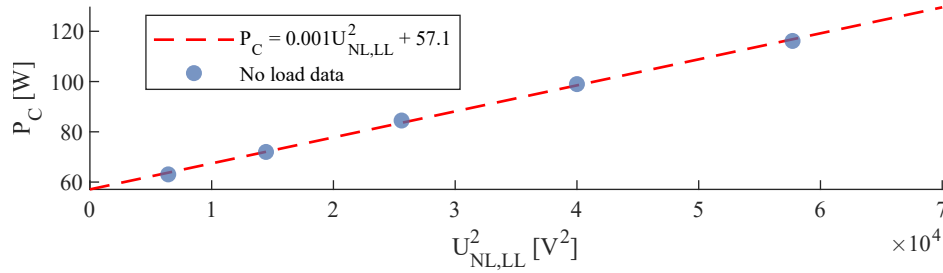
Figure 6.1: Curve for windage and friction loss extrapolation of FAB112M-4
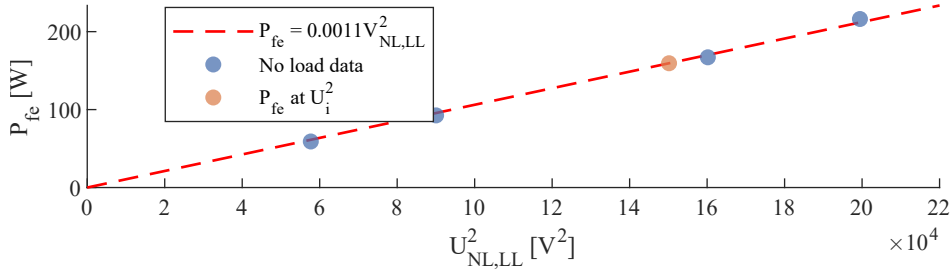
Figure 6.2: Curve for iron loss extrapolation of FAB112M-4

Table 6.6: Estimated parameters from tests performed on FAB112M-4 and Y3PE112M4 seen as Y configured

Parameter	Units	FAB112M-4	Y3PE112M4
X_1	[Ω]	2.50	2.12
X_2	[Ω]	2.50	2.12
X_M	[Ω]	56.9	53.1
R_1 at 25 °C	[Ω]	1.05	1.09
R'_2 at 25 °C	[Ω]	0.87	0.85
R_{fe}	[Ω]	890	899
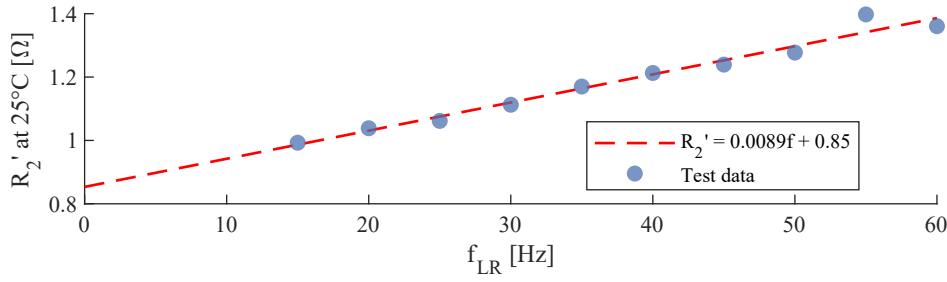
Figure 6.3: R_2' for FAB112M-4 at different testing frequencies, corrected to $25\,°C$
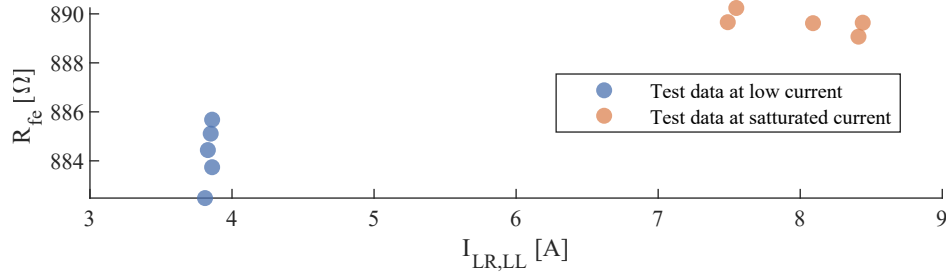
Figure 6.4: R_{fe} for FAB112M-4 at different line to line currents, due to limits on frequency drives used

6.4 Validation of Parameters for the FAB112M-4 and the Y3PE112M4

To validate the equivalent circuit parameters found in Section 6.3, the IEC 60034-2-1:2014 (2014) method 2-1-1H is used as a guideline to calculate ratings. This method is based on efficiency determination using an equivalent circuit. The ratings derived based on the equivalent circuit parameters are then compared to datasheet ratings.

From the datasheets, both machines are rated to perform a continuous duty (S1), as mentioned in Section 2.3 this duty type is specified by IEC 60034-1 (2010). This duty type is defined by operating at a constant load maintained for sufficient time to allow the machine to reach thermal equilibrium. In IEC 60034-1 (2010) thermal equilibrium is defined as the state reached when the temperature rises of several parts of the machine do not vary by more than a gradient of 2 K per hour.

To compare ratings derived from the equivalent circuit parameters and datasheet ratings, comparison at thermal equilibrium is needed. However, datasheets do not state thermal equilibrium during rating. For the Y3PE112M4 a load test can be made to estimate the thermal equilibrium point during datasheet rating. This can be done for the Y3PE112M4 since the cooling system is integrated. For the FAB112M-4 the cooling system is designed to use the airflow of the external fan system implemented. An external fan system for the FAB112M-4 is not available, hence a thermal equilibrium point during datasheet rating cannot be estimated. Instead, the FAB112M-4 is tested at three different temperatures for comparison with the datasheet ratings.

The three different temperatures for the FAB112M-4 are specified through load tests. The load tests are conducted within 3 different temperature intervals, namely 30°C-40°C, 50°C-60°C, and 70°C-80°C. The exact temperature for each load test is then measured. The temperature found during the load testing is then used to correct the temperature-dependant equivalent circuit parameters R_1 and R_2' to compare.

As stated above load testing is needed to estimate a thermal equilibrium point, however, load testing can also be used for validation. Load testing can be used to determine the efficiency of a machine, this can be done directly as stated in IEC 60034-2-1:2014 (2014) method 2-1-1A. The efficiency found directly during a load test is used to validate the efficiency from equivalent circuit parameter calculation and

datasheet ratings.

Furthermore, multiple load tests can be used to form a load curve. The load curve can then be used to separate the losses of the machine tested. A method for loss separation based on load curve testing is found in IEC 60034-2-1:2014 (2014) method 2-1-1B. A method based on IEC 60034-2-1:2014 (2014) method 2-1-1B is used to validate the losses found from equivalent circuit parameter calculation.

6.4.1 IEC60034-2-1 Method 2-1-1H Efficiency Determination by Equivalent Circuit

Based on IEC 60034-2-1:2014 (2014) method 2-1-1H, the efficiency, losses, and ratings are found using the equivalent circuit presented in Chapter 5 with equivalent parameters from Table 6.6.

For convenience in current calculations, impedance, etc., absolute values of the current loops presented in Section 5.1 are utilised, as these are equivalent to equations presented in IEC 60034-2-1:2014 (2014) method 2-1-1H.

To determine the efficiency based on the equivalent circuit the total iron loss ($P_{fe}(s)$) is found using (6.26). Here R_{fe} is a circuit parameter found earlier, while $I_{fe}(s)$ can be found using (5.15) with known parameters.

$$P_{fe}(s) = 3 \cdot R_{fe} \cdot |I_{fe}(s)|^2 \tag{6.26}$$

The stator copper loss ($P_s(s)$) is then found using (6.27), with R_1 being a known parameter and $I_1(s)$ is found using (5.14) with known parameters.

$$P_s(s) = 3 \cdot R_1 \cdot |I_1(s)|^2 \tag{6.27}$$

The rotor copper loss ($P_r(s)$) is then found using (6.28), with R'_2 being a known parameter and $I'_2(s)$ is found using (5.17) with known parameters.

$$P_r(s) = 3 \cdot R'_2 \cdot |I'_2(s)|^2 \tag{6.28}$$

To determine the additional load losses ($P_{LL}(s)$), the assigned value method from IEC 60034-2-1:2014 (2014) is used to estimate the additional load losses at ratings ($P_{rated,LL}$) based on the datasheet. $P_{rated,LL}$ based on datasheet ratings is found using (6.29), where $P_{rated,mech}$ is the rated mechanical output power and $P_{rated,in}$ is the rated electrical input power.

$$P_{rated,LL} = P_{mech,rat} \cdot \left(0.025 - 0.005 \cdot \log_{10} \left(\frac{P_{rated,in}}{1000\,\text{W}} \right) \right) \tag{6.29}$$

The load losses as a fraction of the rated power according to this model, can be seen in Figure 6.5.

The load losses at the rated slip $P_{LL}(s)$ is then found using (6.30), where $I'_{rated,2}$ is calculated using (5.17) with known parameters and rated slip according to the datasheet.

$$P_{LL}(s) = P_{rated,LL} \cdot \left(\frac{I'_2(s)}{I'_{rated,2}} \right)^2 \tag{6.30}$$

Remembering that P_{WF} was determined during parameter estimation using the method in Section 6.2 all losses have been found. The losses are then aggregated to determine the total loss $P_T(s)$ as seen in (6.31).

$$P_T(s) = P_s(s) + P_{fe}(s) + P_r(s) + P_{LL}(s) + P_{WF} \tag{6.31}$$

The electrical input power $P_{in}(s)$ can then be found using (6.32), with $PF_{eq}(s)$ being calculated based on $Z_{eq}(s)$ using (5.19) and (5.20).

$$P_{in}(s) = 3 \cdot U_1 \cdot |I_1(s)| \cdot PF_{eq}(s) \tag{6.32}$$
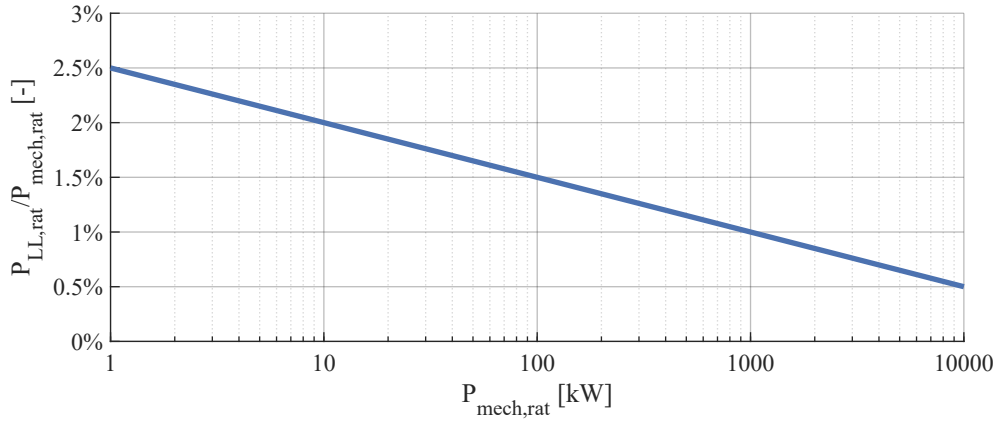
Figure 6.5: Estimated load losses as a fraction of output power according to IEC 60034-2-1:2014 (2014)

.

Using $P_{in}(s)$ and $P_T(s)$ the mechanical output power $P_{mech}(s)$ can then be found using (6.33)

$$P_{mech}(s) = P_{in}(s) - P_T(s) \tag{6.33}$$

Having found input and output power the efficiency can be calculated following (6.34).

$$\eta(s) = \frac{P_{mech}(s)}{P_{in}(s)} \tag{6.34}$$

As seen, this efficiency determination method is slip-dependent. In IEC 60034-2-1:2014 (2014) it is suggested to solve this using an iterative process, stepping the slip until the desired rated mechanical output power is found. The above equations can also be solved using a numerical or analytical solver, inserting the desired rated mechanical output power and solving for slip. To get a crude estimate a graphical solution is also practical.

To compare the method above with the datasheet, ratings are calculated using the method above at the rated output power given in the datasheet. Comparisons between datasheet and equivalent circuit using found parameters for the FAB112M-4 and the Y3PE112M4 can seen in Table 6.7 and Table 6.8 respectively.

Table 6.7: Validation of the FAB112M-4 parameters from Table 6.6 , by using method 2-1-1H from IEC60034-2-1 to compare against ratings from the datasheet.

Parameter	Unit	Datasheet	Equivalent circuit			Tolerance
T_W	[°C]	N/A	40.3	55.5	76.4	N/A
I_{LL}	[A]	8.42	8.17	8.21	8.28	5.77 - 8.41
s	[-]	2.93%	2.94%	3.13%	3.42%	2.35% - 3.52%
τ_{mech}	[Nm]	26.2	26.2	26.3	26.4	26.1 - 26.4
n	[RPM]	1456	1456	1453	1449	1447 - 1465
PF	[-]	0.82	0.82	0.82	0.83	0.79 - 1.00
P_{mech}	[kW]	4.00	4.00	4.00	4.00	-
η	[-]	88.6%	85.9%	85.2%	84.3%	86.9% - 100%
P_T	[W]	515	658	694	748	0 - 604

It is seen in the tables, that the efficiency and the total loss consistently are outside tolerances for both machines. This may indicate possible erroneous parameters or loss estimation methods, hence to validate losses and efficiency, other test methods are used to determine losses and efficiency.

Table 6.8: Validation of the Y3PE112M4 parameters from Table 6.6 , by using method 2-1-1H from IEC60034-2-1 to compare against ratings from the datasheet.

Parameter	Unit	Datasheet	Equivalent circuit	Tolerance
T_W	[°C]	N/A	65.5	N/A
I_{LL}	[A]	7.95	8.29	5.77 - 8.40
s	[-]	2.67%	3.15%	2.13% - 3.20%
τ_{mech}	[Nm]	26.2	26.3	26.0 - 26.3
n	[RPM]	1460	1453	1452 - 1468
PF	[-]	0.82	0.82	0.79 - 1.00
P_{mech}	[kW]	4.00	4.00	-
η	[-]	88.7%	84.8%	87.0% - 100%
P_T	[W]	510	715	0 - 597

6.4.2   IEC60034-2-1 Method 2-1-1A Direct Measurement

To validate machine efficiency, a direct measurement method is used. The direct measurement method is based on IEC 60034-2-1:2014 (2014) method 2-1-1A, here a load test is done by loading the machine with an external load machine. When the test machine is loaded, electrical input power P_{in} is measured using a three phase power analyser, while mechanical speed n and torque τ are measured using a dynamometer. Immediately after testing, the stator winding temperature is recorded, using the difference in resistance method, the same method used during locked rotor testing based on (6.23).

A more detailed description of the load test experiment can be found in Appendix I, with the load test data provided in Appendices H.4 and J.1 for the FAB112M-4 and Y3PE112M4, respectively.

Having found the mechanical speed and torque, the mechanical power can be calculated using (6.35).

$$P_{mech} = \tau \cdot \frac{2 \cdot \pi \cdot n}{60} \tag{6.35}$$

Having measured both the electrical input power and calculated the mechanical output power from measured torque and speed, the direct efficiency η can be found using (6.36).

$$\eta = \frac{P_{mech}}{P_{in}} \tag{6.36}$$

η is found for both the FAB112M-4 and the Y3PE112M4 at around 4 kW mechanical power. For the Y3PE112M4 the load was maintained until thermal equilibrium, while for the FAB112M-4 three different tests were done at three different temperatures. The thermal equilibrium point for the Y3PE112M4 and the three measured temperatures for the FAB112M-4 are also the temperatures used in Section 6.4.1. Efficiency results can be seen in Table 6.9 and Table 6.10 for the FAB112M-4 and Y3PE112M4 respectively.

Table 6.9: Directly measured efficiency using method 2-1-1A from IEC60034-2-1 for the FAB112M-4

T_W [°C]	P_{mech} [kW]	P_{in} [kW]	η [-]
76.4	3.99	4.63	86.2%
55.5	4.00	4.63	86.3%
40.3	3.99	4.64	86.2%

Comparing the measured efficiencies in Table 6.9 and Table 6.10 with those found in Table 6.7 and Table 6.8, they do not seem to match. The efficiencies found using the direct measurement method are

Table 6.10: Directly measured efficiency using method 2-1-1A from IEC60034-2-1 for the Y3PE112M4

T_W [°C]	P_{mech} [kW]	P_{in} [kW]	η [-]
65.5	4.02	4.61	87.2%

higher than the ones estimated using the equivalent circuit parameter method. However, the direct measurement method 2-1-1A in IEC 60034-2-1:2014 (2014) is not recommended for use on a three phase machine. It can also be seen that the efficiencies at different temperatures are similar. This is unexpected as the efficiency in an induction machine is expected to show a decreased efficiency at higher temperatures, due to the increase in winding and rotor resistance. Nevertheless, it indicates where the efficiency of a machine is, but to estimate efficiency and compare loss components more precisely, another method is needed.

6.4.3 IEC60034-2-1 Method 2-1-1B Summation of Losses

The method recommended by IEC 60034-2-1:2014 (2014) for efficiency estimation on a three phase machine up to 2 MW rated mechanical power is method 2-1-1B. Method 2-1-1B is also called the summation of losses method, as it separates the losses by estimating each loss individually to better separate measurement errors. Hence to measure the loss distribution in a machine, a method based on IEC 60034-2-1:2014 (2014) method 2-1-1B is used. This method is not related to any equivalent circuit parameters, thus later when estimating, e.g., rotor copper losses R_2' is not used.

Method 2-1-1B is based on doing load tests as described in Section 6.4.2, for load points at 125%, 115%, 100%, 75%, 50%, and 25% of the rated mechanical output of 4 kW for both machines. Along with P_{in}, τ, and n the line to line current $I_{LT,LL}$, stator winding resistance $R_{1LT,LL}$, ambient temperature T_{amb}, and winding temperature T_W must also be measured at each load point tested. The test at 100% rated load has already been made during Section 6.4.2, by reusing this test the winding temperature at 100% rated load is equal. The method also uses a no load test to determine windage and friction loss and iron losses as described in Section 6.2. For convenience, the no load test performed to estimate parameters in Section 6.3 is also reused.

First, the stator copper losses at 100% rated loading is calculated directly using (6.37).

$$P_s = 1.5 \cdot I_{LT,LL}^2 \cdot R_{1LT,LL} \tag{6.37}$$

Then the rotor copper losses at 100% rated loading are calculated directly using (6.38). Remember that P_{fe} was determined from a no load test during equivalent parameter calculation with calculation method shown in Section 6.2, with U_i based on datasheet data. However, P_{fe} can be found in the same way again, basing U_i of the 100% rated load test.

$$P_r = (P_{in} - P_s - P_{fe}) \cdot s \tag{6.38}$$

In the IEC 60034-2-1:2014 (2014), a correction factor is used on the machine coolant to correct it to 25 °C. In the case of both machines, the coolant is the surrounding air, hence T_{amb} is used as the coolant temperature. The correction factor is calculated as shown in (6.39).

$$k_\theta = \frac{235°C + T_W + 25°C - T_{amb}}{235°C + T_W} \tag{6.39}$$

The coolant correction factor is then used to correct the measured slip, stator copper loss, and rotor copper loss, as shown in (6.40), (6.41), and (6.42) respectively.

$$s_\theta = k_\theta \cdot s \tag{6.40}$$

$$P_{s,\theta} = P_s \cdot k_\theta \tag{6.41}$$

$$P_{r,\theta} = (P_{in} - P_{s,\theta} - P_{fe}) \cdot s_\theta \tag{6.42}$$

The corrected stator copper loss $P_{s,\theta}$ and the corrected rotor copper loss $P_{r,\theta}$ is then used to correct the measured electrical input power P_{in} as shown in (6.43).

$$P_{in,\theta} = P_{in} - (P_s - P_{s,\theta} + P_r - P_{r,\theta}) \tag{6.43}$$

The corrected electrical power input $P_{in,\theta}$, is later used to determine efficiency.

Then for each load point, the windage and friction losses, found earlier from a no load test as explained in Section 6.2, are adjusted to match the slip of each load point. The adjustment is done as shown in (6.44).

$$P_{WF,s} = P_{WF} \cdot (1 - s)^{2.5} \tag{6.44}$$

The residual loss for each load test is then found using (6.45), with P_{mech} calculated as shown earlier in (6.35).

$$P_{Lr} = P_{in} - P_{mech} - P_s - P_r - P_{fe} - P_{WF,s} \tag{6.45}$$

Having found the residual loss, it is assumed to follow a linear tendency shown in (6.46).

$$P_{Lr} = A \cdot \tau^2 + B \tag{6.46}$$

The slope of the linear tendency (A) can be calculated using (6.47), where i is the number of load points summed.

$$A = \frac{i \cdot \sum(P_{Lr} \cdot \tau^2) - \sum P_{Lr} \cdot \sum \tau^2}{i \cdot \sum(\tau^2)^2 - (\sum \tau^2)^2} \tag{6.47}$$

The offset of the linear tendency (B) is calculated following (6.48).

$$B = \frac{\sum P_{Lr}}{i} - A \cdot \frac{\sum \tau^2}{i} \tag{6.48}$$

From IEC 60034-2-1:2014 (2014) the intercept B should be considerably smaller (<50%) than the additional load losses P_{LL} at rated torque. Otherwise, the measurements may be erroneous and should be checked.

Furthermore, the correlation between the linear tendency line calculated and the data points measured should be checked. The correlation coefficient (γ) can be calculated by following (6.49).

$$\gamma = \frac{i\sum(P_{Lr} \cdot \tau^2) - (\sum P_{Lr}) \cdot (\sum \tau^2)}{\sqrt{(i \cdot \sum(\tau^2)^2 - (\sum \tau^2)^2) \cdot (i \cdot \sum P_{Lr}^2 - (\sum P_{Lr}^2)^2)}} \tag{6.49}$$

If γ is less than 0.95, delete the worst load point and repeat the regression. Then, if γ becomes ≥ 0.95, use the second regression otherwise retake the test after investigating possible errors.

Having checked for errors and found the linear regression coefficients, the additional load losses P_{LL} can be found using (6.50). The additional load losses need only be found for the point at 100% rated mechanical output power.

$$P_{LL} = A \cdot \tau^2 \tag{6.50}$$

Then to determine efficiency at 100% rated load, the windage and friction are adjusted according to slip at this point but also according to coolant temperature following (6.51).

$$P_{WF,\theta} = P_{WF} \cdot (1 - s_\theta)^{2.5} \tag{6.51}$$

The total loss at 100% rated load is then estimated using (6.52).

$$P_T = P_{s,\theta} + P_{fe} + P_{r,\theta} + P_{LL} + P_{WF,\theta} \tag{6.52}$$

The efficiency can then be calculated based on $P_{in,\theta}$ and P_T, with the calculation method presented in (6.53).

$$\eta = \frac{P_{in,\theta} - P_T}{P_{in,\theta}} \tag{6.53}$$

Losses and efficiencies calculated from load curve testing based on IEC 60034-2-1:2014 (2014) method 2-1-1B can be seen in Table 6.11 and Table 6.13 for the FAB112M-4 and Y3PE112M4 respectively.

Consequently, for comparison the losses and efficiencies calculated based on the equivalent circuit parameters and IEC 60034-2-1:2014 (2014) method 2-1-1H is shown in Table 6.12 and Table 6.14 for the FAB112M-4 and Y3PE112M4 respectively.

Table 6.11: Losses separated based on method 2-1-1B separation of losses from IEC60034-2-1 for the FAB112M-4

T_W	$P_{s,\theta}$	$P_{r,\theta}$	$P_{WF,\theta}$	P_{LL}	P_{fe}	P_T	P_{mech}	$P_{in,\theta}$	η
[°C]	[W]	[W]	[W]	[W]	[W]	[W]	[kW]	[kW]	[-]
76.4	250	141	52.4	51.6	163	658	3.99	4.63	85.8%
55.5	233	128	52.9	51.0	168	633	4.00	4.63	86.3%
40.3	229	121	53.1	51.8	165	620	3.99	4.64	86.6%

Table 6.12: Losses separated based on method 2-1-1H equivalent circuit from IEC60034-2-1 for the FAB112M-4

T_W	P_s	P_r	P_{WF}	P_{LL}	P_{fe}	P_T	P_{mech}	P_{in}	η
[°C]	[W]	[W]	[W]	[W]	[W]	[W]	[kW]	[kW]	[-]
76.4	259	148	57.1	132	150	745	3.99	4.74	84.3%
55.5	238	135	57.1	112	151	693	4.00	4.69	85.2%
40.3	223	125	57.1	99.1	152	656	3.99	4.65	85.9%

Table 6.13: Losses separated based on method 2-1-1B separation of losses from IEC60034-2-1 for the Y3PE112M4

T_W	$P_{s,\theta}$	$P_{r,\theta}$	$P_{WF,\theta}$	P_{LL}	P_{fe}	P_T	P_{mech}	$P_{in,\theta}$	η
[°C]	[W]	[W]	[W]	[W]	[W]	[W]	[kW]	[kW]	[-]
65.5	246	129	29.7	31.8	164	601	4.02	4.61	87.0%

Table 6.14: Losses separated based on method 2-1-1H equivalent circuit from IEC60034-2-1 for the Y3PE112M

T_W	P_s	P_r	P_{WF}	P_{LL}	P_{fe}	P_T	P_{mech}	P_{in}	η
[°C]	[W]	[W]	[W]	[W]	[W]	[W]	[kW]	[kW]	[-]
65.5	262	137	32.6	138	151	721	4.02	4.74	84.8%

There are small differences between the losses, but the tendencies seem to follow each other. However, the load losses seem to have larger deviations between the methods, compared with the other losses.

Furthermore, load losses found using load curve testing seemingly do not vary with temperature. Whereas load losses found using the equivalent circuit parameter method are temperature-dependent. This is caused by the resistance being temperature dependent, which is used to calculate the current for scaling the estimated load losses, in the equivalent circuit parameter calculation.

The additional load losses found in Table 6.11 and Table 6.13, may then be considered more correct. Hence the equivalent circuit parameter method may be adjusted to use the measured additional load losses, instead of load losses estimated based on an empirical model.

6.4.4 Readjusting Additional Load Losses in IEC60034-2-1 Method 2-1-1H Efficiency Determination by Equivalent Circuit

To adjust the method presented in Section 6.4.1, the load losses found in Section 6.4.3 can be used instead of the empirical model from IEC 60034-2-1:2014 (2014). This is done to compare against load measurements at rated mechanical load more accurately. A comparison against load measurements can be seen in Table 6.15 and Table 6.16 for the FAB112M-4 and Y3PE112M4 respectively.

Table 6.15: Comparison between equivalent circuit methods with adjusted load losses and load measurements for the FAB112M-4.

Parameter	Unit	Equivalent Circuit			Load measurements			Tolerance
T_W	[°C]	40.3	55.5	76.4	40.3	55.5	76.4	N/A
I_{LL}	[A]	8.08	8.11	8.13	8.16	8.09	8.09	5.77 - 8.41
s	[-]	2.89%	3.08%	3.33%	2.83%	3.00%	3.33%	2.35% - 3.52%
τ_{mech}	[Nm]	26.2	26.2	26.3	26.2	26.2	26.3	26.1 - 26.4
n	[RPM]	1457	1454	1450	1458	1455	1450	1447 - 1465
PF	[-]	0.82	0.82	0.82	0.82	0.82	0.83	0.79 - 1.00
P_{mech}	[kW]	3.99	4.00	3.99	3.99	4.00	3.99	-
η	[-]	86.9%	86.5%	86.0%	86.6%	86.3%	85.8%	86.9% - 100%
P_T	[W]	602	623	651	620	633	658	0 - 604

Table 6.16: Comparison between equivalent circuit methods with adjusted load losses and load measurements for the Y3PE112M4.

Parameter	Unit	Equivalent circuit	Load measurements	Tolerance
T_W	[°C]	65.5	65.5	N/A
I_{LL}	[A]	8.16	8.08	5.77 - 8.40
s	[-]	3.08%	3.07%	2.13% - 3.20%
τ_{mech}	[Nm]	26.4	26.4	26.0 - 26.3
n	[RPM]	1454	1454	1452 - 1468
PF	[-]	0.82	0.82	0.79 - 1.00
P_{mech}	[kW]	4.02	4.02	-
η	[-]	87.1%	87.0%	87.0% - 100%
P_T	[W]	597	601	0 - 597

As seen in Tables 6.15 and 6.16, the equivalent circuit and load measurements are relative close to each other. However, the efficiencies are at the lower end compared to the tolerances. Reasons behind this may be measurement accuracy, run-in time, manufacturer test conditions, machine design targets, and drive used for load tests.

Guidelines for the accuracy of measuring instruments and power supplies are presented in the IEC 60034-2-1:2014 (2014). Looking at the equipment used the accuracy classes for both supply and

measurement instruments seem to be met according to IEC 60034-2-1:2014 (2014). However, the equipment datasheets state that calibration after a certain period, often once a year, is needed. It is unknown when maintenance such as calibration has been performed last, thus the accuracy class of the instruments may have drifted.

IEC 60034-2-1:2014 (2014) and IEEE std 112 - 2017 (2017) both state that the run-in time of the bearings must have passed. Often bearings have to operate for a certain period to distribute oil, wear down irregularities etc. This lowers the bearings' frictional losses, however, it is hard to tell how much friction is lowered or for how long the run-in has to last. A small run-in period of a couple of hours has been made for both machines, in this case.

The manufacturer test conditions are somewhat unclear, they should follow IEC 60034-2-1:2014 (2014) to get an IE class, but often loopholes or communication with production makes this hard. From talking to people inside the industry, the execution may differ from IEC 60034-2-1:2014 (2014) specifications. Examples include not waiting for the machine to hit thermal equilibrium during efficiency testing, testing without seals installed or not having surface treated all machine parts yet. Furthermore, ambient temperature is unknown and the exact methodology used from IEC 60034-2-1:2014 (2014) is unknown.

The machine design target itself should also be considered since the IE efficiency number is an upper limit. Thus if a designer and manufacturer is confident in its capability to produce machines within the lower end of the efficiency tolerances, this may be beneficial for cost reduction. Costs such as lamination qualities or copper windings could be reduced by keeping the efficiency at the lower end of tolerances.

As mentioned earlier accuracy of the supply and measurement instruments are given in IEC 60034-2-1:2014 (2014), but no accuracy class of the drive for the external loading machine is given. The setup used to load both machines is an external PMSM machine with a drive controlled by an algorithm scripted in Matlab. During testing the PMSM then tries to apply a constant load given by the algorithm scripted in Matlab. However, the accuracy of the Matlab algorithm and the PMSM was found to vary with up to 100 W at times. The variance was recorded on the dynamometer, and concluded that even if the dynamometer had drifted it could not be measuring so incorrectly. However, the sampling frequency and number of samples used to determine an average within the dynamometer could be affecting the measurements. To take this into account different sampling settings were tested, and pictures were taken of the three phase power analyzer and dynamometer data simultaneously or directly after each other. Multiple pictures of the dynamometer data were also taken as a means to find an average.

Overall from the equipment available and methods used the experiments have been carried out to the best of one's abilities. Furthermore looking at the IEC 60034-2-1:2014 (2014) and IEEE std 112 - 2017 (2017) both standards seem to be complied with. From the results obtained using the adjusted additional load losses and equivalent circuit parameter calculation method, the equivalent circuit parameters found in Section 6.3 seem valid.

Chapter 7

MotorCAD Modelling

The equivalent circuit method presented in Chapter 6, is seen to estimate the efficiency capabilities of an induction machine well. However, to use the equivalent circuit method, tests need to be performed on a physical machine. Instead when dealing with machine design, simulations to predict induction machine parameters are needed, without necessarily having to construct a new physical machine each time.

To do so the program MotorCAD is chosen as a calculation tool. MotorCAD is an electrical machine modelling program, which can be used to model squirrel cage induction machines. The program uses machine geometry and material data to predict the machine's performance.

To validate the use of MotorCAD as a calculation tool, the FAB112M-4 and Y3PE112M4 have been modelled using MotorCAD. The MotorCAD models constructed is then validated based on data from Chapter 6 and their datasheets.

7.1 Obtaining the MotorCAD Model Inputs

To model an induction machine in MotorCAD, the program requires data regarding the physical parameters of the machine. To obtain this information for the FAB112M-4 and Y3PE112M4, the machines have been dismantled to allow for measurements and observations. Please note that specific numerical values obtained from these measurements are confidential and are not disclosed.

7.1.1 Stator and Rotor Geometry

The stator and rotor have been pulled out of the machine, and the stack length has been measured. Subsequently, the stator and rotor sections were cut, as illustrated in Figures 7.1 and 7.2, showcasing the Y3PE112M4 post-cutting. To make measurements of the geometry easier, a small stack of the laminates has been removed, as seen in Figures 7.3 and 7.4.

Figure 7.1: Stator after cutting
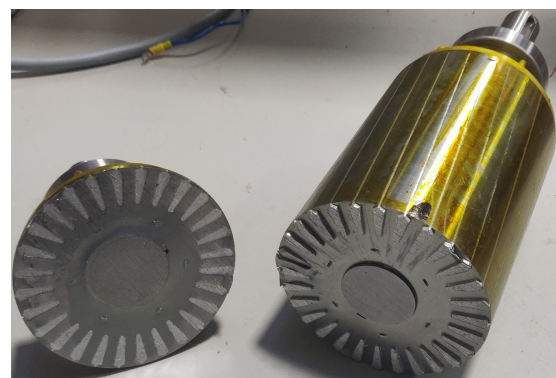
Figure 7.2: Rotor after cutting

The Geometry of the stator and rotor teeth is then measured using a calliper, and thicknesses are measured using a micrometre.
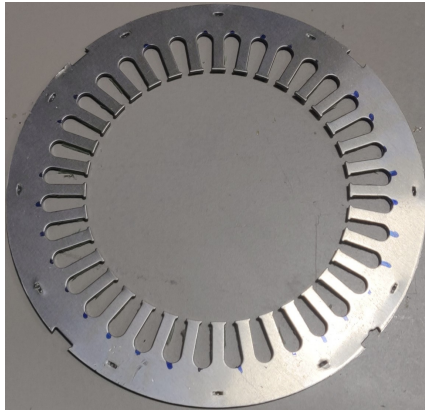
Figure 7.3: Stator laminate stack
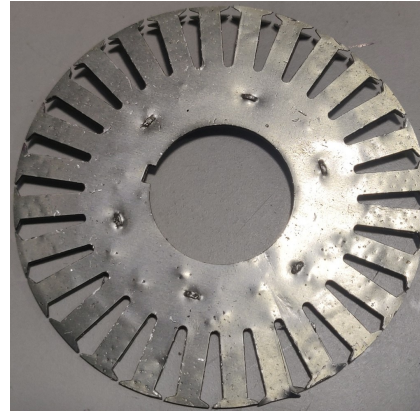
Figure 7.4: Rotor laminate stack

7.1.2 Winding Configuration

To determine the winding configuration of the machines, coils are pulled from the rotor, as seen in Figures 7.5 and 7.6.
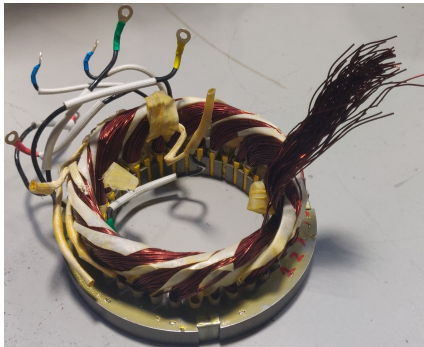
Figure 7.5: FAB112M-4 stator coils
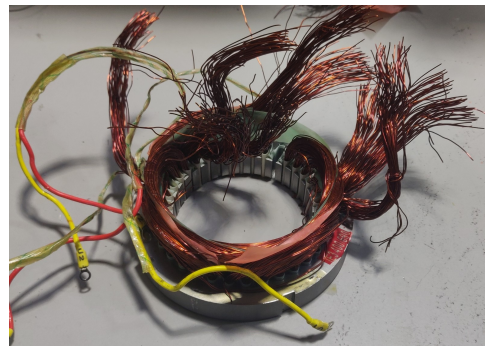
Figure 7.6: Y3PE112M4 stator coils

For the FAB112M-4, which features single-layered windings, the measurement of winding turns and noting coil spans is sufficient. However, the Y3PE112M4, with two winding layers, requires counting multiple coils to ensure accurate winding distribution and slot fill. The final winding configurations are depicted in Figures 7.7 and 7.8.

The laminate material of the FAB112M-4 is known to be an M600-50A magnetic steel, whereas the laminate material of the Y3PE112M4 is unknown, but is assumed to be the same material type. Multi-Wing has supplied data for the M600-50A used in the FAB112M-4.

With the geometries and winding configurations determined, MotorCAD is employed to calculate the models.
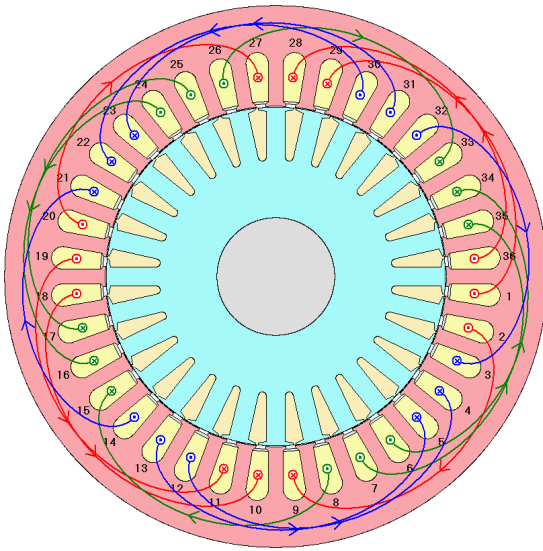
Figure 7.7: FAB112M-4 Winding configuration
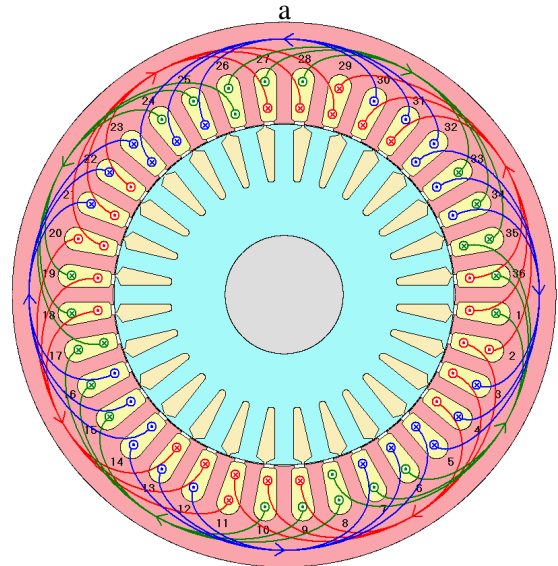
Figure 7.8: Y3PE112M4 Winding configuration

7.2 MotorCAD Ratings

Having set up the MotorCAD models from available material data and machine geometry, the models need validation. As previously done in Chapter 6, ratings from the datasheet with tolerances are used for comparison. Furthermore, ratings found using the equivalent circuit method in Section 6.4.4, are also used for comparison, as these are based on physical measurements. Comparison between MotorCAD, datasheet, and Section 6.4.4 equivalent circuit ratings is seen in Table 7.1 and Table 7.2 for the FAB112M-4 and the Y3PE112M4 respectively.

Table 7.1: Comparison of ratings between the MotorCAD model, the datasheet and the equivalent circuit method from Section 6.4.4 for the FAB112M-4.

Parameter	Unit	Datasheet	Equivalent circuit			MotorCAD			Tolerance
T_W	[°C]	N/A	40.3	55.5	76.4	40.3	55.5	76.4	N/A
I_{LL}	[A]	8.42	8.09	8.11	8.14	8.01	8.03	8.05	5.77 - 8.41
s	[-]	2.93%	2.90%	3.08%	3.34%	2.71%	2.87%	3.10%	2.35% - 3.52%
τ_{mech}	[Nm]	26.2	26.2	26.3	26.3	26.2	26.2	26.3	26.1 - 26.4
n	[RPM]	1456	1457	1454	1450	1459	1457	1454	1447 - 1465
PF	[-]	0.82	0.82	0.82	0.82	0.83	0.83	0.84	0.79 - 1.00
P_{mech}	[kW]	4.00	4.00	4.00	4.00	4.00	4.00	4.00	-
η	[-]	88.6%	86.9%	86.5%	86.0%	86.9%	86.5%	86.0%	86.9% - 100%
P_T	[W]	515	603	623	653	604	624	652	0 - 604

Looking at the FAB112M-4 comparison presented in Table 7.1, most of the MotorCAD ratings comply with tolerances. The efficiencies at higher temperatures do not abide by the datasheet tolerances, but they seem to follow the efficiencies found using Section 6.4.4. However, the power factors do not comply with the datasheet nor results from Section 6.4.4. This indicates that the apparent, reactive, and real power distribution is off. Which suggests there might be a problem regarding the modelling of resistance or reactance, as they are used to decide the power factor angle, as seen earlier in (5.20).

For the comparison done in Table 7.2 regarding the Y3PE112M4 MotorCAD model validation, the current and power factor are both higher than in the datasheet. This suggests that a higher percentage of the current and power drawn is used actively. Thus, the MotorCAD model can produce a magnetic field

Table 7.2: Comparison of ratings between the MotorCAD model, the datasheet and the equivalent circuit method from Section 6.4.4 for the Y3PE112M4.

Parameter	Unit	Datasheet	Equivalent circuit	MotorCAD	Tolerance
T_W	[°C]	N/A	65.5	65.5	N/A
I_{LL}	[A]	7.95	8.12	7.82	5.77 - 8.40
s	[-]	2.67%	3.06%	2.77%	2.13% - 3.20%
τ_{mech}	[Nm]	26.2	26.3	26.2	26.0 - 26.3
n	[RPM]	1460	1454	1458	1452 - 1468
PF	[-]	0.82	0.82	0.85	0.79 - 1.00
P_{mech}	[kW]	4.00	4.00	4.00	-
η	[-]	88.7%	87.1%	87.2%	87.0% - 100%
P_T	[W]	510	593	588	0 - 597

strong enough, to keep mechanical power at the rating, using less current. The high power factor and lower current may suggest a problem regarding the modelling of resistance or reactance.

To better understand why both MotorCAD models show high power factors, their resistances and reactances are checked. In MotorCAD it is possible to show a T-circuit with parameters calculated based on input data. The T-circuit model in MotorCAD is equal to the equivalent circuit model presented earlier in Section 5.1, which also was used in Chapter 6. Hence the reactances and resistances from the MotorCAD model and those calculated in Section 6.3 should be similar.

7.3 MotorCAD Equivalent Circuit Parameters

Inspecting the equivalent circuit parameters, calculated by MotorCAD, allows for the identification of standouts when compared to the measured parameters. Comparisons between MotorCAD and measured parameters from Section 6.3 are found in Tables 7.3 and 7.4 for the FAB112M-4 and Y3PE112M4 respectively. In the tables, ε is the absolute error relative to the measured parameter in percentage, it is defined as stated in (7.1). ε is introduced as there are no known tolerances for the measured parameters, hence the absolute error is used to indicate standouts more distinctly.

$$\varepsilon = \frac{|MotorCAD\ paramter - Measured\ paramter|}{Measured\ paramter} \tag{7.1}$$

Table 7.3: Comparison of MotorCAD and measured equivalent circuit parameters for the FAB112M-4

Parameter	Units	Measured	MotorCAD	ε
X_1	[Ω]	2.50	1.01	59.6%
X_2'	[Ω]	2.50	3.76	50.4%
$X_1 + X_2'$	[Ω]	5.00	4.77	4.60%
X_M	[Ω]	56.9	58.9	3.51%
R_1 at 25°C	[Ω]	1.05	1.10	4.76%
R_2' at 25°C	[Ω]	0.87	0.85	2.30%
R_{fe}	[Ω]	890	1332	49.7%

Looking at the comparisons in Tables 7.3 and 7.4, the parameters X_1 and X_2' from MotorCAD seem to deviate drastically from the measured values. This discrepancy likely arises due to the assumption made during calculations based on measurements, where X_1 is equated to X_2'. This assumption stems from the ratio determination method outlined in Section 6.2, which assumes the machines adhere to design A

Table 7.4: Comparison of MotorCAD and measured equivalent circuit parameters for the Y3PE112M4

Parameter	Units	Measured	MotorCAD	ε
X_1	[Ω]	6.37	1.94	69.5%
X_2'	[Ω]	6.37	11.4	79.0%
$X_1 + X_2'$	[Ω]	12.7	13.3	4.72%
X_M	[Ω]	159	187	17.6%
R_1 at 25 °C	[Ω]	3.26	3.21	1.53%
R_2' at 25 °C	[Ω]	2.55	2.44	4.31%
R_{fe}	[Ω]	2693	3916	45.4%

standards according to ANSI/NEMA MG 1-2021 (2021). MotorCAD does not have the ratings of the machines available, hence it cannot choose a ratio based on a design type. Instead, MotorCAD employs an analytical formula, which calculates the expected ratio between X_1 and X_2'.

Thus, comparing X_1 and X_2' individually is not favourable, as the ratio between X_1 and X_2' used in MotorCAD and the ratio assumed during measurement calculations are different. Instead, the sum $X_1 + X_2'$ should be compared, as the difference in the ratio is then ignored. This step is already shown in the tables, where the MotorCAD leakage reactance sum is within 5% of the measurement leakage reactance sum.

Furthermore, the iron loss resistance, R_{fe}, for both machines also differs drastically between MotorCAD models and measurements. In MotorCAD R_{fe} is based on the iron loss data provided for the specified laminate materials. Often laminate material data is based on measurements performed before processing. This is due to costs, as measuring the laminate material properties after processing involves the construction of measurement tools capable of handling complex geometries. However, the processing of magnetic steel changes its properties, such as iron loss, as described in Mierczak et al. (2020). Processing often increases the iron loss in the laminate material, hence the processed laminate material inside the machine is expected to result in a lower R_{fe}. This effect is also seen in the tables, as the measured R_{fe} is lower, than the R_{fe} in MotorCAD based on non-processed material data.

Mierczak et al. (2020) also discusses how different types of processes or the order in which processes take place affect the material's BH curve. MotorCAD uses the specified material BH curve to, among others, estimate its reactances in the T-circuit model. From the tables, the FAB112M-4 MotorCAD model reactances are seen to be within 5% of the measured reactances, excluding the X_1 and X_2' individual comparison. So, even though the BH curve might change due to processing it does not seem to affect the material data used in the FAB112-4 MotorCAD model significantly. However, the Y3PE112M4 has a noticeable deviation when comparing MotorCAD X_M and measured X_M. This deviation may be caused by material changes, but is more likely due to the unknown composition of the laminates, as mentioned in Section 7.1.2.

The rest of the deviations in the tables are within 5% of the measured values. These smaller deviations are often due to measurement inaccuracies, both when measuring geometrical data for the MotorCAD model, but also when measuring the parameters. Other assumptions also have an effect, such as assuming the copper wires to be completely round or having the exact extruded diameter throughout the whole wire. Hence deviation within 5% of the measured values is deemed acceptable. However, it was seen that some parameters are outside tolerances, as explained above mostly the material data seem to be the root cause. In MotorCAD calibration coefficients are often used to correct such deviations, as having to calibrate material data is common.

In conclusion, the FAB112M-4 and Y3PE112M4 models in MotorCAD require calibration of material data, due to the effect of processing. However, the purpose of the MotorCAD models for the FAB112M-4 and Y3PE112M4 is to assess the accuracy of MotorCAD calculations without calibration.

Therefore, the calibration of these models is unnecessary.

7.4   Introduction to the UMP-3C3-210-25-4 as Initial Design Basis

Multi-Wing's UMP-3C3-210-25-4 induction machine is used as an initial design basis, as this is Multi-Wing's attempt at creating a short-stacked induction machine. This allows for a more accurate prediction of performance, if a well-fitting model of the UMP-3C3-210-25-4 is achieved. The performance characteristics of the UMP-3C3-210-25-4 are made to be similar to those of the FAB112M-4, and can be found in Table 7.5.

Table 7.5: Performance characteristics of the UMP-3C3-210-25-4 induction machine

Characteristics	Units	Performance values
Freq.	[Hz]	50.0
Rated torque	[Nm]	25.5
Rated voltage Δ/Y	[V]	400/690
Rated current Δ/Y	[A]	7.86/4.55
Rated power	[kW]	4.00
Power factor	[-]	0.83
Poles	[-]	4
Speed	[1/min]	1462
Efficiency	[-]	88,6%
IE class	[-]	IE3
Frame size	[-]	UMP 210
Insulation class	[-]	H
Duty type	[-]	S1
Ambient temperature	[°C]	$-20\,°C$ to $45\,°C$
Cooling type	[-]	IC418

The UMP-3C3-210-25-4 has an OD of 256 mm compared to the 215 mm OD of the FAB112M-4 excluding its terminal box. Due to the larger diameter, the total length of the UMP is 330 mm, whereas the FAB112M-4 has a length of 350 mm. However, it should be noted that the shaft of the UMP-3C3-210-25-4 is a smaller diameter and therefore also 6.5 mm shorter than the FAB112M-4's shaft. Thus the actual length reduction achieved is 13.5 mm, if the shaft change is ignored.

The internal geometries of the UMP-3C3-210-25-4 have been determined in the same way as those of the FAB112M-4 and Y3PE112M4, by disassembling the machine and cutting the rotor and stator. The final stator and rotor geometry with the winding configuration is seen in Figure 7.9.

The UMP-3C3-210-25-4 shares an identical slot count in the rotor and stator with the FAB112M-4, albeit featuring larger slots owing to its increased diameter. In terms of length, the UMP-3C3-210-25-4 has a rotor and stator lamination stack length of around 90 mm. This is shorter than the FAB112M-4, which features a stator and rotor lamination stack length of around 150 mm. The stack lengths differ by 60 mm, yet the UMP-3C3-210-25-4 is only 13.5 mm shorter than the FAB112M-4 on the outside accounting for the change in shaft length. This is simply due to the machine being less densely packed as illustrated in Figures 7.10 and 7.11, which shows a rough sketch of the housings using MotorCAD.

Thus, it is evident that designing a more densely packed machine could reduce the current length of the UMP-3C3-210-25-4 by up to 46.5 mm. This reduction can be achieved if the full potential of the lamination stack length decrease is utilised and the shaft length change is maintained.

The absolute limit on how densely the machine can be packed is determined by the UL 1004-1 (2020)
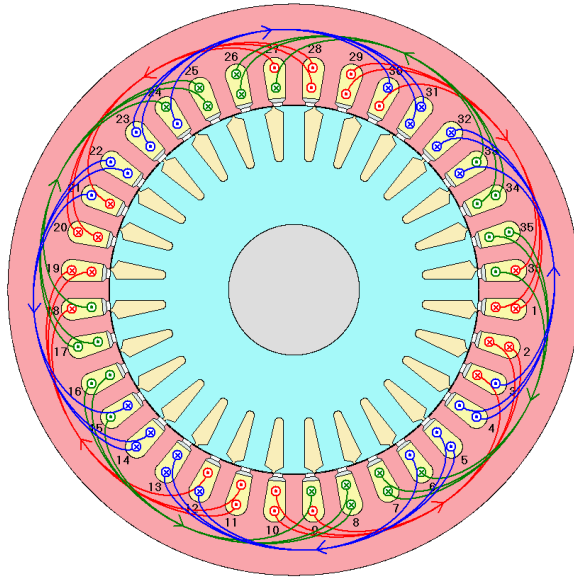
Figure 7.9: Winding configuration of the UMP-3C3-210-25-4
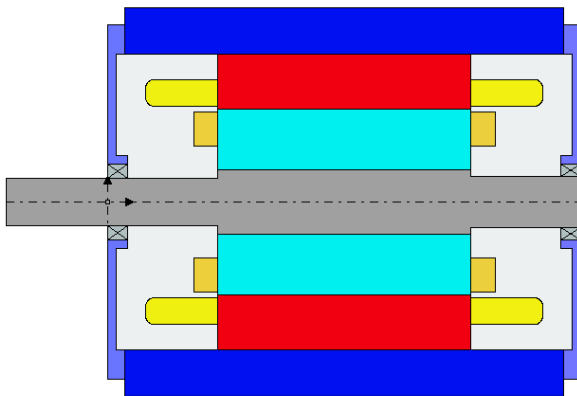
Figure 7.10: FAB112M-4 housing in MotorCAD
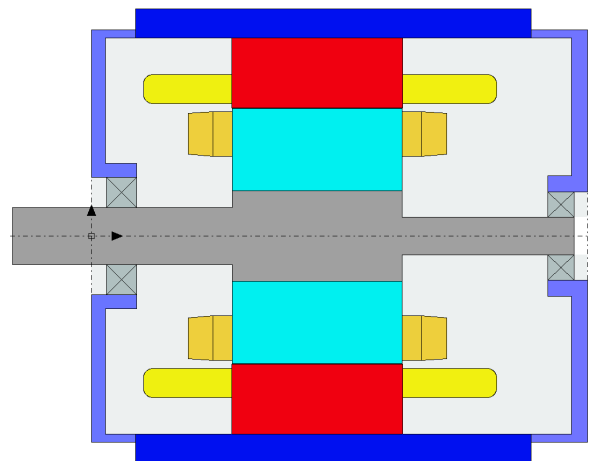
Figure 7.11: UMP-3C3-210-25-4 housing in MotorCAD

standard, which dictates that the minimum distance between stator windings and housing/end bells must be more than 2.4 mm.

Multiple reasons may underlie the current housing length choice of the UMP-3C3-210-25-4. Thermal limitations or assembly constraints are plausible explanations. However, it is likely due to stock keeping, as the same housing is used in seven different machine versions with various pole numbers and mechanical power output. Using the same housing across multiple machine models simplifies stock-keeping significantly, thus reducing costs.

Given the machine is manufactured by an external supplier in China and information regarding stock keeping is unavailable, stock-keeping considerations are disregarded in this project. However, investigating whether the current housing profile can accommodate the reduction in surface area without encountering thermal issues, or necessitates the design of a new housing profile, remains important.

7.5 MotorCAD Electromagnetic Model of the UMP-3C3-210-25-4

The development of a good electromagnetic model is essential, to allow for the evaluation of how different modifications impact the performance of the machine. This is due to the loss determination and distribution determined through electromagnetic modelling, being used in the thermal model to evaluate the cooling performance.

Parameter estimation and efficiency tests have also been performed for the UMP-3C3-210-4 in the same way as described for the FAB112M-4 and Y3PE112M4 in Chapter 6. Test data from the DC, no load, locked rotor and load test on the UMP-3C3-210-25-4 is found in Appendices K.1 to K.4 respectively.

7.5.1 Calibration of Electromagnetic Model

As mentioned in Section 7.3, MotorCAD models often need calibration, to model, e.g., the iron losses of an induction machine accurately.

Table 7.6 shows the MotorCAD equivalent circuit parameters of the UMP-3C3-210-25-4 before calibration.

Table 7.6: Comparison of equivalent circuit parameters for the UMP-3C3-210-25-4 MotorCAD model before calibration and the measured parameters at 25 °C.

Parameter	Units	Measured	MotorCAD	ε
X_1	[Ω]	7.95	2.57	67.7%
X_2'	[Ω]	7.95	13.5	69.6%
$X_1 + X_2'$	[Ω]	15.9	16.1	0.9%
X_M	[Ω]	184	201	9.0%
R_1 at 25 °C	[Ω]	3.38	3.48	3.0%
R_2' at 25 °C	[Ω]	2.27	2.31	1.8%
R_{fe}	[Ω]	3210	4452	38.7%

As it can be seen from Table 7.6, the iron loss resistance R_{fe} and mutual reactance X_m are parameters that should be calibrated. Furthermore, R_1 is also be calibrated as it is a directly measurable value through, e.g., a multimeter. Whereas the errors in R_2' and the leakage reactances $X_1 + X_2'$ are considered negligible.

MotorCAD features a calibration tool using no load testing data, to calibrate mutual inductance and iron loss. This method creates a lookup table of calibration factors for both R_{fe} and X_m. However, the

validity of using these calibration factors when applying changes to the machine geometry is uncertain and manual calibration is used instead.

The first calibration applied, is calibration of the magnetising reactance ($X_1 + X_m$). The MotorCAD model is set to produce the same output power as measured during no-load testing and a saturation multiplier on X_m is then used to adjust the parameter until the calculated value of $X_1 + X_m$ approximately match the measured value.

The iron loss resistance R_{fe} is also adjusted based on available data using stator and rotor iron loss build factors. These build factors are multipliers used to adjust the R_{fe} parameter directly.

The resistivity of the copper windings is also adjusted slightly, to match the measured value of R_1 better.

As a last change in MotorCAD, the additional load loss calculation method is changed. As a default MotorCAD uses the additional load loss formula presented in (6.29) on page 43, which was shown to overestimate the additional load losses. The calculation method is therefore changed, so MotorCAD calculates the additional load losses as a percentage of the output power, which in this case is set to 1.73%. The additional load losses in MotorCAD then result in the additional load losses calculated using the method from Section 6.4.3.

An overview of the MotorCAD options which have been changed, can be seen in Table 7.7.

Table 7.7: Comparison between default values and calibrated parameter values used in the calibrated UMP-3C3-210-25-4 MotorCAD model.

MotorCAD option	Default value	New value	Percentage change
Stator saturation multiplier	1	1.027	2.7%
Rotor saturation multiplier	1	1.027	2.7%
Stator iron loss build factor	1	1.387	38.7%
Rotor iron loss build factor	1	1.387	38.7%
Copper resistivity	$1.724 \cdot 10^{-8}\,\Omega\text{m}$	$1.673 \cdot 10^{-8}\,\Omega\text{m}$	3.0%
Additional load loss calculation	Same as (6.29)	1.73% of output power	-

7.5.2 Mechanical Losses

In the evaluation of machine losses, it is important to account for mechanical losses, specifically windage and friction. In the context of the UMP-3C3-210-25-4 machine, the windage losses are mainly attributed to the end-ring fins. These windage losses are deemed negligible in comparison to the more substantial frictional losses arising from the bearings.

Both the driving end and non-driving end bearings are from the manufacturer SKF, which offers a calculation tool on its website. This tool has been utilised to generate the loss curves observed in Figures 7.12 and 7.13, taking into account the weight of the rotor.

As it can be seen from Figures 7.12 and 7.13, the bearing loss of the driving end, is significantly higher than the rear bearing. This is due to the driving end bearing featuring a rubber seal to increase the ingress protection of the bearing. However, it could be investigated if it is strictly necessary or whether it can be exchanged for a bearing with fewer losses.

The windage and friction losses measured from the no-load tests amount to 52.2 W, whereas SKF specifies a loss of approximately 17 W. The variance in losses may stem from several factors, including bearings not being fully run-in, radial pressure, manufacturing tolerances, or friction from the shaft seal.

To achieve the best modelling in MotorCAD, using real-world data makes the most sense. One way to input the correct data into MotorCAD is to supply MotorCAD with a summation of the loss curves
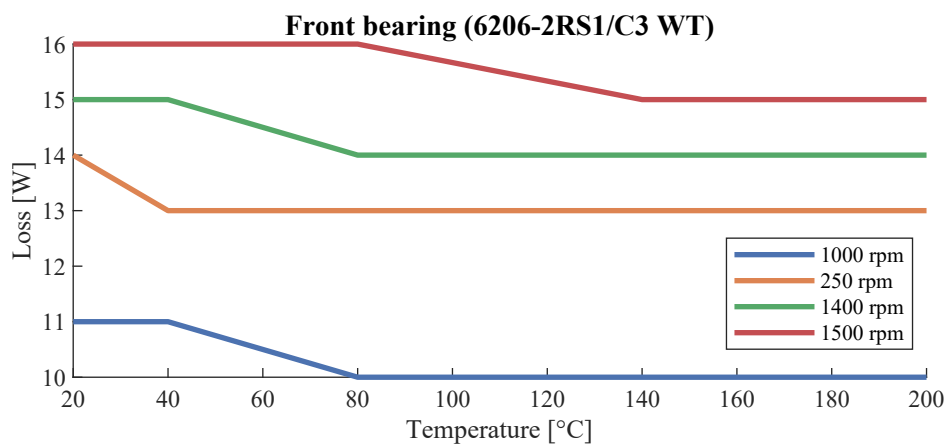
Figure 7.12: Bearing loss curve for the UMP-3C3-210-25-4 front bearing
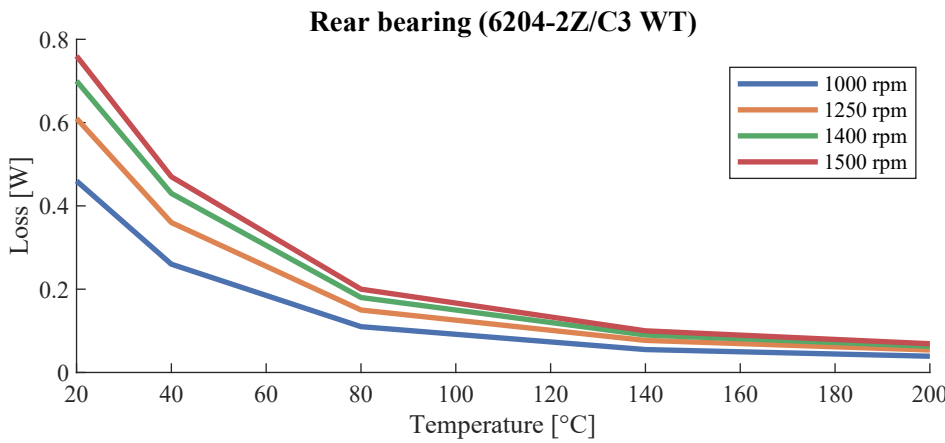
Figure 7.13: Bearing loss curve for the UMP-3C3-210-25-4 rear bearing

shown in Figures 7.12 and 7.13. The curves can then be adjusted using a multiplication factor to achieve the appropriate losses on the bearings. However, MotorCAD is not allowing an uneven distribution of the friction losses when using this method. This becomes a problem later when calculating the thermal model, as the loss distribution should be accurate. Instead, MotorCAD can be set to use a constant loss model, where the user can distribute the friction losses between the bearings.

The exact distribution is indeterminable from the available data. But assuming the front bearing has more loss than the rear bearing, based on SKF data, a distribution of 70/30 is chosen.

7.5.3 Validation

Having calibrated the UMP-3C3-210-4 MotorCAD model, validation of the calibrated MotorCAD results is carried out.

Calibrated Equivalent Circuit Parameter Comparison

Firstly a comparison between the equivalent circuit parameters is made, as an improvement from the non-calibrated parameters in Table 7.6 is expected. The equivalent circuit parameter comparison between measured parameters and the calibrated MotorCAD model for the UMP-3C34-210-4 is seen in Table 7.8.

Table 7.8: Comparison of equivalent circuit parameters for the calibrated UMP-3C3-210-25-4 MotorCAD model and measurements.

Parameter	Units	Measured	MotorCAD	ε
X_1	[Ω]	7.95	2.57	67.7%
X_2'	[Ω]	7.95	13.3	67.3%
$X_1 + X_2'$	[Ω]	15.9	15.9	0.19%
X_M	[Ω]	184	191	3.80%
R_1 at 25 °C	[Ω]	3.38	3.38	0.06%
R_2' at 25 °C	[Ω]	2.27	2.31	2.07%
R_{fe}	[Ω]	3210	3210	0.00%

As expected the calibrated model shows an improvement, as calibrated parameters are within 4% of measured parameters. Only X_1 and X_2' compared individually are noticeably different from the measured values, but as explained in Section 7.3 this is expected. X_1 and X_2' are only shown to imply what ratio MotorCAD expects the machine to have.

With equivalent circuit parameters close to measurements, ratings are expected to be within tolerance. Hence comparison against datasheet values and tolerances is also performed.

Calibrated Rating Comparison

The comparison between the datasheet ratings and the calibrated UMP-3C3-210-25-4 MotorCAD model can be seen in Table 7.9. A couple of deviations are noticeable when comparing these parameters. The mechanical torque specified in the datasheet is outside datasheet tolerances, with tolerances calculated as specified in IEC 60034-1 (2010). This may indicate an error in the specified mechanical torque.

Furthermore, the power factor calculated from the calibrated MotorCAD model is higher than indicated by the datasheet. This might be due to the ratio between X_1 and X_2', as shifting the ratio of these in the MotorCAD model changes the calculated power factor. However, there is no basis for changing this ratio, as the ratio has not been measured, hence no data exists for comparison and calibration.

Furthermore, the efficiency of the calibrated model at higher temperatures is outside tolerances. This is not of concern as the UMP-3C3-210-25-4 thermal equilibrium point could be at a lower temperature. Hence the model seems to fit the datasheet ratings decently, but the error in the datasheet compromises its integrity a bit. Thus comparison between the calibrated UMP-3C3-210-25-4 MotorCAD model and load test measurements is also done.

Table 7.9: Comparison between the calibrated UMP-3C3-210-25-4 MotorCAD model and datasheet ratings

Parameter	Unit	Datasheet	Calibrated MotorCAD			Tolerance
T_W	[°C]	N/A	38.7	56.3	78.1	N/A
I_{LL}	[A]	7.86	7.87	7.88	7.91	5.77 - 8.29
s	[-]	2.53%	2.41%	2.58%	2.79%	2.03% - 3.04%
τ_{mech}	[Nm]	25.5	26.1	26.1	26.2	26.0 - 26.3
n	[RPM]	1462	1464	1461	1458	1454 - 1470
PF	[-]	0.83	0.84	0.84	0.85	0.80 - 1.00
P_{mech}	[kW]	4.00	4.00	4.00	4.00	-
η	[-]	88.6%	87.3%	86.9%	86.4%	86.9% - 100%
P_T	[W]	515	580	602	629	0 - 604

Calibrated Load Test Comparison

The MotorCAD e-magnetic model is validated against actual load data by matching temperature and power output with the values from the load testing data. The load testing data is obtained through measurements when loading the machine to around the rated mechanical power output. Except for the efficiency which is calculated following Section 6.4.3, as recommended by IEC 60034-2-1:2014 (2014). Section 6.4.3 also describes the load testing more in-depth. The comparison between load test data and the calibrated UMP-3C3-210-25-4 MotorCAD model can be seen in Table 7.10.

Table 7.10: Comparison between the calibrated UMP-3C3-210-25-4 MotorCAD model and measurement results from load testing.

Parameter	Unit	MotorCAD			Load measurements			Tolerance
T_W	[°C]	38.7	56.3	78.1	38.7	56.3	78.1	N/A
I_{LL}	[A]	7.93	7.91	7.92	8.12	8.06	8.04	5.77 - 8.29
s	[-]	2.44%	2.59%	2.80%	2.60%	2.87%	3.20%	2.03% - 3.04%
τ_{mech}	[Nm]	26.4	26.2	26.3	26.4	26.3	26.3	26.0 - 26.3
n	[RPM]	1463	1461	1458	1461	1457	1452	1454 - 1470
PF	[-]	0.84	0.84	0.85	0.83	0.83	0.84	0.80 - 1.00
P_{mech}	[kW]	4.04	4.02	4.01	4.04	4.02	4.01	-
η	[-]	87.3%	86.9%	86.3%	87.4%	86.2%	86.2%	86.9% - 100%
P_T	[W]	587	605	630	590	640	644	0 - 604

As it can be seen in Table 7.10, the performance characteristics of the MotorCAD model, show a higher power factor than the load test measurements. This also means that the current is lower in the MotorCAD model compared to the load test measurements. However, the small deviation in power factor and current is deemed acceptable.

The differences in machine efficiency between measurements and MotorCAD are also less than 35 W when comparing at 56.3 °C. Furthermore, the efficiency observed from measurements at 56.3°C and 78.1°C are equal. This is unexpected as the efficiency should increase along with the temperature increase. This may indicate a small error during measurement.

The method used to calculate efficiency and total power loss also calculates the loss distribution. This makes it possible to directly compare the calibrated UMP-3C3-210-25-4 MotorCAD model loss distribution with measurements. This comparison can be seen in Table 7.11.

Table 7.11: Comparison between loss distribution in the calibrated UMP-3C3-210-25-4 MotorCAD model, and measured loss distribution according to the summation of losses method from Section 6.4.3.

Loss symbol	Unit	MotorCAD			Load measurement		
T_W	[°C]	38.7	56.3	78.1	38.7	56.3	78.1
P_s	[W]	223	236	254	237	248	265
P_r	[W]	104	110	119	113	123	137
P_{WF}	[W]	52.2	52.2	52.2	48.8	48.5	48.1
P_{LL}	[W]	72.0	71.6	71.4	60.1	87.4	60.4
P_{fe}	[W]	135	135	134	132	134	134
P_T	[W]	587	605	630	590	640	644

As expected the losses are close to measurements, however, the additional load losses at 56.3°C are higher than measurements at other temperatures. Three data points are insufficient to conclude anything definitively, and measurements follow IEC 60034-2-1:2014 (2014), by being performed as described in Section 6.4.3.

Hence deviations concerning measurements are deemed acceptable as they can be explained and are rather small. The MotorCAD e-magnetic model then represents the real world to a satisfactory degree, the e-magnetic model is combined with a thermal model to evaluate potential design changes.

7.6 MotorCAD Thermal Modelling of the UMP-3C3-210-25-4

As previously mentioned in Section 7.4, it is essential to assess whether reducing the housing length leads to thermal issues, necessitating the development of a thermal model. MotorCAD offers its own thermal modelling capabilities, which can be combined with e-magnetic modelling to generate a converged solution. MotorCAD uses an equivalent thermal circuit using thermal conductance and resistance.

7.6.1 Geometry of Thermal Model

MotorCAD uses simplified geometry when performing thermal modelling. This means that the exact machine geometry can not be used. Figure 7.14 shows the MotorCAD housing geometry, whereas the actual machine housing geometry is shown in Figure 7.15 from CAD-modelling.

The most important feature is not the geometry itself, but the resulting surface areas of the machine parts. Table 7.12, compares the MotorCAD and CAD models' surface areas.

Table 7.12: Comparison between surface areas of CAD model and MotorCAD thermal model

	Unit	Surface area			
		Housing	Front end bell	Rear end bell	Total
CAD model	[cm^2]	3908	1030	1136	6074
MotorCAD	[cm^2]	3827	969	1061	5857
Relative error	[-]	-2.1%	-5.9%	-6.6%	-3.6%

Comparing the models, the MotorCAD model is seen to have a surface area smaller than the CAD model on all surfaces. The end bells show the highest errors in surface area, this is due to the absence of
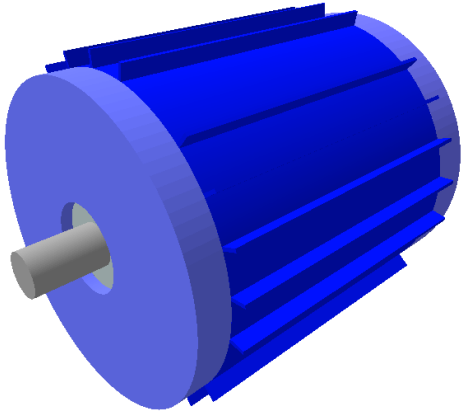
Figure 7.14: MotorCAD housing
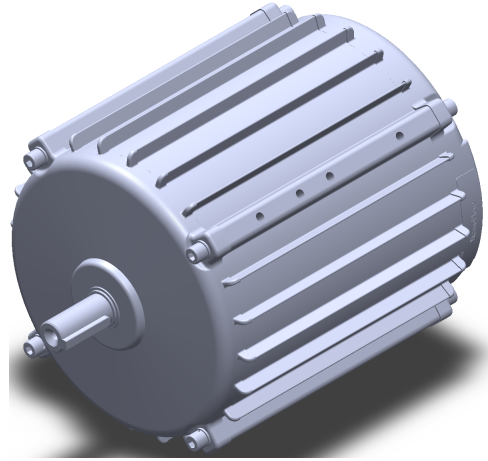
Figure 7.15: CAD model of real housing

surface complexity and sloped sides. However, most of the surface area is found on the centre housing, which has an error of -2.1% while the total surface area has an error of -3.6%.

Because the MotorCAD model is geometrically different, the mass and surface areas of components are erroneous. To adjust the mass of components, MotorCAD features a mass multiplier. Thus the stator, rotor, housing and end bells have been weighed to allow for accurate adjustments of the masses in MotorCAD.

To compensate for the lack of surface area ($A_{surface}$), a multiplication factor (H_{factor}) on the heat transfer coefficients (H) is used, as it provides the same result as a multiplication of the surface area. This is because the heat transfer coefficient and surface area are used to calculate the thermal resistance as seen in (7.2).

$$R_{thermal} = \frac{1}{H_{factor} \cdot H \cdot A_{surface}} \tag{7.2}$$

The multiplication factor (H_{factor}), is calculated using (7.3), where $A_{surface,real}$ is the real surface area and $A_{surface,MCAD}$ is the surface area in the MotorCAD model.

$$H_{factor} = \frac{A_{surface,real}}{A_{surface,MCAD}} \tag{7.3}$$

7.6.2 Cooling Options

MotorCAD features a range of different options and settings that can be used to simulate various cooling situations. The main cooling mechanisms represented in MotorCAD are; Radiation, natural convection, and forced convection both on the surface and end spaces.

MotorCAD uses the surface areas of different parts of the machine, together with emissivity values to calculate the heat transfer coefficients.

In this case, only the external radiation is considered, which is painted with a black (RAL9005) paint. The emissivity in MotorCAD based on the colour is set to around 0.92. (Jandrlic and Reskovic; 2015)

Natural convection in MotorCAD uses different default heat transfer coefficients, based on the surface. These heat transfer coefficients are adjusted as explained earlier using (7.3). Whereas the forced convection options are more complex, thus requiring more adjustments.

Given that the end space, defined as the area surrounding the stator end windings and the rotor rings, is enclosed, only the rotor ring fins induce forced convection within this space. However, forced convection on the machine surface is driven by an air stream from the attached fan. MotorCAD calculates the impact of this air stream by considering the airspeed and a profile determining how the airspeed decreases along the machine's axial distance from the fan.

To achieve the right airspeed, an airspeed measurement probe is employed while the machine is installed in a fan pack. The resulting airspeed drop profile is illustrated in Figure 7.16, with an initial airspeed of approximately 14.5 m/s. A full test procedure can be found in Appendix L, while the test data is found in Table K.8.
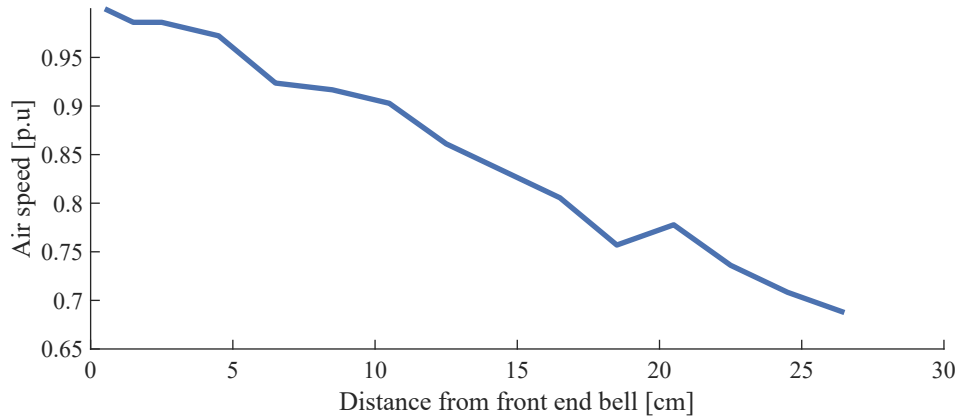
Figure 7.16: Measured air speed drop across the UMP-3C3-210-4 running with a fan

7.6.3 Validation

To ensure the accuracy of the thermal model, validation is conducted through comparison with a DC load test and a fan load test where the machine is running with a fan.

DC Load Test

This test is performed by running a DC-current through the three phases of the machine while observing the temperature rise over time. The test data is found in Appendix K.5, while the full test documentation is found in Appendix M.

The idea is to introduce copper losses in the windings that heat the machine. The advantage is the size and location of the losses are known, which then is replicated when the MotorCAD thermal model is made. Furthermore, no cooling is applied, hence the DC load test can be used to identify problems with the model when no forced convection is applied.

To achieve an even distribution of losses across all three phases, the DC-current has to be distributed equally. However, the UMP-3C3-210-25-4 is wound as a delta configuration without access to the individual phase terminals. Hence, achieving an even distribution of losses with a single wiring configuration is not possible. Instead, the electric wiring is continuously cycled between three different wiring configurations as shown in Figure 7.17.

Assuming that $R_a \approx R_b \approx R_c \approx R_1$, the average power loss for a single phase is then calculated as shown in (7.4).

$$P_{Cu} = \frac{V_s^2}{2R_1} = \frac{2I_s^2}{9R_1} \tag{7.4}$$
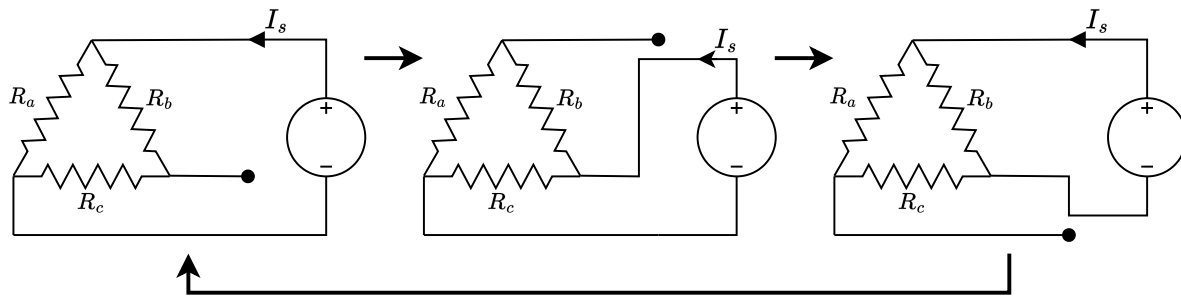
Figure 7.17: Cycles of wiring configurations during DC-current thermal test

Since the phase resistance changes with temperature, the heat dissipated through the windings also changes. During testing the voltage is changed so the current remains approximately constant, with the resulting estimated power losses shown in Figure 7.18.
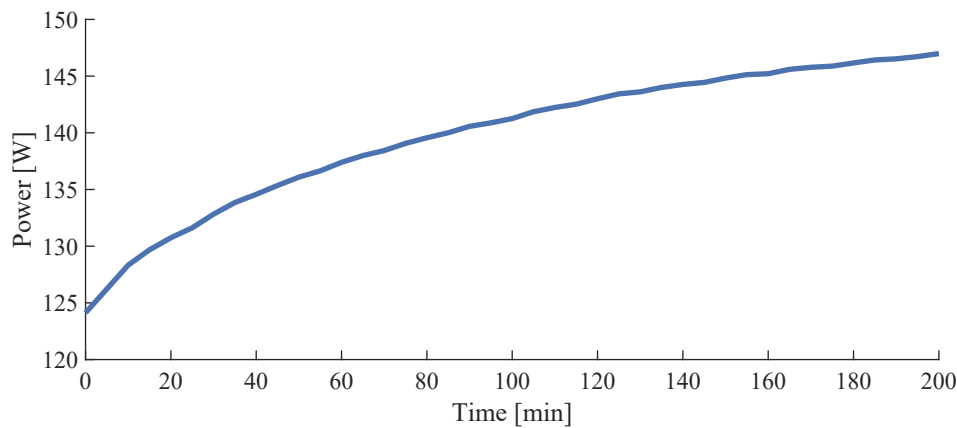
Figure 7.18: Estimated power loss as a function of time during DC thermal testing

MotorCAD only takes a single value of power loss as input, so the average power loss of 140.1 W is used instead.

The temperatures recorded during the DC test are the windings, bearings, rear bell and central housing temperatures.

The results of the thermal model transient analysis from MotorCAD are shown together with the experimental data in Figures 7.19 to 7.21.
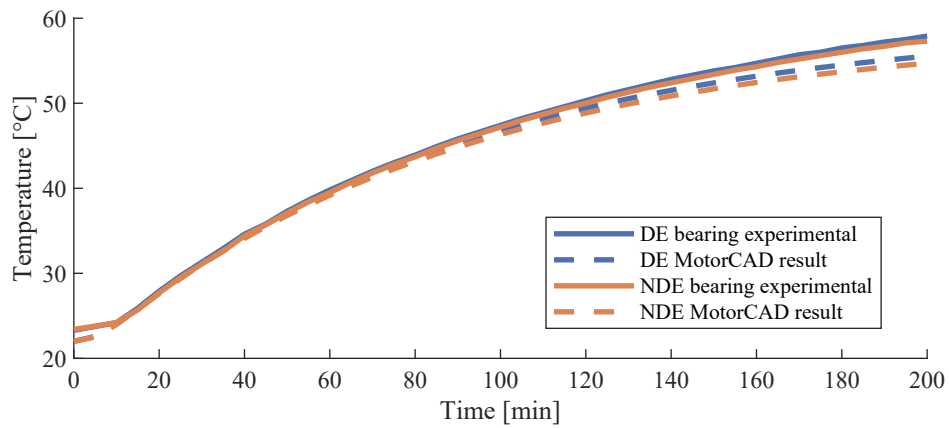
Figure 7.19: Comparison of bearing temperatures from DC thermal test
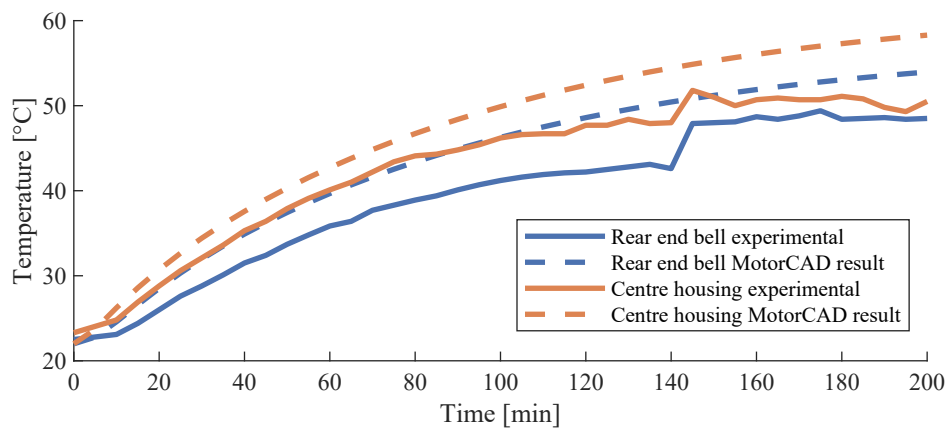
Figure 7.20: Comparison of housing temperatures from DC thermal test
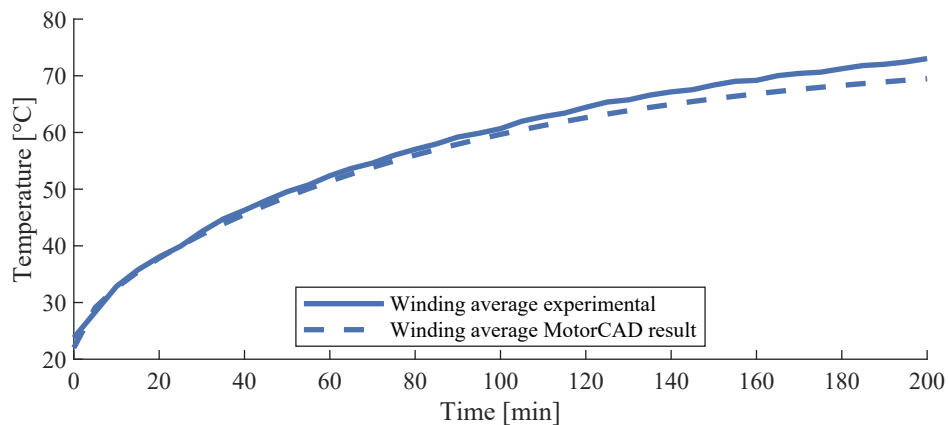
Figure 7.21: Comparison of winding temperatures from DC thermal test

As seen from the figures, the MotorCAD thermal model predicts the temperatures well, except for the housing temperatures which are showing temperatures that are too high. However, it should be noted that during the DC thermal test, the externally mounted thermocouples used to measure the housing temperature started to loosen from the housing. This is indicated by the jump in temperatures at the 140-minute mark in Figure 7.21, where readjustments to the thermocouples are made to fasten them.

Fan Load Test

To simulate a practical operational scenario of the machine, it is installed in a fan pack assembly, as depicted in Figure 7.22.
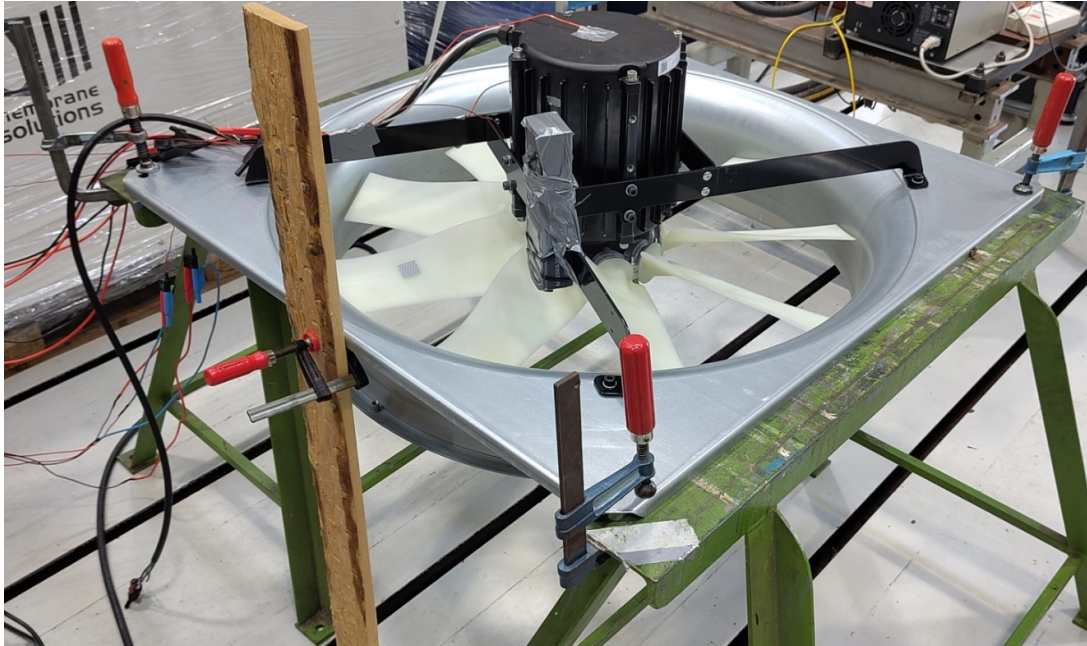
Figure 7.22: Picture of fan load thermal test setup

The experiment's objective is to determine the machine's thermal equilibrium point when cooling is applied through air movement. The machine is operated at a supply voltage of 380 V, a deviation from the nominal 400 V due to equipment constraints. Upon initiation, the machine is accelerated to its operational speed, and temperature readings of bearings, housing, rear end bell, and windings are recorded at 10-minute intervals until thermal equilibrium is reached. A comprehensive overview of this test methodology is found in Appendix N, and the test data is reported in Appendix K.7.

The rotational speed of the fan is determined using a tachometer, registering at approximately 1469 rpm, thereby establishing the operational load point for use in MotorCAD, when comparing the thermal model results to measurements.

MotorCAD is unable to couple the e-magnetic model with the thermal model when performing transient thermal analysis, so in the case of the fan load test, only the steady state results are available.

Table 7.13 shows the temperatures after thermal equilibrium is reached together with the MotorCAD thermal model steady state results.

Table 7.13: Comparison between thermal equilibrium temperatures and MotorCAD thermal model steady state temperatures

	Unit	Temperature				
		Housing	**Rear bell**	**DE bearing**	**NDE bearing**	**Winding**
Measured	[°C]	32.3	34.6	38.2	38.4	52.2
MotorCAD	[°C]	37.4	37.3	44.5	43.7	51.9
Error	[-]	15.9%	7.9%	16.5%	13.8%	0.4%

As seen in Table 7.13, the temperatures calculated using the MotorCAD thermal model are relatively close to those measured. However, the housing temperature and bearing temperatures show errors above

10%.

The cause of this issue could partly be discrepancies between the location of measurement in MotorCAD and during the tests. Figure 7.23 shows the locations of measurements in MotorCAD, and Figure 7.24 shows how the thermocouples are placed on the machine during DC load and fan load tests. The exact measurement points of the winding and bearing temperatures are unknown, as the temperature sensors came preinstalled.
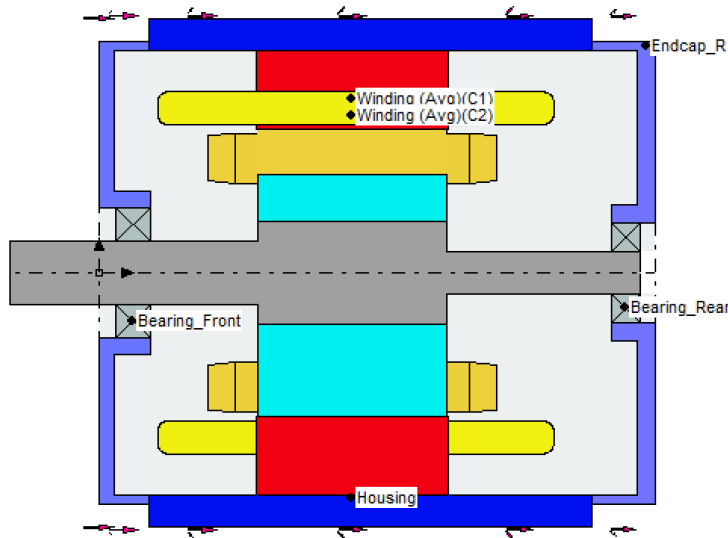
Figure 7.23: MotorCAD thermal measurement points
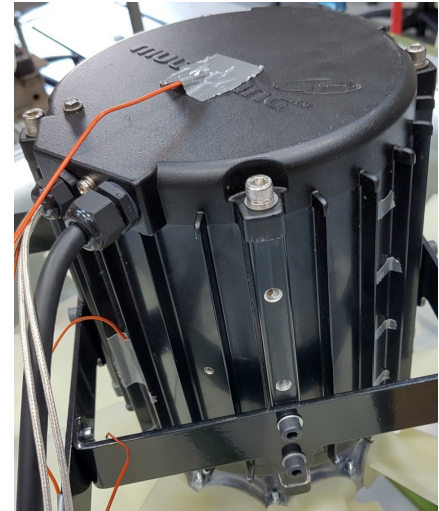
Figure 7.24: Picture of physical thermal measurement points

Another cause could be that the surface temperature of the housing differs from the internal housing temperature. Or that the windage losses are modelled as friction, and thus appear as a loss in the bearings.

It should also be noted that, while the error percentage are high, the difference in temperature is only around 5 °C. The starting temperature when performing the fan load test showed a difference of 1.6 °C between the highest and lowest reading. Thus the temperature measurement equipment might also play a role.

Despite the thermal model from MotorCAD being unable to predict the temperatures with high precision. The thermal model can provide an answer in the right temperature range, albeit on the conservative side. Thus the thermal model should predict if thermal issues arise as a consequence of shortening the machine.

With a satisfactory e-magnetic and thermal model setup for the UMP-3C3-210-25-4, design improvements can be considered and examined.

Chapter 8

Modification Proposals

If the current UMP-3C3-210-25-4 design should be changed, it is important to only make changes that are worth the extra cost in terms of production and development. To do so, only materials and products already available at Multi-Wings supplier are considered to keep production costs low.

To evaluate the feasibility of a design, it is compared against the validated MotorCAD model representing the existing UMP-3C3-210-25-4 design. This model demonstrates an efficiency of 87.65% at a temperature of 25°C. This efficiency serves as a lower limit against which the effectiveness of any design alterations must adhere to.

8.1 Electromagnetic Modification Proposals

In Section 7.4, it was mentioned that the laminate stack length of the UMP-3C3-210-25-4 is 60 mm shorter than that of the FAB112M-4. However, it is unknown whether this stack length is the shortest achievable or if modifications can be made to shorten it even more. Reducing the laminate stack length often reduces the internal machine components' length, creating more space inside the housing and allowing for a shorter housing design.

It is assumed that the UMP-3C3-210-25-4 is already designed with the minimum feasible laminate stack length and suffers a reduction in efficiency if the laminate stack lengths are shortened further. Therefore, the efficiency at the current length must be increased to compensate for the anticipated drop in efficiency due to the reduced laminate stack lengths.

Often to improve efficiency the electromagnetic aspect of the machine is considered. To change the electromagnetic aspect in a cost-effective way strategies such as material selection, winding changes, and an increase in laminate OD are chosen. Changing these things could potentially improve the electromagnetic aspect of the machine, leading to stack length reduction.

8.1.1 Material Choice

One aspect that can easily be altered in the machine design is the choice of laminate material. The current design employs SURA M600-50A as the laminate material, with an iron loss of 6 W/kg at 1.5 T (60 Hz) and a thickness of 0.5 mm. This material can be changed, as the supplier has multiple rotor and stator laminate materials, which can use already available stamping tools. Available laminate materials from the supplier, with data available for MotorCAD simulation, can be seen in Table 8.1.

As previously explained, a build factor and saturation factor have been applied to correct the material parameters in MotorCAD. Despite changing the material used, these factors remain applied. The factors remain applied, as they are based on material parameter changes due to the manufacturing process used. It is assumed that the manufacturing process for the laminates remains unchanged, as it should be independent of the material change.

To determine whether a reduction in stack length is possible, by changing the laminate material of the stator and rotor, MotorCAD is used. In MotorCAD a sweep of rotor laminate stack length is made, by starting with a length of 96 mm and then reducing it by 1 mm down to a stack length of 86 mm. The

Table 8.1: Different available laminate materials

Laminate material	Loss per mass [W/kg] at 1.5 T (60 Hz)	Thickness [mm]
SURA M310-50A	3.10	0.50
SURA M350-50A	3.50	0.50
SURA M470-50A	4.70	0.50
SURA M600-50A	6.00	0.50
SURA M800-50A	8.00	0.50

sweep is made for the available materials presented in Table 8.1. For the convenience of automation, this procedure is done through the MotorCAD Python scripting option, the Python script used is found in Appendix O.1. The script is then applied to the validated UMP-3C3-210-25-4 MotorCAD model from Chapter 7. Efficiency results, from changing the material in the validated model and running a length sweep, are presented in Figure 8.1.
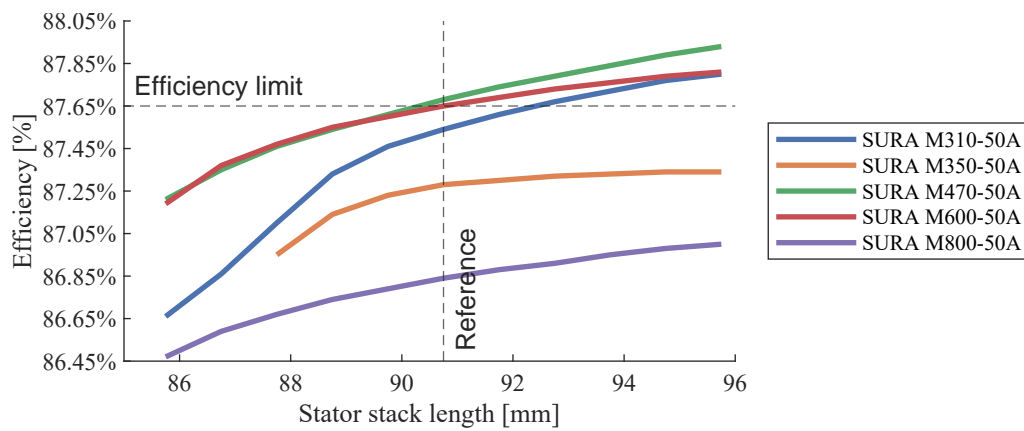
Figure 8.1: Efficiency sweep of different stator lengths, for different laminate qualities

As indicated in Figure 8.1, only M470-50A, aside from the original M600-50A, is a viable option, as it has a reduced length compared to the original, while being above the lower efficiency limit. However, the feasibility of using the M470-50A instead is questionable, as the reduction achieved is less than one millimetre. A reduction this small is not necessarily achievable in reality, as uncertainties are introduced when using models. In addition, the M470-50A material is expected to be more expensive than the M600-50A, due to the reduction in loss per mass. Hence if the material is changed, the machine becomes more expensive, while obtaining a negligible length reduction.

Furthermore, it is worth noting that the materials from Table 8.1 with a lower loss per mass index have efficiency performance below the limit. This is due to the materials' different B-H curves, as illustrated in Figure 8.2, which shows B-H curves of the different laminate qualities.

In general, laminate materials saturate more easily as iron losses decrease. Therefore, if the machine is already highly saturated at the load point, changing the material to one with lower iron losses may negatively impact the ability to generate a strong magnetic field. The flux densities of the UMP-3C3-210-25-4 as reported by MotorCAD, is shown in Table 8.2 and Figure 8.3 shows the MotorCAD FEM analysis flux density plot.

The calculated flux densities show that the machine is already well saturated in some areas, and therefore if the material's B-H curve is changed so it saturates more easily, the performance is negatively impacted.

In conclusion, the UMP-3C3-210-25-4 does not benefit from changing the material, due to the high

magnetic saturation for which it is designed.
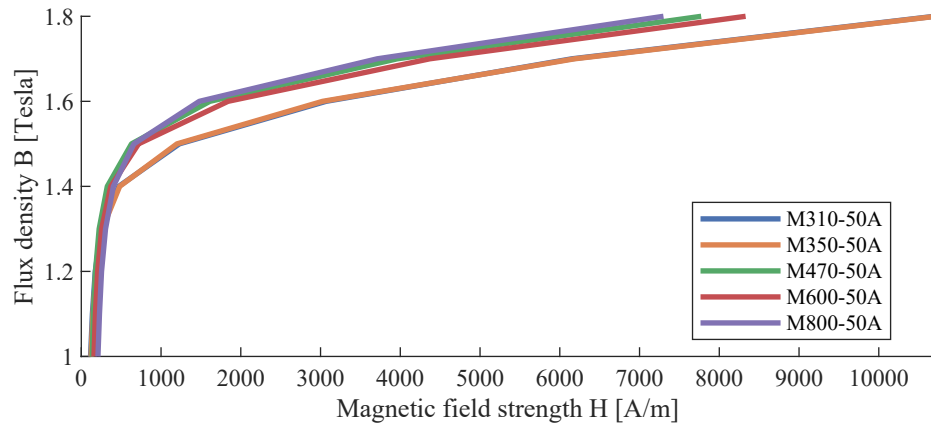
Figure 8.2: Comparison between laminate material B-H curves above 1 Tesla

Table 8.2: Flux density values reported by MotorCAD for the UMP-3C3-210-25-4 model at 25 °C

Location	Calculated flux density [Tesla]
Airgap (mean)	0.6035
Airgap (peak)	0,8535
Stator tooth (peak)	1.714
Stator back iron (peak)	1.547
Rotor tooth (peak)	1.604
Rotor back iron (peak)	1.326
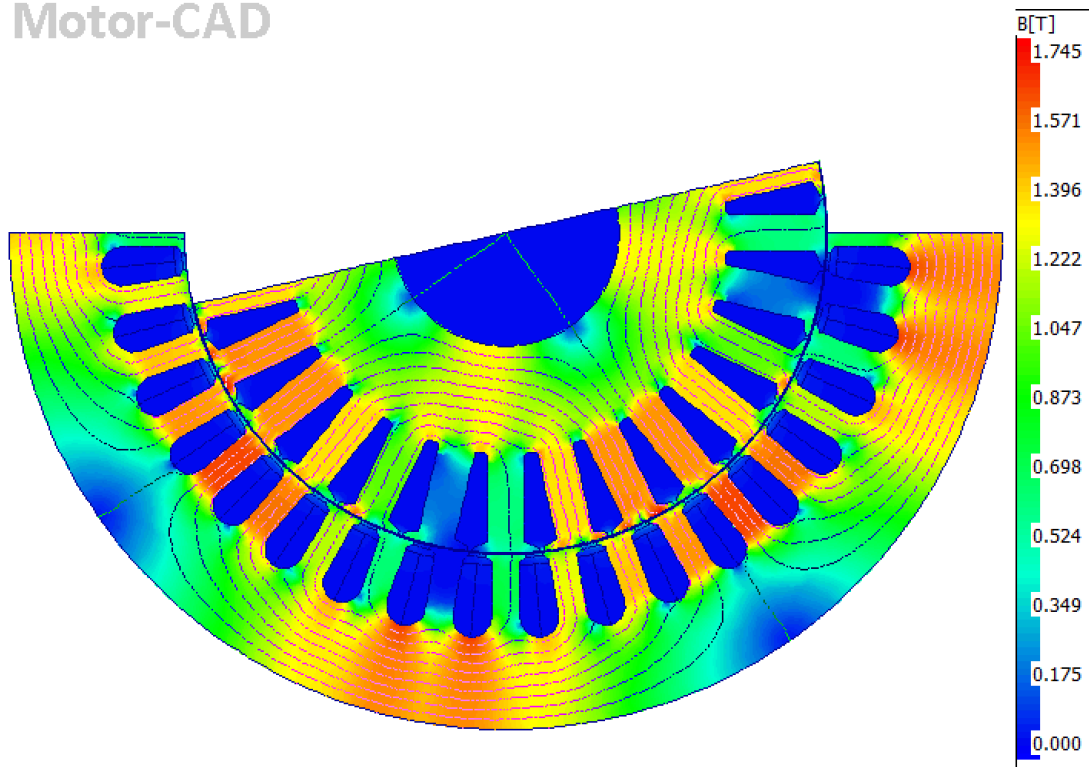
Figure 8.3: FEM analysis results from MotorCAD, showing the flux density in the UMP-3C3-210-25-4 at 4kW load

8.1.2 Winding Choice

Choosing the right winding configuration is crucial for optimising the performance of the machine. A shorter stack requires a stronger magnetic field, which can be achieved by either increasing the current in the windings or adding more turns.

By changing the amount of turns, the turns ratio between the stator and rotor changes. Therefore the value of X_2' and R_2', are changed if the amount of turns in the stator is changed.

Increasing the current also raises the copper losses. To mitigate these losses, the cross-sectional area of the copper wire can be increased to reduce resistance. However, increasing the wire diameter increases the slot fill, which is the fraction of the stator slot area occupied by wires and insulation materials. This makes winding the stator more challenging from a production standpoint.

Understanding the distinction between copper fill (ff_{cu}) and slot fill (ff_{slot}) is also important. Copper fill refers to the ratio between the stator slot area (A_{slot}) and the copper total copper area (A_{cu}) seen in (8.1).

$$ff_{cu} = \frac{A_{cu}}{A_{slot}} \tag{8.1}$$

Whereas slot fill (ff_{slot}) refers to the fraction of the stator slot area occupied by the total area of the wires (A_{wire}), insulation ($A_{insulation}$), and wedge (A_{wedge}), as seen in (8.2).

$$ff_{slot} = \frac{A_{wire} + A_{insulation} + A_{wedge}}{A_{slot}} \tag{8.2}$$

To increase the copper fill without increasing the slot fill, a better wire grade can be used. IEC 60317-0-1 (2013) specifies three different wire grades, with varying insulation thicknesses. The three different wire grades are shown for a few selected wire diameters in Table 8.3.

Table 8.3: Selected enamelled wire dimensions according to IEC 60317-0-1 (2013)

Conductor diameter [mm]	Maximum wire diameter [mm]		
	Grade 1	Grade 2	Grade 3
0.475	0.519	0.541	0.562
0.530	0.576	0.600	0.623
0.560	0.606	0.630	0.653
0.600	0.649	0.674	0.698
0.670	0.722	0.749	0.774
0.710	0.762	0.789	0.814
0.800	0.855	0.884	0.911
0.850	0.909	0.939	0.968
0.900	0.959	0.989	1.018
0.950	1.012	1.044	1.074
1.000	1.062	1.094	1.124
1.060	1.124	1.157	1.188
1.120	1.184	1.217	1.248

From Table 8.3 it is seen that the ratio between conductor diameter and total wire diameter grows larger as the wire diameter increases. Hence the maximum copper fill factor increases if the diameter of the wire increases. However, increasing wire diameter also increases wire stiffness making installation and handling during processing more difficult.

The maximum feasible slot fill depends on wire type and slot geometry, with values normally ranging from 60-70%. However, achieving slot fill factors of 70-80% are possible but challenging, often requiring specialised tooling and more time for winding.(Alderks; 2019)

Determining the actual fill factor of the UMP-3C3-210-25-4 is difficult to do in practice as the wire diameter varies depending on where it is measured. Furthermore, the end wires are covered in a thin layer of impregnation. The wire size in MotorCAD has therefore been chosen from a list of standard metric sizes within MotorCAD. The wire size used in MotorCAD has a conductor diameter of 0.750 mm and a total wire diameter of 0.832 mm. This is not one of the wire sizes presented in Table 8.3, but it is the closest option to the measured values.

Furthermore, MotorCAD is used to determine the slot area but does not model the liner and wedge geometry correctly as is indicated by the slot cross-section in Figure 8.4, where a comparison between the MotorCAD slot and actual slot is seen.

Figure 8.4: Difference between slot cross-section of UMP-3C3-210-25-4 in reality and in MotorCAD

As it can be seen in Figure 8.4, the slot is filled more in reality than MotorCAD might indicate. It also appears to be well-filled, thus the fill factor is assumed to be at the limit. With this in mind, MotorCAD reports a wire fill factor of 67.3%.

To determine feasible wire size options, the grade 1 wire options shown in Table 8.3 are used to generate a list of candidate combinations of wire diameter, turns, connection (Delta/Star), and strands in hand. Strands in hand refer to multiple wires wound together as a single unit to improve flexibility. The combinations, which can be found in Appendix P.1, aim to have approximately the same fill factor as the original design. Only grade 1 wire options are considered because they provide the highest copper fill factor.

The number of turns for each wire combination (N_{turns}) is determined by the wire diameter (D_{wire}), desired slot fill factor ($sf_{desired}$), slot area (A_{slot}), and number of strands available ($N_{strands}$), as defined in (8.3):

$$N_{turns} = \left\lfloor \frac{2 \cdot sf_{desired} \cdot \pi \cdot N_{strands}}{D_{wire}^2} \right\rfloor \tag{8.3}$$

Where $\lfloor \rfloor$ denotes that the result is floored. Meaning that the resulting wire size configuration never surpasses the desired fill factor.

To identify candidates, a Python script tests all combinations listed in Appendix P.1 without altering the laminate stack. It then reports the efficiency, enabling further examination of the most promising designs. The script can be found in Appendix O.2, while the resulting efficiencies is provided in

Appendix P.3. It should be noted, that the results where a 4 kw output was not possible, are also included in the results table marked by N/A.

Furthermore, MotorCAD lacks the capability to implement the custom wiring pattern utilised in the e-magnetic model when altering the number of turns through scripting. Consequently, MotorCAD is configured to employ a lapped winding pattern with a throw of 8 as it allows for interfacing with the Python script. However, this adjustment results in a reduction in the efficiency of the e-magnetic model at 25 °C to 87.45%, as opposed to the original 87.65%. Hence, it is essential to compare the results generated by the Python script in this context against an efficiency of 87.45%, acknowledging the updated wiring pattern.

Table 8.4 shows the wiring combinations with efficiencies above the threshold of 87.45%.

Table 8.4: Winding configurations in Appendix P.1 with efficiencies above 87.45%

Option	Diameter [mm]		Number of turns	Strands in hand	Connection	Efficiency
	Conductor	Wire				
18	0.540	0.576	30	4	Delta	87.60%
57	0.710	0.762	17	4	Star	87.59%
75	0.850	0.909	16	3	Star	87.59%
95	1.000	1.062	17	2	Star	87.55%
102	1.120	1.184	28	1	Delta	87.69%

From Table 8.4 it is seen that five different combinations show efficiencies above the 87.45% threshold, which indicates a reduction in stack length is feasible. To further examine these possibilities, a sweep across 80.75-95.75 mm stator stack lengths is performed, and the results are reported in Figure 8.5.
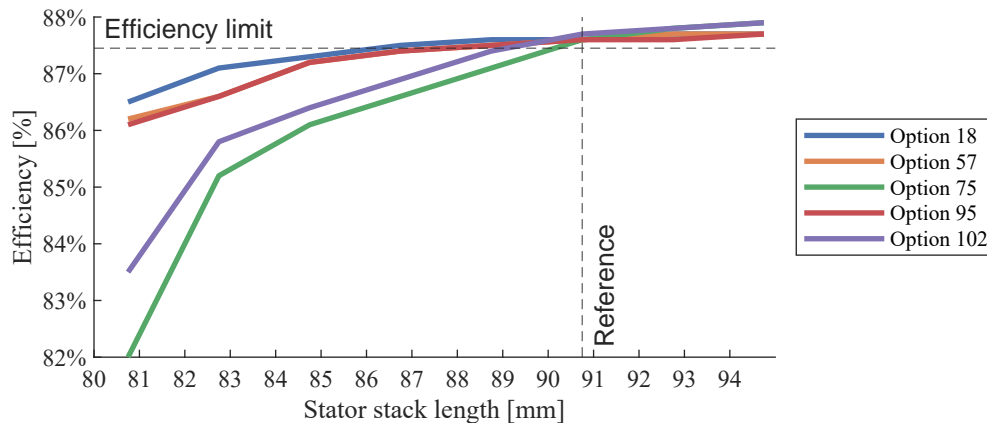
Figure 8.5: Efficiency sweep across 80.75-95.75 mm stator stack lengths for combinations shown in Table 8.4

From Figure 8.5 it is seen that the option which allows for the shortest possible stack length is wire option 18. If this wire option is chosen the stack length could be reduced to approximately 86.75 mm, which is a reduction of 4 mm. This is a 4.4% reduction in stator length, but only a 1.2% reduction in the total machine length. Thus the effort required to produce and validate a machine with such a winding configuration is not worth such a small reduction.

Earlier it was mentioned that slot fill factors normally lie between 60-70%. However, an improvement to 70-80% is possible but at the cost of complicating the winding process. Complication of the winding process might be worth it if the reduction of length obtained is large enough.

To investigate how much an improvement in slot fill factor impacts the efficiency of the machine. The same calculations are performed again but with a slot fill factor of 73.1%, using the wire size

combinations found in Appendix P.2. The full results of this calculation are found in Appendix P.4, and the combinations with efficiencies above the threshold of 87.45% are shown in Table 8.5.

Table 8.5: Winding configurations in Appendix P.2 with efficiencies above 87.45% using original stator/rotor stack length

Option	Diameter [mm]		Number of turns	Strands in hand	Connection	Efficiency
	Conductor	Wire				
132	0.560	0.606	30	4	Delta	87.90%
150	0.670	0.722	28	3	Delta	87.95%
153	0.670	0.722	17	5	Star	88.01%
168	0.800	0.855	30	2	Delta	87.98%
179	0.850	0.909	17	3	Star	87.88%
189	0.900	0.959	16	3	Star	87.99%
203	1.060	1.124	17	2	Star	88.02%
206	1.120	1.184	31	1	Delta	87.88%
225	0.750	0.832	16	4	Star	87.73%

As indicated by Table 8.5, the efficiencies are improved as expected. To determine the potential minimum stator stack length, a sweep is again performed, which is seen in Figure 8.6.
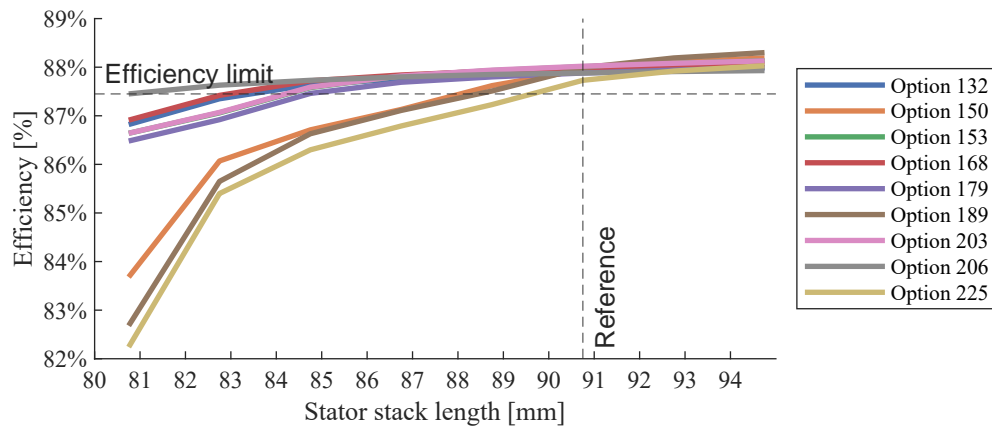
Figure 8.6: Efficiency sweep across 80.75-95.75 mm stator stack lengths for combinations shown in Table 8.5

As seen in Figure 8.6, the potential reduction in stack length is approximately 10 mm. Due to expected production difficulties associated with the increased fill factor, this reduction of 10 mm is not further investigated.

There's also a possibility that the winding pattern can be modified to try and increase the efficiency. This could be a change from double to single-layered winding or a change in how the windings are distributed.

As a source of inspiration the windings patterns of the FAB112-4 and Y3PE112M4 shown in Figures 7.7 and 7.8 are tested in the MotorCAD model for the UMP-3C3-210-25-4. The results are reported in Figure 8.7, where it can be seen that neither of the two winding patterns meet the efficiency limit at stator lengths of less than 90.75 mm.

In conclusion, altering the winding pattern and wire size in the UMP-3C3-210-25-4 does not yield any significant reduction that justifies the time and resources invested. It is important to note that the assessments were conducted within the constraints of the available options. Hence, the wire sizes considered were limited to those listed by the manufacturer, and the layouts were derived from the
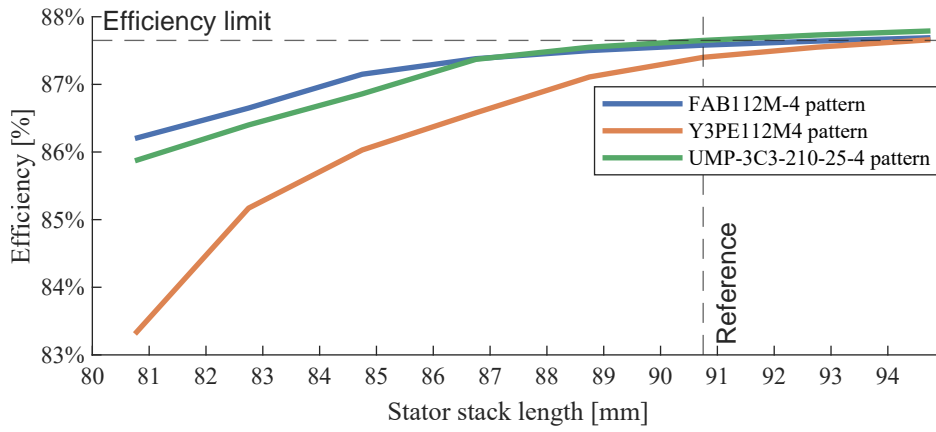
Figure 8.7: Efficiency sweep using the winding patterns from FAB112M-4 and Y3PE112M4 machines

available machines. While other options for, e.g., wire layout or wire size exist on the market, they were not reported as available by the manufacturer.

8.1.3 Increase in Stator and Rotor Diameter

In addition to examining changes in laminate materials and winding patterns, it is also possible to investigate the effects of the different available laminate sizes.

When increasing the OD of the stator and rotor, a larger slot area can be obtained, allowing for more copper to be accommodated. This results in an increased capacity to generate a stronger magnetic field. Additionally, the larger diameter reduces saturation in the laminates, further enhancing the magnetic field strength. With a stronger magnetic field, there's potential to reduce the length of the stator and rotor, achieving the desired compactness.

Multi-Wing's supplier already produces machines with a stator OD of 260 mm, hence switching to this laminate size would be relatively simple. As it is the supplier from China, and not Multi-Wing, which produces the machines, the geometry of the 260 mm OD laminate is unknown. For the other laminate geometries, a machine with the laminate was taken from the stock at Multi-wing and disassembled for measurements. However, no machine with the 260 mm OD laminate is available, hence the geometry of this laminate has to be estimated.

To estimate the geometry of the 260 mm OD laminate, the measured laminate geometries of the FAB112M-4 and UMP-3C3-210-25-4 are used to scale. The difference in geometry based on the size in OD is used to create a proportional change in the laminate geometry based on the size of the stator.

This is illustrated by equation (8.4), which shows an example of how the width of the teeth changes with the stator diameter. Similar equations are derived for other parts of the geometry to fully scale the entire laminate design based on the OD. The rotor and stator laminate geometries are then scaled to match a 260 mm OD stator, except for the air gap and slot insulation, which are kept at their original dimensions.

$$w_{tooth}(D_{stator}) = \frac{w_{tooth,UMP} - w_{tooth,FAB}}{D_{stator,UMP} - D_{stator.FAB}} \cdot (D_{stator} - D_{stator,FAB}) + w_{tooth,FAB} \tag{8.4}$$

With a larger slot area, the wiring has to be changed, if the same slot fill factor is to be achieved. As an initial starting point, a slightly larger wire size and a small increase in the number of turns are used, which can be seen in Table 8.6.

Table 8.6: Winding combination used in the first iteration of the scaled machine design

Conductor diameter	Wire diameter	Number of turns	Strands in hand	Slot fill	Copper fill	Connection
0.800 mm	0.855 mm	32	2	53.8%	47.1%	Delta

To find the minimum feasible stator stack length a sweep in the range of 54.75-90.75 mm is made. The sweep is done in the interval by stepping the stack length by 2 mm, and results from the sweep are shown in Figure 8.8.
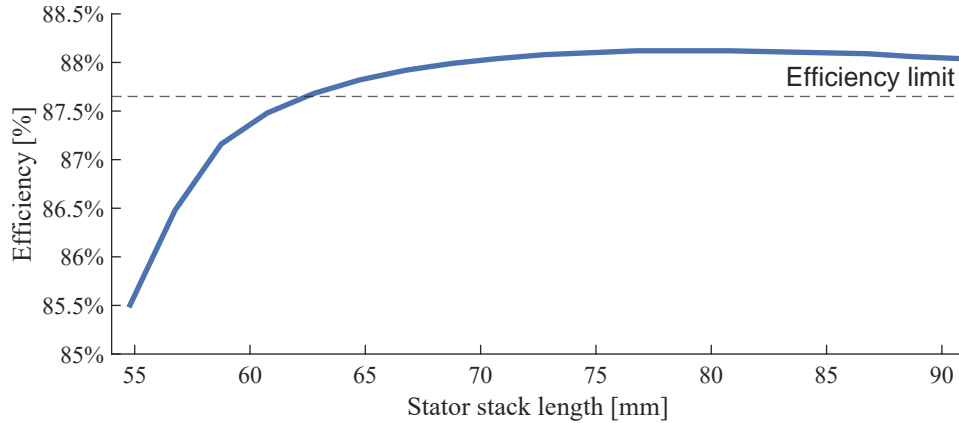
Figure 8.8: Sweep of stator stack lengths for the first iteration of the scaled machine design

Based on the sweep in Figure 8.8, a stator stack length of approximately 62.75 mm is found to be the minimum value.

This is a length reduction of 28 mm, but also an increase in volume of 6% when considering a cylinder defined by the length and diameter of the stator. Thus the decrease in length is achieved at the cost of increased material use. The machine also risks blocking more of the airflow, if the diameter is increased.

It should also be recognised that the increased wire size and turns result in longer end-windings. MotorCAD uses (8.5) and (8.6) to calculate the end winding overhang in the front and rear respectively.

$$Ohang_F = \frac{MLT - 2 \cdot (Ext_F + Ext_R)}{2 \cdot \pi} + Ext_F \tag{8.5}$$

$$Ohang_R = \frac{MLT - 2 \cdot (Ext_F + Ext_R)}{2 \cdot \pi} + Ext_R \tag{8.6}$$

Where Ext_F/Ext_R are the winding extension before the windings start to bend and *MLT* is the mean length per turn.

MotorCAD automatically calculates the mean length per turn based on the stator length and then assumes the end windings follow a semi-circular path defined by the mean coil pitch (cp_{mean}), as shown in Figure 8.9.

The coil pitch is calculated for each individual coil and then averaged to determine the mean coil pitch as illustrated in Figure 8.10

As the diameter of the stator is increased, the mean coil pitch also increases because the distance between slots grows. Thus the end winding overhang ends up being longer when using a 260 mm OD
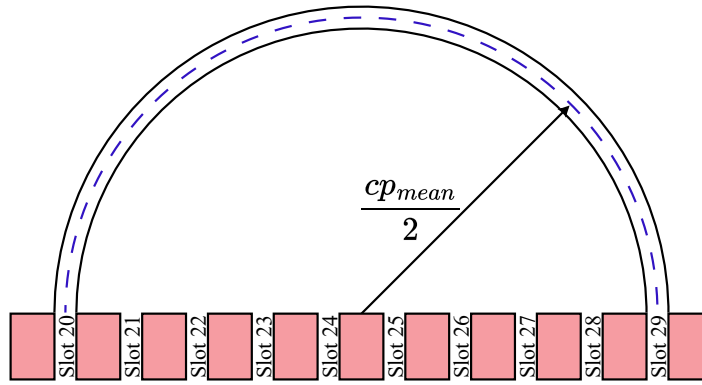
Figure 8.9: MotorCAD's definition of mean length per turn
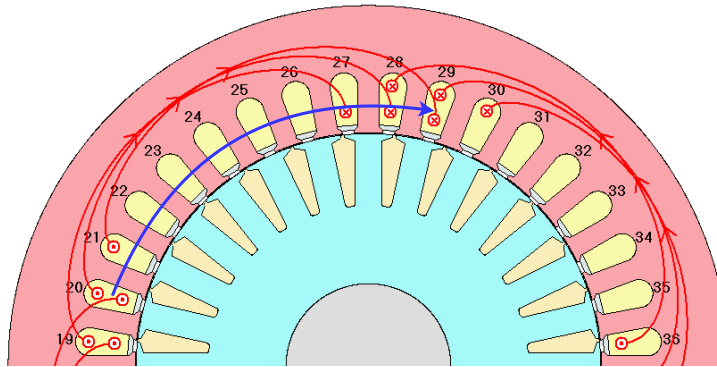
Figure 8.10: MotorCAD's definition of mean coil span

stator laminate compared to the original 210 mm OD design. Based on calculated *MLT* values from MotorCAD, the difference between the overhang length, if the extensions are ignored, turns out to be 14.75 mm. Therefore the total length reduction is 12.25 mm when the difference in winding overhang is included.

Thus, changing the laminate size to an OD of 260 mm can shorten the housing. However, it requires the use of more material, increasing the cost. It is worth noting that the calculations performed, are based on a coarse estimation regarding the laminate geometry, as the exact laminate geometry used in laminates of OD 260 mm at the fabrication site is unknown. The optimal winding size and configuration have also not been examined. However, to limit the scope of this project, this optimisation is not performed.

8.2 Housing Redesign

After investigating potential changes to the internal components of the UMP-3C3-210-25-4, the focus shifts to the housing design. The housing of the UMP-3C3-210-25-4 can be easily shortened, as the extrusion length can be reduced by cutting it at a different length.

The current design of the UMP-3C3-210-25-4 features a lot of free space inside the machine, as explained earlier in Section 7.4. Therefore, the housing redesign aims to reduce this free space, leading to a reduced length.

As previously mentioned in Section 7.4, the UL 1004-1 (2020) states that the minimum distance between stator windings and housing/end bells must be more than 2.4 mm.

8.2.1 Development of Design Proposal

To aid in designing a new housing, the CAD model of the old housing design is used together with a simplified sketch of the rotor and housing, allowing the machine to be recreated as a CAD assembly, as seen in Figure 8.11.
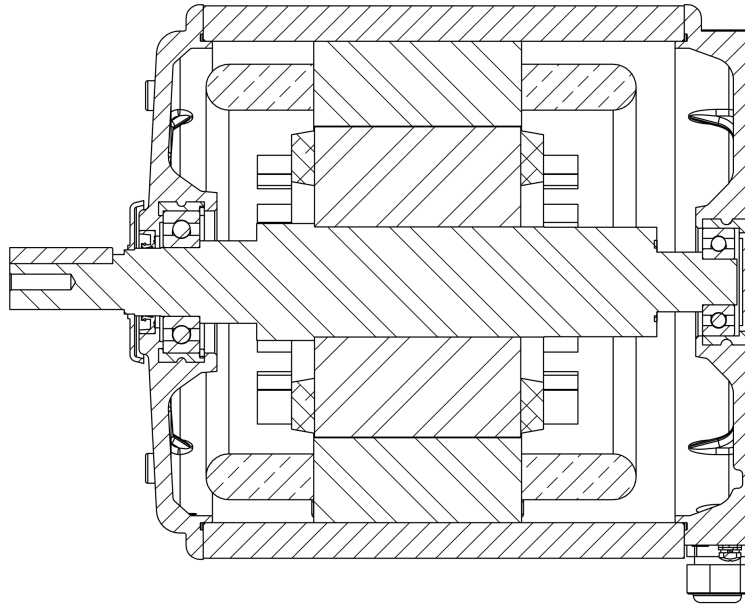
Figure 8.11: Cross-section of CAD assembly with original housing

As seen from the CAD model assembly of the original housing, the stator housing has free space at both ends, with most of it located at the rear.

A revised housing and shaft design is then proposed, as seen in Figure 8.12.
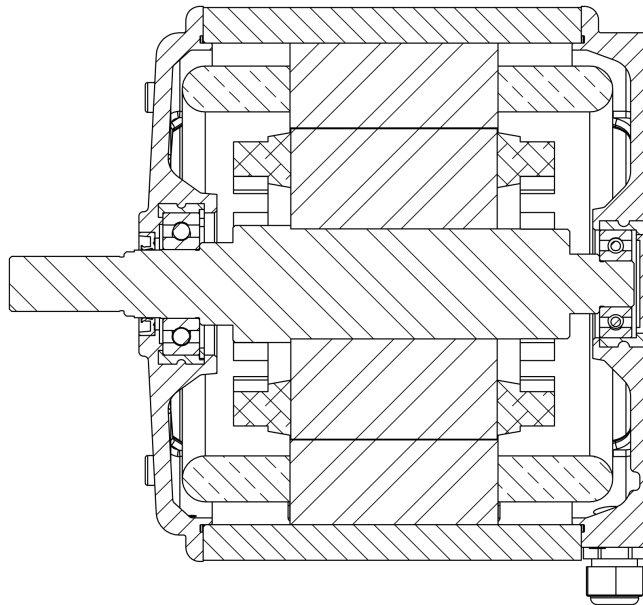
Figure 8.12: Cross-section of CAD assembly with shortened housing

To determine the end winding clearances, Solidworks features a clearance detection tool that can check for clearance issues between components. With the proposed design, the clearance between the front

end bell and end windings is reduced from 8.47 mm to 4.59 mm, and the clearance between the rear end bell and end windings is reduced from 21.9 mm to 5.49 mm. The clearance between the end bells and end windings is higher because of a ground screw connection located on the inside of the rear end bell, as seen in Figure 8.13. The clearance to this ground screw is 4.31 mm. It should be noted that the reduction in clearances do not directly relate to the length reduction of the machine, as the locations of clearance measurement change with the new design proposal.
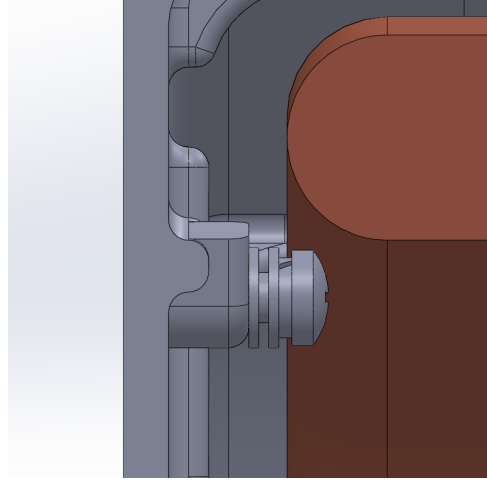
Figure 8.13: Image of ground screw inside CAD assembly of shortened housing design

These clearances are larger than what is strictly necessary according to the UL 1004-1 standard, but to allow for some tolerance in the end winding thickness and length, the clearances are kept at this level.

The total reduction in machine length achieved with the design proposal is 45 mm, which is more than any of the electromagnetic design changes investigated in Section 8.1.

As previously mentioned in Section 7.6, a shortening of the housing also means less surface area available for cooling. Therefore, it is important to check if the UMP-3C3-210-25-4 can maintain safe temperatures despite the shorter housing.

To determine if the proposed housing design's cooling ability is sufficient, the thermal model of the UMP-3C3-210-4, which has already been verified in Section 7.6.3, is modified to include a shorter housing. The thermal model uses the cooling model determined from the fan load test of the UMP-3C3-210-4 to simulate the machine being cooled by a fan.

Since the machine is supposed to be rated at 4 kW, the simulations are performed with a 4 kW load. The machine is then simulated at different ambient temperatures with a 4 kW load, for the original and the proposed shorter housing design. The resulting temperatures of parts of the machines are shown as a function of the ambient temperatures in Figure 8.14 and Figure 8.15 for the original and the proposed shorter housing, respectively.

As seen, there is a linear correlation between ambient temperatures and the machine's temperatures, albeit with different gradients depending on what part of the machines are being observed. Because the numbers are hard to read in Figures 8.14 and 8.15, Table 8.7 shows the machine temperatures for three different ambient temperatures. It can be seen that the temperatures of the machines differ by 3-4 °C between the original and shortened housing design.

The results in Table 8.7 indicate that the maximum temperatures inside the machine do not exceed the 180 °C maximum temperature indicated by the insulation class H of the machine. Furthermore, as mentioned before, the load in this case is higher than the expected fan load of the machine, so the
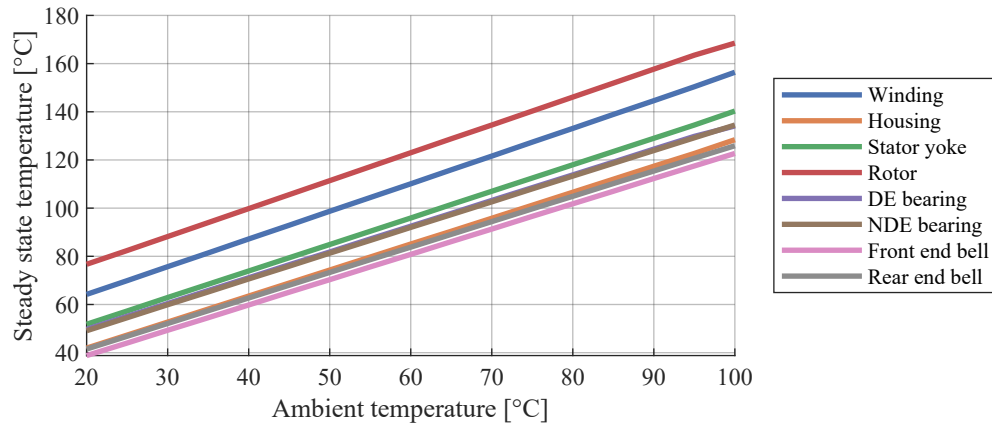
Figure 8.14: Simulated steady-state temperatures of original housing design at different ambient temperatures
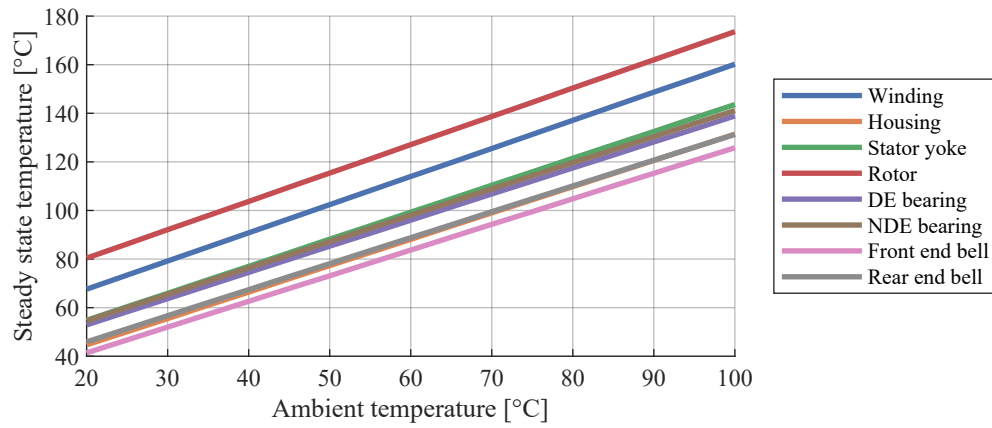
Figure 8.15: Simulated steady-state temperatures of proposed housing design at different ambient temperatures

Table 8.7: Comparison between MotorCAD thermal simulation results for old and new housing design

Housing	Temperatures [°C]				
	Ambient	Winding	Housing	Rotor yoke	Stator yoke
Original	25	69.9	47.3	82.4	57.3
Shortened	25	73.4	50.1	86.2	60.4
Original	45	92.9	68.9	105.5	79.4
Shortened	45	96.6	71.9	109.6	82.7
Original	100	156.1	128.1	169.2	140.0
Shortened	100	160.3	131.6	173.7	143.7

temperatures are expected to be lower in reality.

As long as the thermal capabilities of the UMP-3C3-210-4 meet the needs of Multi-Wings customers and are kept within thermal ratings, the small increase in temperature from the proposed housing design is deemed acceptable.

8.2.2 Manufacturing and Assembly of Design Proposal

Having determined through simulation that the proposed housing design has sufficient cooling, a physical machine is constructed based on the modification proposal to validate the design proposal.

An unassembled UMP-3C3-210-4 is modified and assembled to create a prototype.

The housing is first cut short using electric discharge machining to avoid damaging the fins. To install the stator at the correct place in the housing, a specially made ring is used to prop up the stator laminate stack to a specific height. Bolts at the end of the stator adjust the height of the housing as it is placed on top of the stator, as illustrated in Figure 8.16.
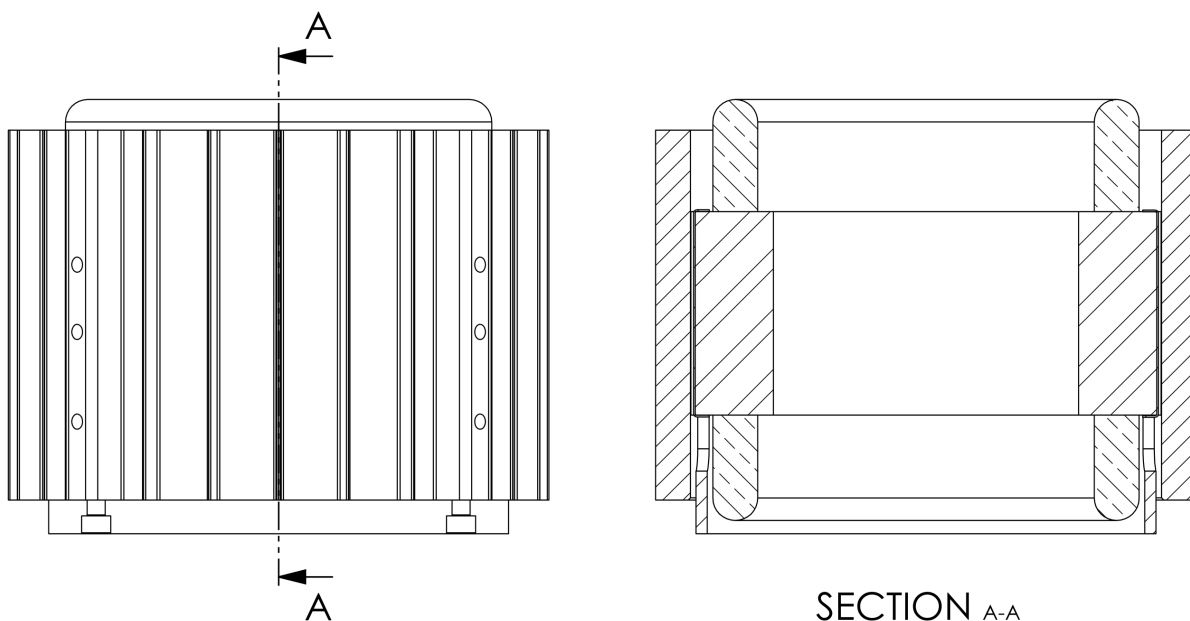
Figure 8.16: Height alignment of stator inside housing using a specially manufactured ring to support the stator

As the stator is press-fitted inside the housing, the housing is heated to approximately 200 °C, expanding it enough to fit over the stator.

The rotor shaft is turned down to size using a lathe, and the rear bearing is fitted directly onto it. The front bearing is held in place by a snap ring mounted on the front end bell. The snap ring cannot be mounted if the bearing is attached to the rotor shaft first due to space limitations. Therefore, the front bearing is installed in the front end bell first and then pressed onto the rotor shaft, as seen in Figure 8.17.

The rotor is then fed through the stator, and the front end bell is screwed in place.

As the received parts did not have temperature sensors installed, thermocouples were attached inside the machine to allow for real-time measurement of temperatures.

Ideally, measuring the winding temperature should be achieved using a measurement probe installed inside a stator slot. In this case, this was not possible, so a thermocouple was attached to the end windings instead, as seen in Figure 8.18.
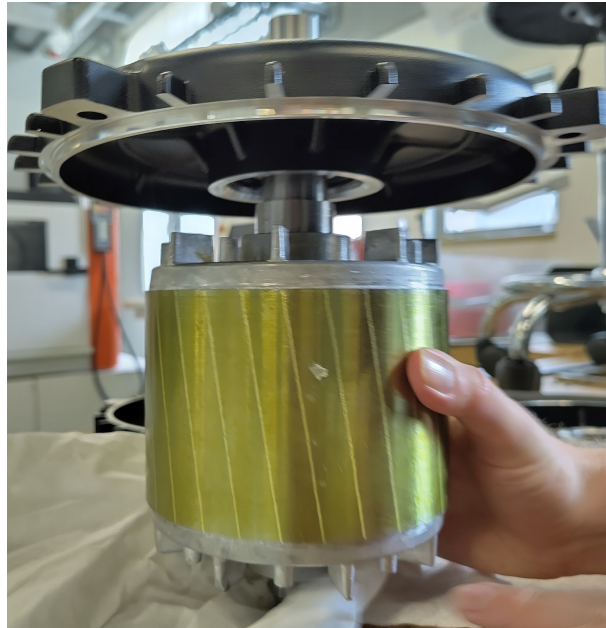
Figure 8.17: Photo of the modified rotor with the front end bell attached
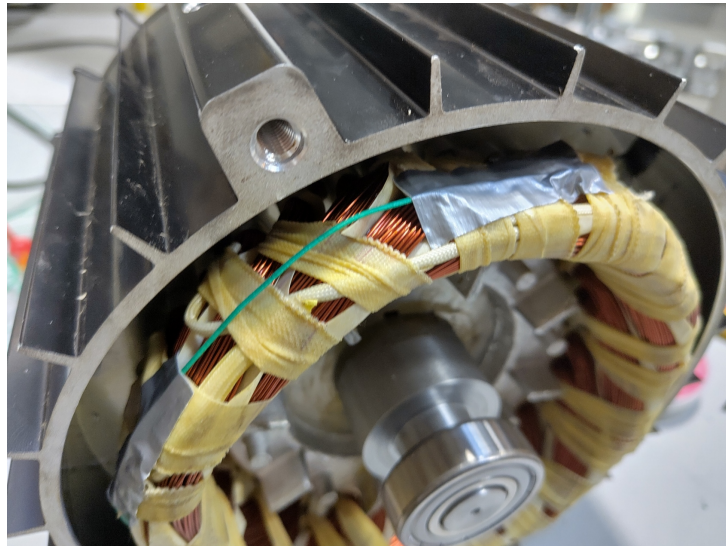
Figure 8.18: Photo of thermocouple attachment to end winding

Another thermocouple was mounted to measure the temperature of the rear bearing's outer ring using a small hole, as seen in Figure 8.19.
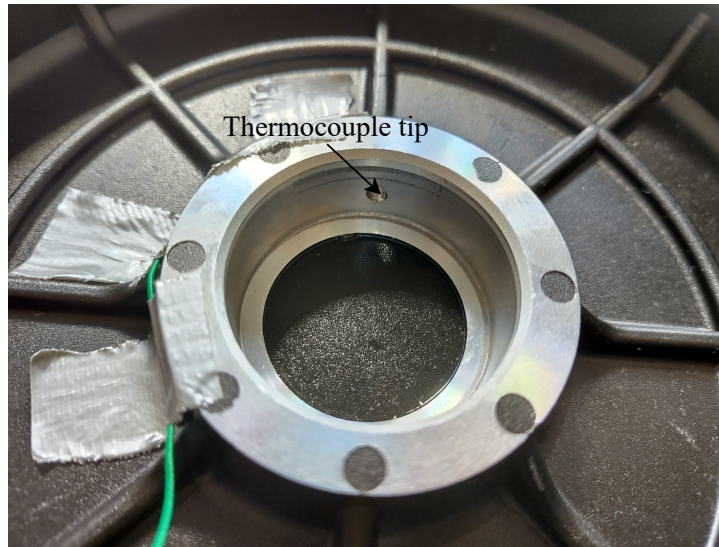
Figure 8.19: Photo of thermocouple attachment to rear bearing

The rear end bell is then attached, along with various seals and screws.

8.2.3 No load Testing of Prototype

To ensure that the prototype functions as intended, a no-load test is performed to determine if the performance is significantly different from the original UMP-3C3-210-4. In this case, the no-load test is not run until thermal settling, as it is very time-consuming and only an approximation is needed.

Table 8.8 shows the measurement results of the reference and prototype with a 400 V input. Full data from the no-load test can be found in Appendix Q.2.

Table 8.8: Comparison of no load measurements between original machine and the prototype performed at 400 V

Housing	Current [A]	Power [W]	Power factor [-]
Original	3.64	245	0.097
Shortened	3.80	241	0.092

As seen in Table 8.8, the differences in measurements at 400 V are small. Furthermore, when calculating the windage and friction losses, they appear almost identical to the reference machine, as seen in Table 8.9.

Table 8.9: Comparison between measured no load losses of unmodified reference machine and the prototype

Housing	Iron loss [W]	Friction and windage loss [W]
Original	134	52.2
Shortened	135	53.2

With the results of the no-load test being close to those measured on the machine with the original housing, it is safe to assume that nothing major has gone wrong when assembling the prototype.

8.2.4   Fan load Test With Prototype Machine

The main goal of the prototype is to test if the machine can keep cool as indicated by simulations. Therefore, a fan load test identical to the one performed in Section 7.6.3 is performed using the prototype machine.

The full test data can be found in Appendix Q.3, and the final steady-state temperatures are reported in Table 8.10.

Table 8.10: Comparison between MotorCAD thermal simulation results for old and new housing design

Housing	Temperatures [°C]				
	Ambient	**Winding**	**Housing**	**DE bearing**	**Rear end bell**
Original	21.4	52.2	32.3	38.2	34.6
Shortened	23.8	53.2	36.0	40.6	37.0
Difference	2.4	1	3.7	2.4	2.4

It is seen that the maximum temperature difference between the original housing and the new prototype is measured at the housing as 3.7 °C, despite an increase in ambient temperature of 2.4 °C. The windings show an increase of 1 °C, which was expected to be higher due to a higher ambient temperature. This might be attributed to the windings being measured at the top of the end windings, which are cooled by the fins of the rotor ring, suggesting the average winding temperature is likely higher.

In general, it seems that the temperature differences could easily be due to measurement uncertainties or differences in machine efficiency rather than the inferior cooling performance observed through simulations.

In conclusion, there is no significant difference in the cooling performance of the prototype machine compared to the original machine. Therefore, the length of the housing is not a limiting factor in terms of the machine's thermal performance.

Furthermore, the suggested housing design is a cost-effective method to reduce the length. This is due to the reduction in material usage, the adjustable housing length provided by extrusion, and having only to reprogram the CNC lathe for a new shorter shaft. Thus, new tools, materials, and production steps are avoided. Hence a reduction of 45 mm in machine length compared to the UMP-3C3-210-25-4 has been proved realisable.

Chapter 9

Discussion

This chapter seeks to discuss the decisions and methods used in the redesign of the UMP-3C3-210-25-4 induction machine, focusing on their consequences and validity. The discussion also covers the modifications implemented in the machine's redesign, assessing their success and identifying areas for potential improvement.

9.1   Choice of Equivalent Circuit Model Type

The equivalent circuit model, presented in Chapter 5, is used to model induction machines in a steady state. As mentioned in Section 5.1, the R_{fe} component of the equivalent circuit could be removed, as demonstrated by Sen (2013). According to Sen (2013), when R_{fe} is removed, its losses are combined with windage and friction losses. This is based on the assumption that, when a machine is operated at a constant voltage and frequency, the sum of the iron, windage, and friction losses remains constant at operating speeds.

One benefit of this method is that it eliminates the need for the constant loss separation, explained in Section 6.2, reducing the complexity of the no-load test. It also simplifies the calculation methods for estimating equivalent circuit parameters. However, combining iron losses with windage and friction losses complicates the comparison of losses between MotorCAD and actual measurements. MotorCAD models the loss components separately, making it advantageous to compare each loss component individually. Separating these losses also makes it easier to understand how reducing each loss component could impact the machine's efficiency. Furthermore, the reduced complexity of the no-load test is not particularly significant, as no-load testing still needs to be performed in general. The same reasoning applies to the simplification of calculations as calculation methods are easily implemented into numerical programs.

Space and time harmonics can also be considered, by using additional equivalent circuits to model the harmonics. By investigating the harmonics of the machine, the efficiency drop due to harmonics could potentially be reduced. However, modelling these parameters would require further testing, possibly involving equipment beyond the scope of this project. (Liang and Luy; 2006)

It is also important to consider that the equivalent circuit presented in Chapter 5 is identical to the equivalent circuits presented in IEEE std 112 - 2017 (2017) and IEC 60034-2-1:2014 (2014). Adhering to these standards, especially IEC 60034-2-1:2014 (2014), enables the use of the equivalent circuit to estimate machine efficiency according to IEC 60034-30-1:2014 (2014). Compliance with IEC 60034-30-1:2014 (2014) is essential as it determines whether or not a machine is IE3-rated, which is a legal requirement.

9.2   Equivalent Circuit Parameter Determination

The equivalent circuit parameters are important for accurately modelling and analysing the performance of the redesigned UMP-3C3-210-25-4. To ensure precise and reliable results, it is essential to select appropriate testing methods and correctly conduct these.

9.2.1 Choice of Test Methods for Determination

To measure the parameters of the equivalent circuit, DC resistance measuring, locked rotor testing, and no-load testing were chosen. This choice is straightforward as multiple sources, such as IEC 60034-2-1:2014 (2014) and Sen (2013) explain these test methods, including explanations of calculation methods.

However, it would also be possible to use other test methods to measure, e.g., iron losses or reactances, which could enable the separation of the leakage reactances. The downside to using test methods to measure iron losses more directly is that they often require non-standard equipment or multiple testing phases, making them time-consuming and expensive if the non-standard equipment is unavailable. (Mierczak et al.; 2020)

9.2.2 Accuracy and Precision of Measured Equivalent Parameters

During no load testing on the FAB112M-4 and Y3PE112M4, the winding resistance R_1 was measured before starting the test and again after the last no-load test was performed. It was assumed that the value of R_1 remained the same for all no-load tests, which was incorrect because the temperatures would have increased with each run. Additionally, the FAB112M-4 and Y3PE112M did not reach a stable temperature before measurements were taken, leading to further inaccuracies.

However, these mistakes were corrected during the no-load test of the UMP-3C3-210-25-4. In this case, the winding resistance R_1 was measured immediately after each run, and the machine was allowed to reach thermal equilibrium before each measurement. Correcting the error for the UMP-3C3-210-25-4 is crucial, as it is used as an initial design basis.

Some parameters for the FAB112M-4 and the Y3PE112M4 are affected by this error. However, the impact is assumed to be minimal. Furthermore, the resistance for the UMP-3C3-210-25-4 no-load tests (the tests without the mistake) varies by 0.48 Ω, as shown in Appendix K.2. The variance of 0.48 Ω is not acceptable if the R_1 at every no load voltage point was needed to determine R_1 at operation. However, since the resistance found is used to calculate the copper loss during no-load testing, the 0.48 Ω variance is not significantly impactful as the current is the defining term. Furthermore, the approximated copper loss is then used to determine constant losses by subtracting it from the measured power. Therefore, the error impacts the determination of iron losses and windage and friction losses, but only slightly, as the measured power is more determinative than the copper loss error.

Other than the error regarding the measurement of no load DC resistance, the equipment used is also prone to uncertainties. It is also unknown whether or not the machines used for testing were run in, as this might impact the friction from the bearings. In general, the tests performed are based on IEC 60034-2-1:2014 (2014), including the equipment accuracy classes, the test method, and the calculation method. Therefore, accuracy and precision comply with European standards, excluding the noted mistakes.

9.2.3 Validation Against Ratings

As the equivalent circuit parameters were determined, it became necessary to validate whether the measurements were performed correctly or if mistakes were made, necessitating a new test. For this purpose, the estimated equivalent circuit parameters were used to calculate the machine ratings and to compare those with the datasheet ratings. As is discussed in Chapter 2, the nameplate ratings are subject to tolerances and therefore the nameplate ratings do not necessarily reflect the actual machine performance. To account for this, the tolerances were included during the comparison. As long as the ratings calculated from the equivalent circuit parameters are within or around the given tolerance values, they are considered valid.

It was observed that the equivalent circuit models showed efficiencies, lower than what was stated in the datasheets. Thus, to further investigate the discrepancy between the datasheets and the equivalent circuits, load testing was performed on the machines. Performing the load tests made it possible to estimate machine efficiency by using the direct measurement or separation of losses method from IEC 60034-2-1:2014 (2014). The determined efficiency would then be used for further validation.

However, the validity of the load tests performed is questionable, as mechanical power measurements were seen to fluctuate by up to 100 W. This fluctuation is also described in Section 6.4.4, where the accuracy of the driver used to keep the mechanical load steady is questioned.

In IEC 60034-2-1:2014 (2014), requirements for the measuring equipment are mentioned, however, there are no requirements regarding the load equipment, and how much the load can fluctuate.

IEC 60034-2-1:2014 (2014) states requirements regarding the linear relationship of measured data and their correlation factor. This is done for the separation of loss methods in Section 6.4.3, affecting which load measurements are deemed viable. Thus, if too much fluctuation is seen through the correlation factor and linear relationship between each test, they are not used.

9.3   MotorCAD Modelling

As the project uses MotorCAD to predict changes in machine performance, this section provides an overview of how MotorCAD was utilised. It also discusses the insights gained from the simulations and how these impacted the design proposals.

9.3.1   MotorCAD as a Modelling Tool

This project uses MotorCAD as modelling software due to its availability through the university. While MotorCAD can perform the necessary calculations, it is not the only software commercially available for such tasks. Throughout the project, some limitations of MotorCAD were encountered, such as the inability to represent the geometry in the thermal model correctly. These limitations might not have been an issue if other software was used. However, this remains speculative since alternative software was not investigated as part of this project.

Additionally, the project could have been completed using purely analytical methods and estimations instead of a combination of analytical and Finite Element Methods (FEM). Analytical methods would have allowed for the use of optimisation theory on analytical expressions, such as identifying the shortest length analytically instead of performing time-consuming sweeps. However, the drawback of analytical modelling is its potential inaccuracy compared to FEM. Moreover, setting up analytical models requires more time compared to the automated calculations in MotorCAD. Setting up an optimisation algorithm for analytical methods would also require a significant amount of time to ensure accurate parameter selection and convergence, further extending the project's duration.

9.3.2   Validation Methods

To validate MotorCAD as a modelling software, MotorCAD results were compared to datasheet ratings, load tests, and equivalent circuit parameters determined in Chapter 6. This validation procedure relies on the accuracy of datasheet ratings, load tests and estimated equivalent circuit parameters. It was found through load test measurements that the machine performance did not match the datasheet ratings, and the efficiency was outside the tolerances. The accuracy of the load test measurements is questionable due to issues with fluctuating readings during load testing.

However, the estimated equivalent circuit parameters were found to estimate the machine characteristics well. Therefore, the equivalent circuit parameters were used for comparison and helped identify which

parts of the MotorCAD model are inaccurate.

As the estimated equivalent circuit parameters are based on no-load and locked rotor testing, these tests could also directly have been used for comparison. Directly comparing the no load tests to MotorCAD could have provided useful information about the accuracy of the stator leakage and mutual reactance parameters. Instead, it was chosen to use the no load tests to calibrate the model directly, without comparison between no load measurements and MotorCAD modelling. Additionally, locked rotor data were not compared against MotorCAD, as the comparison to equivalent circuit parameters and no load test calibration were deemed enough.

9.3.3 Calibration of MotorCAD Electromagnetics

Calibration factors were introduced into the MotorCAD models to adjust the values of mutual reactance (X_m) and iron loss resistance (R_{fe}). The calibration factors used included a saturation factor to lower the value of mutual reactance and a build factor on both the rotor and stator to reduce R_{fe}. Instead of these multipliers, other factors in MotorCAD could have been utilised. E.g., stacking factors related to laminate stacking density, direct inductance multipliers on leakage and mutual reactances, end winding multipliers, and build factors on the shaft and magnetic axial length.

Adjusting more or all of these multipliers could potentially have made the electromagnetic model more accurate. However, it is important to consider whether these build factors remain valid despite changes to the machine design. This project did not validate if the used build factors changed with modifications to the machine, thus it is only assumed that the used build factors remain approximately the same despite changes in geometry.

The resistivity of the copper used in the windings was adjusted to set R_1 to the measured value. However, it remains unclear whether this discrepancy in R_1 arises from variations in resistivity or differences in end winding length. In the MotorCAD model, the end winding overhang is set to a specific length based on measurements. Yet, according to the MotorCAD documentation, this parameter does not alter the end winding length used in calculations and is only utilised in the thermal model.

MotorCAD also offers an end winding length multiplier, which could be used instead. Using this multiplier ensures that the end winding length in MotorCAD matches reality more closely, thus influencing R_1. The end winding length is also used to calculate the end winding inductance. Additionally, employing the end winding length multiplier would likely provide better scaling and accuracy when modifying the winding type or configuration.

Lastly, the method for calculating additional load losses in MotorCAD was modified to compute these losses as a percentage of the output power. This adjustment was based on measurement data from the separation of losses method, which indicated lower additional load losses than those estimated by MotorCAD's standard method. While this approach ensures that additional load losses are accurate at the rated load, the assumption that these losses remain a fixed fraction of the output power may not hold true at all speeds.

9.3.4 Thermal Modelling in MotorCAD

For the UMP-3C3-210-25-4, a thermal model was also set up in MotorCAD. The accuracy of the thermal model was limited by how well MotorCAD could represent the machine's geometry and by the knowledge of material properties. After some adjustments to the heat transfer coefficients to compensate for a lack of surface area, the thermal model was found to be around 5 °C off compared to reality.

This inaccuracy was partly attributed to the ability to measure the temperature correctly in verification tests and partly to model accuracy. However, the thermal model showed errors above 15%, questioning the validity of the model and its use. More time could have been spent further adjusting material

parameters and heat transfer coefficients to gain a more accurate model. However, this would likely have resulted in the same conclusions regarding whether the machine could be shortened from a thermal perspective.

9.3.5 Accuracy and Precision of Fan Load Tests

To obtain a cooling model, a fan load test was performed on the UMP-3C3-210-25-4 and the prototype machine. During this test, the machine was mounted pointing downwards, causing the fan to suck air from the ground, which increased the system impedance. Changing the system impedance changes the fan load point, and therefore also the machine load point. Additionally, the test used a 380 V supply instead of the rated 400 V due to equipment limitations, causing a limitation of the machine's output. The measurement accuracy of the airspeed was poor, with significant fluctuations due to turbulence, making the airspeed profile questionable.

However, since fan load changes depending on use case and ambient temperatures, it is unlikely that any fan load test would accurately represent actual working conditions.

9.4 Redesign of The UMP-3C3-210-25-4

Following the MotorCAD modelling discussion, the focus shifts to the redesign of the UMP-3C3-210-25-4 machine. This section explores the redesign efforts, discussing what modification proposals were examined and the choices made.

9.4.1 Material Choices

In an attempt to reduce the iron losses of the UMP-3C3-210-25-4, alternative laminate materials were examined. Simulations showed, that choosing a laminate material with less core losses did not increase efficiency due to saturation issues. Likewise, choosing a material with more core losses but less saturation also did not provide an increase in efficiency.

Only materials available from Multi-Wings' Chinese supplier were considered. However, alternative supplier materials that might have fewer saturation issues were not explored. The investigation did not consider grain-oriented versus non-grain-oriented materials, which could also potentially reduce the machine's length further. (Cassoret et al.; 2014)

Other materials used in the machine, such as rotor bars and winding materials, were also not examined in detail. The only winding materials with better conductivity than copper are silver or gold, which are significantly more expensive. The cast aluminium used in the rotor rings could be replaced with higher-quality aluminium or copper bars, but these options would also increase the cost.

9.4.2 Winding Configurations

An investigation into possible winding combinations was performed. The fill factor of the current design was used as a limit to determine if a wire combination was feasible. It was decided that the maximum fill factor would remain the same as the current one. However, the current fill factor was hard to determine and thus associated with inaccuracies. Further examination of the maximum fill factor could have been relevant, as it was demonstrated that increasing the fill factor to 73.1% could potentially reduce the stator length by 10 mm. However, increasing the fill factor increases the material used and time consumed when winding. Furthermore, it is unknown whether the fabrication site could produce a higher fill factor. This could have been investigated, but other methods of length reduction were prioritised instead.

The use of a Python script to run a list of winding combinations in MotorCAD introduced limitations to the winding configuration. This meant that when simulating different winding options, the winding pattern was changed from the custom pattern on the UMP-3C3-210-25-4 to a lapped pattern, resulting in decreased efficiency according to simulations. Without the Python script, the results would have been more precise and trustworthy but would have taken much longer than the time required by the script.

Different winding layout configurations were also tested. The winding configurations tested were based on the layouts observed in the FAB112M-4 and Y3PE112M4. This is due to the machines having the same number of slots, making the layouts interchangeable. From the tested layouts none was found to reduce the machine length. Layouts with more concentrated or distributed windings were not tested as they often require a different number of stator slots.

9.4.3 Scaling of Laminate OD

An increase in laminate OD to reduce the required laminate stack length was also examined. It was decided to use a 260 mm OD laminate, as Multi-Wings' supplier use this size in other projects. However, the exact geometry was unavailable to this project and therefore a direct scaling method was used to estimate the geometry of a 260 mm OD laminate. In this process, the air gap and insulation material were not scaled. The choice of a small air gap could become an issue, as maintaining air gap tolerance becomes increasingly difficult with larger machines. Additionally, direct scaling likely results in less optimised laminate geometry compared to the original size.

However, the FEM results from MotorCAD for flux density, shown in Figure 9.1 and Table 9.1, indicate that both the flux density values and the areas of high magnetic saturation are similar to those in the 210 mm OD laminate design. This suggests that the laminate geometry is already well-designed from a saturation perspective.
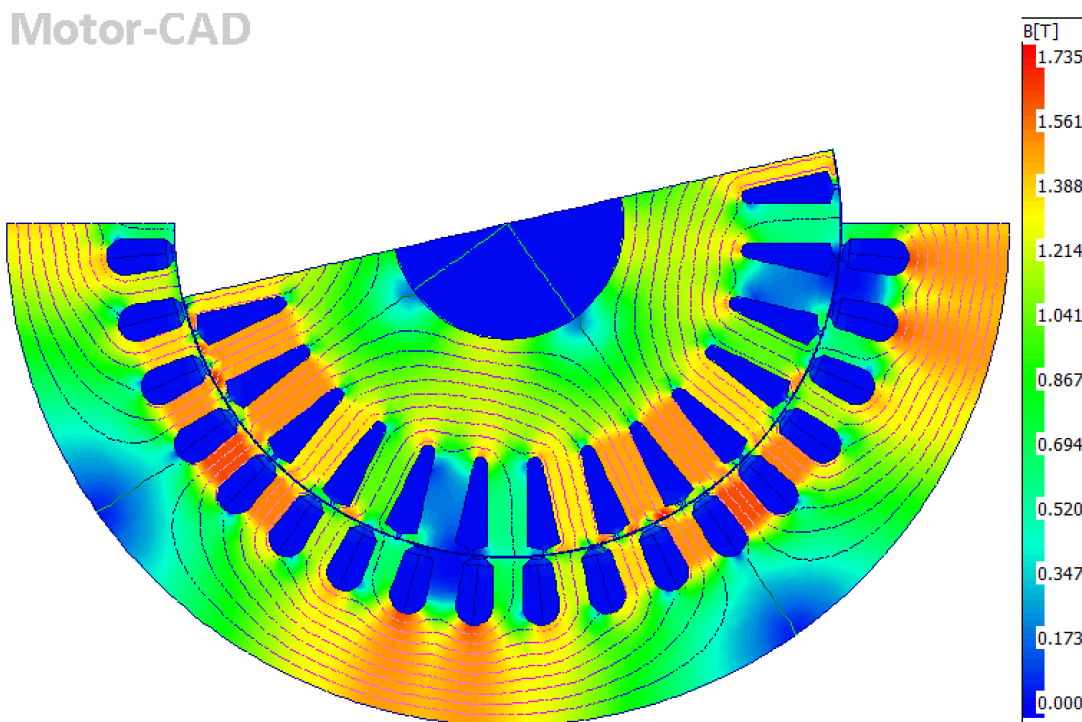
Figure 9.1: FEM analysis results from MotorCAD, showing the flux density in the scaled machine design at 4kW load

When evaluating the 260 mm OD laminate design, the wiring configuration was not properly investigated. Instead, a configuration similar to the original wiring in the UMP-210-25-4 was chosen.

Table 9.1: Flux density values reported by MotorCAD for the scaled machine model at 25 °C

Location	Calculated flux density [Tesla]
Airgap (mean)	0.6074
Airgap (peak)	0.859
Stator tooth (peak)	1.678
Stator back iron (peak)	1.493
Rotor tooth (peak)	1.564
Rotor back iron (peak)	1.247

The 260 mm OD laminate design might benefit from selecting a different wiring combination, potentially further reducing the machine's final length.

Additionally, using an alternative method for calculating the end winding length might have produced different results, potentially leading to a greater reduction in length. This parameter is also highly dependent on production methods.

9.4.4 Redesign of Housing

A redesign of the housing was made by reducing the length of the extruded part of the housing. The redesign was made in compliance with UL 1004-1 (2020), as the windings need a clearance of at least 2.4 mm to non-live machine parts. A Length reduction of 45 mm was made out of the 46.5 mm possible, as tolerances were added to ensure UL compliance was kept.

When redesigning the housing, only the extruded part of the machine was considered. Redesigning the end bells could have allowed for further length reduction, though likely less than 10 mm. This would also change the machine's thermal properties and require new casting moulds, increasing initial production costs. A completely new housing design could increase the fin count, potentially lowering machine temperatures and expanding the rated ambient temperature. Additionally, investigating better bearings could reduce friction losses, translating to a reduction in stack length.

9.4.5 Validation of Prototype

The redesign was verified by performing a no-load test and a fan load test on a constructed prototype machine. While the electromagnetic performance of the prototype is expected to be the same as the original UMP-3C3-210-25-4, there could be differences. If the electromagnetic performance significantly differs from the original, the fan load test results would be invalid. To ensure validity, a load test and a locked rotor test could have been conducted to estimate equivalent circuit parameters. However, no significant differences were seen when comparing the power drawn and operating speed during the fan load test to the original UMP-3C3-210-25-4. Furthermore, the no load test conducted on the prototype showed no significant difference in iron loss or windage and friction loss compared to the original.

Neither the original UMP-3C3-210-25-4 nor the prototype has been tested at temperatures higher than ambient. Consequently, the maximum ambient temperature for the machines has not been formally validated in this project. Additionally, the thermal performance at 60 Hz and 4.6 kW, which would result in higher temperatures, has not been evaluated. This was not investigated because the UMP-3C3-210-25-4's datasheet does not specify operation at 60 Hz. Furthermore, if electrical frequency increases the mechanical speed is also expected to increase. It is unknown how the airflow profile used in modelling would change if the mechanical speed increased. It is also unknown whether the fan used at 50 Hz is used at 60 Hz in Multi-Wing projects.

9.4.6 Production methods

As mentioned in Section 8.1.1, it is expected that the material properties of laminate materials change, as the laminates are processed. In Mierczak et al. (2020), it was mentioned that the order of processing methods impacts how the laminate material properties change. Hence it would have been advantageous to investigate how the laminates are processed, and if improvements could be made to the production method. It would also be advantageous to investigate how other production methods could be improved to reduce the machine length. This could include investigating production methods such as compression of end windings or reduction of air gap between stator and rotor. However, this would be a time-consuming process requiring detailed knowledge of how Multi-Wings supplier fabricates and assembles their machines.

Chapter 10

Conclusion

This study aimed to redesign the UMP-3C3-210-25-4 induction machine to reduce total machine length while maintaining performance characteristics and remaining cost-effective.

To redesign the UMP-3C3-210-25-4 the modelling software MotorCAD was used to predict how changes to the machine would impact the machine characteristics. The MotorCAD model constructed of the UMP-3C3-210-25-4 was validated through estimated equivalent circuit parameters, datasheet ratings, and load testing performed on the UMP-3C3-210-25-4.

The redesign process investigated several strategies to achieve a possible reduction in machine length, with some of the key findings listed below.

- Change of laminate material for both stator and rotor laminates was investigated, but no significant possibilities were seen for the laminate materials considered.
- Changing the wire type for the windings showed potential if the slot fill factor could be increased from 67.3% to 73.1%. Using a new wire type for the winding and the higher slot fill factor showed a potential reduction of 10 mm in stator stack length. However, it is unsure whether reducing the length by 10 mm at the cost of a 5.8% increase in slot fill is cost-effective, or if the fabrication site can increase the slot fill by 5.8%.
- Increasing the stator and rotor diameter to an OD of 260 mm was investigated, with the potential to reduce the stack length by 28 mm. However, due to the increase in end winding extension, the possible machine length reduction is 12.25 mm, at the cost of increased material usage. This reduction is based on linear scaling of the geometry, and the exact laminate geometry is unknown. The increase in material usage raises concerns about cost-effectiveness.
- During the disassembly of the UMP-3C3-210-25-4, free space was discovered inside the machine, indicating a potential length reduction of up to 46.5 mm. MotorCAD thermal simulations confirmed the machine could operate with the reduced length while maintaining its characteristics. A new housing design, reducing the machine length by 45 mm, was created and validated through fan load testing, showing performance similar to the original housing. This redesign also provided a practical and feasible solution for Multi-Wing.

In conclusion, several options to possibly reduce the length of the UMP-3C3-210-25-4 have been investigated within the project scope. From the investigated options it was found that the housing of the original UMP-3C3-210-25-4 could be shortened by 45 mm while reducing material usage. Thus, a redesign has been made to shorten the UMP-3C3-210-25-4 while maintaining its performance characteristics and ensuring cost-effectiveness.

Chapter 11

Future work

The project provided insights and explored various possibilities towards length reduction of the UMP-3C3-210-25-4 induction machine. However, from this project, several areas are also seen to warrant further investigation. Hence this section outlines potential future work areas, to either investigate further shortening of the UMP-3C3-210-25-4 or improve already implemented methods.

11.1 Thermal Modelling

As mentioned in the discussion, concerns were raised regarding the thermal modelling of the UMP-3C3-210-25-4 in MotorCAD. To address these concerns additional work regarding testing and modelling of the thermal properties might be advantageous.

11.1.1 Modelling of Fan Flow Profile

The fan speed measurement test, performed in this project should be revised to improve the thermal model. Instead of measuring at a single distance from the machine surface, it would be better to create a surface plot by measuring several points in both the radial and axial directions. This would provide a clearer overview of how the wind speed develops, which could be useful information when creating the thermal model.

Furthermore, equipment limitations led to the fan load test being performed at 380V instead of 400V. This should be addressed, and the fan load test should run at 400V instead. The fan load test was also performed with the machine in a vertical direction, which changes the system impedance, decreasing the airspeed. Thus a new fan load test should be performed with the machine in a vertical position.

11.1.2 Thermal Impact of Airspeed

As the use case might vary from customer to customer, the fan used might also vary, hence introducing different load points and air speeds generated by the fan. Thus it would be a good idea to model how the change in air speed impacts the machine's thermal properties.

To do so a range of airspeed could be modelled, using the MotorCAD model, at different ambient temperatures to predict whether the machine could handle the specific use cages. The tested airspeed could then be graphically mapped to determine how increasing the airspeed is advantageous or not. The graphs can then be used to more precisely determine what fans can be operated at what ambient temperatures while keeping the thermal class of the machine.

11.1.3 Thermal Model Based on Measurements

From the thermal modelling in MotorCAD, it was seen that the relation between ambient temperature and machine temperature is linear. This linear relation could be used in combination with measurements to establish a model predicting at what ambient temperatures the thermal class is kept. Hence component temperatures could be measured at three different ambient temperatures, or more, then

assuming a linear relation extrapolated to higher ambient temperatures. This creates an empirical model capable of predicting at what ambient temperatures the machine can operate.

Making a thermal model between the machine part temperatures and ambient temperatures based on data, would also help in validating the MotorCAD thermal modelling made.

11.1.4 Specification of Thermal Situations

In Section 2.3.5 Multi-Wing requested the ambient temperature rating of the machine to be between -50 - 100°C. It was also mentioned that the machine should be able to run at 60 Hz with a load point of 4.60 kW. This was not tested in this project due to reasoning mentioned in Section 9.4.5, but would in general be a good idea to do. To investigate this characteristic, load point, air flow profile etc. is needed to specify the thermal load situation more precisely.

To test at a higher frequency and new load point, a load case should be given with a fan available, as the airflow profile then is measurable. The measured airflow profile can then be used in combination with MotorCAD to determine whether the thermal class is kept at the operation point.

11.2 Design of Housing

Another area which warrants further investigation is the design of the housing, as only the extruded housing profile was considered in this project.

11.2.1 Redesign of End Bells

Redesign of the end bells was not considered as part of this project, since it requires new casting moulds. However, if a redesign is performed on the end bells, a possible reduction in length seems possible, although it is unlikely to reduce the length by more than a few mm.

If a redesign of the end bells is considered, it would likely make sense to redesign the housing entirely. This would allow for a new housing design to include more fins, which could help cool the housing. With a better cooling performance, the motor would run colder, increasing the efficiency under load. Furthermore, it would allow the machine to operate at higher ambient temperatures.

11.2.2 Bearing Choice

To reduce the friction losses in the UMP-3C3-210-25-4, choosing another set of bearings would be a possibility. As it was demonstrated in Figure 7.12 on page 60, the front bearing demonstrates a significantly higher friction loss than the rear bearing according to SKF's online calculator. Therefore, it would seem advantageous to replace this bearing. If the bearings are changed, the friction reduction could then be examined by performing a new no-load test.

11.3 Design of Electromagnetics

As restrictions were imposed on the electromagnetic parts of the machine, it would be advantageous to investigate how removing some of these restrictions could impact the electromagnetic performance.

11.3.1 Laminate Geometry Redesign

To fully determine if the 260 mm laminate size can be used to shorten the stack length, the complete geometric details must be obtained. This can be achieved either from the supplier's documentation or by disassembling a machine that uses the 260 mm laminate.

Further work regarding the winding configuration on the 260 mm, should also be done to investigate what winding configurations enable the most reduction in length.

11.3.2   Optimisation Possibilities

By using Python scripting to interface with MotorCAD, it enables the use of optimisation algorithms. Making an optimisation algorithm and removing the restrain regarding laminate geometry, an optimal laminate geometry could be found. Additionally, when choosing to use new laminate designs. A new geometry could also provide more freedom in the choice of windings, materials, and other design elements.

11.3.3   Laminate Sizes and End Winding Overhang

During the investigation into the 260 mm laminate size, it was noted that the end winding overhang also increased, limiting the total length reduction. Therefore, it would be valuable to examine how the total length is affected by variations in the stator laminate outer diameter (OD). To achieve this, the direct scaling method could be used to estimate the geometry for different laminate sizes. For each laminate size, the ideal wire combination would need to be identified, followed by a sweep to determine the minimum length. While this process would require significant simulation time, the framework for the investigation is already in place.

11.3.4   Geometry of Wires

In this project, simulations showed that an improved copper fill factor could provide a reduction in stator and rotor stack length. Copper wires are available in a wide range of sizes and shapes, that was not considered as part of this project. If square wires are used instead of circular wires, the fill factor can be increased significantly according to Tong (2022). Thus an investigation into alternative wire shapes, with the intention of increasing the fill factors could prove useful. If rectangular wires are to be used, it would also be a good idea to redesign the slot to best utilise the rectangular shape of the conductors.

11.3.5   Leakage Reactance Ratio

If a better electromagnetic model is desired, the leakage reactance ratio should be investigated further. Khade (2013) suggests an estimation method, which uses a locked rotor test, DC stator resistance test and two new tests known as no stator test and no rotor tests. As the name suggests these are measurements performed on the rotor and stator before they are assembled. By performing these tests, a separation of the leakage reactances becomes possible.

11.3.6   Available Laminate Materials

In this project, only the laminate materials currently available to Multi-Wing's supplier was considered. It would therefore be relevant to see if there are other material suppliers available who offers materials with different properties. If a material with the same iron loss, but less saturation is available on the market, it could potentially turn out to be worth investing in.

11.4   Production Methods

To improve the electromagnetic performance of the machine, changes in production methods should be considered. As demonstrated by Mierczak et al. (2020), residual stresses from thermal and mechanical treatments cause changes in the permeability and power loss of the stator and rotor core. It also showed

that the order in which production methods were used, could significantly influence the core materials properties.

Other production methods should also be investigated, such as reduction of air gap tolerance between the stator and rotor or if the end windings could be compressed further.

11.5 Other Machine Types

The choice of a 4-pole induction machine has not been discussed as part of this project. However, if the fan pack length is important to a customer, it could be worth investigating whether an alternative machine technology is a better solution. Since the end winding overhang is currently taking up a large part of the machine's internal space, it would be beneficial to reduce this overhang. This could be achieved by increasing the number of stator poles but would require a variable frequency drive to keep the same mechanical speed. Therefore this solution becomes more expensive and includes power electronics. If power electronics are part of the solution other machine types such as PMSMs should be considered as well. PMSMs can achieve a significantly higher power density than induction machines and could use concentrated windings technology, significantly reducing the end winding overhang. (Finken et al.; 2008)

There is also the possibility to rethink the design and use a machine with an external rotor. These types of machines allow for the fan blades to be mounted on the rotating housing of the machine itself, thus allowing for the machine to be placed further forward in the fan pack. These types of machines are already being used by some of Multi-Wings competitors such as Ziehl-Abegg (2024) or EBM-Pabst (2024).

11.6 Economics

Part of this project was to create a solution that would not increase the costs of the machine. To meet this requirement, the project has focused on material usage and keeping the production simple. Exact prices for different solutions are not possible at this stage, because the material and workmanship prices are not available.

Some of the future work needed to conclude this project would therefore be to investigate the price of different solutions. This would be essential to decide what solution Multi-Wing should go with, or if they should keep the current design and spend their time and resources differently.

Bibliography

Alderks, B. (2019). Windings slot fill and design for manufacturability.
  URL: *https://www.windings.com/slot-fill-and-design-for-manufacturability*

ANSI/NEMA MG 1-2021 (2021). ANSI/NEMA MG 1-2021, *Standard*, National Electrical
  Manufacturers Association, 1300 North 17th Street, Suite 900 Rosslyn, Virginia 22209.

Boldea, I. and Nasar, S. A. (2001). *The induction machine handbook*, The electric power engineering
  series., CRC Press, Boca Raton, Fla.

Cassoret, B., Lopez, S., Brudny, J. F. and Belgrand, T. (2014). Non-segmented grain oriented steel in
  induction machines, *Progress In Electromagnetics Research C* **47**: 1–10.

Council of European Union (2019). Commission regulation (EU) no 2019/1781.
  URL: *https://eur-lex.europa.eu/eli/reg/2019/1781/oj*

EBM-Pabst (2024). Ec-motor dv280: A green heart for large fans.
  URL:
  https://www.ebmpapst.com/at/en/products/motors-and-drive-systems/ec-external-rotor-motors.html

Finken, T., Felden, M. and Hameyer, K. (2008). Comparison and design of different electrical machine
  types regarding their applicability in hybrid electrical vehicles, *2008 18th International Conference
  on Electrical Machines*, pp. 1–5.

Fiorillo, F. (2010). Measurements of magnetic materials, *Metrologia* **47**: S114.

Haque, N., Hughes, A., Lim, S. and Vernon, C. (2014). Rare earth elements: Overview of mining,
  mineralogy, uses, sustainability and environmental impact, *Resources* **3**(4): 614–635.

Helonde, A. and Mankar, M. (2019). Identifying three phase induction motor equivalent circuit
  parameters from nameplate data by different analytical methods, *International Journal of Trend in
  Scientific Research and Development* **Volume-3**: 642–645.

Hess, D. and Soom, A. (1990). Friction at a lubricated line contact operating at oscillating sliding
  velocities, *Journal of Tribology-transactions of The Asme - J TRIBOL-TRANS ASME* **112**.

IEC 60034-1 (2010). Rotating electrical machnies - Part 1: Rating and performance, *Standard*,
  International Electrotechinal Comission, Geneva, CH.

IEC 60034-12:2016 (2016). Rotating electrical machines – Part 12: Starting performance of
  single-speed three-phase cage induction motors, *Standard*, International Electrotechnical Comission,
  Geneva, CH.

IEC 60034-2-1:2014 (2014). Rotating electrical machines – Part 2-1: Standard methods for determining
  losses and efficiency from tests (excluding machines for traction vehicles), *Standard*, International
  Electrotechnical Comission, Geneva, CH.

IEC 60034-30-1:2014 (2014). Rotating electrical machines - Part 30-1: Efficiency classes of line
  operated AC motors (IE code), *Standard*, International Electrotechinal Comission, Geneva, CH.

IEC 60034-6:1991 (1991). Rotating electrical machines - Part 6: Methods of cooling (IC Code),
  Standard, International Electrotechinal Comission, Geneva, CH.

IEC 60085:2007 ED4 (2007). Electriacal Insulation - Thermal Evaluation and Designation, *Standard*, International Electrotechinal Comission, Geneva, CH.

IEC 60317-0-1 (2013). Specifications for particular types of winding wires – Part 0-1: General requirements – Enamelled round copper wire, *Standard*, International Electrotechinal Comission, Geneva, CH.

IEEE std 112 - 2017 (2017). IEEE Standard Test Procedure for Polyphase Induction Motors and Generators (std 112), *Standard*, Institute of Electrical and Electronics Engineers, 3 Park Avenue New York, NY 10016-5997 USA.

Jandrlic, I. and Reskovic, S. (2015). Choosing the optimal coating for thermographic inspection, *Holistic approach to environment* **5**(3): 127–127.

Khade, S. (2013). Measurement of rotor leakage reactance of induction motor, *Int. J. Elect., Electron. Data Commun.* **1**(3): 49–51.

Liang, X. and Luy, Y. (2006). Harmonic analysis for induction motors, *2006 Canadian Conference on Electrical and Computer Engineering*, pp. 172–177.

Mierczak, L., Klimczyk, P., Hennies, D., Denke, P. and Siebert, S. (2020). Influence of manufacturing processes on magnetic properties of stator cores, *2020 International Conference on Electrical Machines (ICEM)*, Vol. 1, pp. 901–908.

Sen, P. (2013). *Principles of Electric Machines and Power Electronics*, Wiley.

Steinmetz, C. P. (1892). On the law of hysteresis, *Transactions of the American Institute of Electrical Engineers* **IX**(1): 1–64.

Tapani Jokinen, Valeria Hrabovcova, J. P. (2013). *Design of Rotating Electrical Machines*, second edition. edn, Wiley, Newark.

Tong, W. (2022). *Mechanical design and manufacturing of electric motors*, second edition. edn, CRC Press, Boca Raton.

UL 1004-1 (2020). UL Standard for Safety for Rotating Electrical Machines - General Requirements, *Standard*, Underwriters Laboratories INC., Northbrook, IL.

Ziehl-Abegg (2024). External rotor motor.
URL: *https://www.ziehl-abegg.com/en/glossary/external-rotor-motor*

Appendix A

Technical Datasheet for FAB112M

MULTI-WING™

Technical data sheet (TDS)

Type:	AC~3 - motor				Project MW:	ENQ
Standard series:	IEC 60034				Type:	FAB112M-4-B14

Electrical data					General data	
Rated power:	4,00	4,60	4,60	kW	Frame size:	112M
Poles:		4			Degree of protection:	IP55
Speed:	1456	1750	1759	1/min	Frame material:	Housing: Aluminium DE-shield/flange: Cast iron NDE-Shield: Cast iron
Rated torque (T$_N$):	26,2	25,1	25,0	Nm	Build form:	B14 FT130
Rated voltage Δ/Y:	230/400	Y440	Y 480	V	Corrosion class:	C3M
Frequency:	50	60	60	Hz	Color:	RAL9005
Rated current:	14,51/8,42	7,97	7,54	A	Insulation class/Temperature rise:	H/(50K)
Power factor (Cos φ):	0,82	0,85	0,82		Insulation system:	Standard
Efficiency 100%:	88,6	89,1	89,5	%	Duty type:	S1 (AO)
Efficiency 75%:	87,4	89,5	89,5	%	Cooling:	IC418 (TEAO)
Efficiency 50%:	85,1	88,7	88,1	%	DE bearing:	6206-2Z/C3 WT
Efficiency class:	IE3	IE2	IE2		NDE bearing:	6206-2Z/C3 WT
Phase resistance @ 25°C:		1,09		Ω	Bearing brand:	SKF
Enviromental conditions					Moment of inertia:	1,513*10^{-4} kgm²
Ambient temperature:		-35 to 90		°C	Vibration grade:	A
Ambient humidity:		0 - 95		%	Rotation direction:	CCW
Tropicalized windings:		N/A			Weight:	35 kg
Altitude above sea level:		1000		m	Noise level (LpA):	55 dB(A)

Additional info		
Cable entry main:	1 x M25x1,5 Plastic cable gland Ø13 - 18mm	Thermal protection (PTO):	1 x 160°C
Cable entry acc.:	1 x M12x1,5 Plastic blind plug	Space heater:	N/A
Cable:	N/A	PTC:	N/A
Shaft:	IECm standard + k6 tolerance Ø28	PT100 bearing:	N/A
Fasteners:	SST - A2	PT100 windings:	N/A

Water slinger DE, Inverter duty operation

Version 1 - 10.07.2023

Technical and ordering data are subject to change / There may be discrepancies between calculated and rating plate data.
Declared values are subject to tolerances in accordance to IEC 60034-1

Appendix B

Technical Datasheet for UMP-3C3-210-4

Technical data sheet (TDS)

Type:	AC~3 - motor		Project MW:	M22-139.2
Standard series:	IEC 60034		Type:	UMP-3C3-210-25-4

Electrical data			General data	
Rated power:	4.00	kW	Frame size:	UMP 210
Poles:	4		Degree of protection:	IP55
Speed:	1462	1/min	Frame material:	Housing: Aluminium DE-shield/flange: Aluminium NDE-Shield: Aluminium
Rated torque (T_N):	25.5	Nm	Build form:	B30
Rated voltage Δ/Y:	400/690	V	Corrosion class:	CX
Frequency:	50	Hz	Color:	RAL9005
Rated current:	7.86/4.55	A	Insulation class/Temperature rise:	F/B
Power factor (Cos φ):	0.83		Insulation system:	Reinforced
Efficiency (100% / 75% / 50%):	88,6 / 89.0/88.0	%	Duty type:	S1 (AO)
Efficiency class:	IE3		Cooling:	IC418 (TEAO)
Breakdown torque (T_{BD}/T_N):	3.15		DE bearing:	6206-2RS1/C3 WT
Locked rotor torque (T_{LR}/T_N):	2.65			
Starting current:	63.7/36.9	A	NDE bearing:	6204-2Z/C3 WT
No-load current:	3.91/2.26			
Phase resistance @ 25°C:	3.51	Ω	Bearing brand:	SKF
Enviromental conditions			Moment of inertia:	$2.35*10^{-3}$ kgm^2
Ambient temperature:	-20 to 45	°C	Vibration grade:	A
Ambient humidity:	30 - 80	%	Rotation direction:	CCW
Tropicalized windings:	N/A		Weight:	35kg
Altitude above sea level:	1000	m	Noise level (LpA):	60 dB(A)

Additional info			
Cable entry main:	1 x M20x1,5 Plastic cable gland	Thermal protection (PTO):	N/A
Cable entry acc.:	N/A	Space heater:	N/A
Cable:	Acc. DWG TBD 1x 1,5meter	PTC:	N/A
Shaft:	IEC standard	PT100 bearing:	N/A
Fasteners:	SST - A2	PT100 windings:	N/A

UL/CSA E- TBD, Double stator winding impregnation

Version   1   -   20.06.2023

Technical and ordering data are subject to change / There may be discrepancies between calculated and rating plate data.
Declared values are subject to tolerances in accordance to IEC 60034-1

Appendix C

IE class tables

Table C.1: Nominal efficiency limits (%) for 50 Hz IE3 according to IEC 60034-30-1:2014 (2014)

Rated power kW	Number of poles/Synchronous speed min^{-1}			
	2/3000	4/1500	6/1000	8/750
0.12	60.8	64.8	57.7	50.7
0.18	65.9	69.9	63.9	58.7
0.20	67.2	71.1	65.4	60.6
0.25	69.7	73.5	68.6	64.1
0.37	73.8	77.3	73.5	69.3
0.40	74.6	78.0	74.4	70.1
0.55	77.8	80.8	77.2	73.0
0.75	80.7	82.5	78.9	75.0
1.1	82.7	84.1	81.0	77.7
1.5	84.2	85.3	82.5	79.7
2.2	85.9	86.7	84.3	81.9
3	87.1	87.7	85.6	83.5
4	88.1	88.6	86.8	84.8
5.5	89.2	89.6	88.0	86.2
7.5	90.1	90.4	89.1	87.3
11	91.2	91.4	90.3	88.6
15	91.9	92.1	91.2	89.6
18.5	92.4	92.6	91.7	90.1
22	92.7	93.0	92.2	90.6
30	93.3	93.6	92.9	91.3
37	93.7	93.9	93.3	91.8
45	94.0	94.2	93.7	92.2
55	94.3	94.6	94.1	92.5
75	94.7	95.0	94.6	93.1
90	95.0	95.2	94.9	93.4
110	95.2	95.4	95.1	93.7
132	95.4	95.6	95.4	94.0
160	95.6	95.8	95.6	94.3
200-1000	95.8	96.0	95.8	94.6

Table C.2: Nominal efficiency limits (%) for 60 Hz IE3 according to IEC 60034-30-1:2014 (2014)

Rated power kW	Number of poles/Synchronous speed min^{-1}			
	2/3600	4/1800	6/1200	8/900
0.12	62.0	66.0	64.0	59.5
0.18	65.6	69.5	67.5	64.0
0.25	69.5	73.4	71.4	68.0
0.37	73.4	78.2	75.3	72.0
0.55	76.8	81.1	81.7	74.0
0.75	77.0	83.5	82.5	75.5
1.1	84.0	86.5	87.5	78.5
1.5	85.5	86.5	88.5	84.0
2.2	86.5	89.5	89.5	85.5
3.7	88.5	89.5	89.5	86.5
5.5	89.5	91.7	91.0	86.5
7.5	90.2	91.7	91.0	89.5
11	91.0	92.4	91.7	89.5
15	91.0	93.0	91.7	90.2
18.5	91.7	93.6	93.0	90.2
22	91.7	93.6	93.0	91.7
30	92.4	94.1	94.1	91.7
37	93.0	94.5	94.1	92.4
45	93.6	95.0	94.5	92.4
55	93.6	95.4	94.5	93.6
75	94.1	95.4	95.0	93.6
90	95.0	95.4	95.0	94.1
110	95.0	95.8	95.8	94.1
150	95.0	95.8	95.8	94.5
185-1000	95.8	96.2	95.8	95.0

Appendix D

Technical Datasheet for Y3PE112M

MOLL-MOTOR

DIE MECHATRONISCHE ANTRIEBSTECHNIK

Datenblatt für Drehstrom-Käfigläufermotoren
datasheet for three-phase squirrel-cage-motors

Teilenummer:
article code:

Y3PE112M4B34F1

U [V]	Δ / Y	f [Hz]	P [kW]	I [A]	n [1/min]	M [Nm]	NOM.Eff at…load [%] 4/4	3/4	2/4	cos φ 4/4	3/4	2/4	I$_A$/I$_N$ I$_I$/I$_N$	M$_A$/M$_N$ T$_I$/T$_N$	M$_K$/M$_N$ T$_B$/T$_N$	IE-CL
400	Δ	50	4	7,95	1460	26,2	88,7	89,4	87,9	0,82	-	-	7,8	2,2	2,3	IE3
690	Y	50	4	4,61	1460	26,2	88,7	89,4	87,9	0,82	-	-	7,8	2,2	2,3	IE3
460	Δ	60	4,6	7,68	1752	25,1	91,7	-	-	-	-	-	-	-	-	-
795	Y	60	4,6	4,44	1752	25,1	91,7	-	-	-	-	-	-	-	-	-

Mechanische Daten / *mechanical data*			
Trägheitsmoment Jmot *moment of inertia Jmot*	0,0139		[kgm²]
Schalldruckpegel LpA (r=1m) 50Hz / 60Hz *noise level LpA(r=1m) 50Hz / 60Hz*	54	61	[dB]
Schwingstufengröße *vibration severity grade*	A		

Ausführungen / *versions*		
Lagertype A/B-Seite *DE/NDE bearing design*	6306-2RZ C3	6306-2RZ C3
Farbe, Farbton *color, paint shade*	RAL7030 (Steingrau) *RAL 7030 (stone grey)*	
Endanstrich *coating (paint finish)*	- -	

Umgebungsbedingungen / *environmental conditions*		
Umgebungstemperatur *ambient temperature*	-20°C - +40°C	
Höhe über Meeresspiegel *altitude above sea level*	1000	[m]

Explosionsschutz / *explosion protection*	
Zündschutzart *type of ex-protection*	keine *none*

Bemerkungen / *remarks*

Allgemeine Daten / *general data*		
Baugröße *size*	112M	
Bauform *type of construction*	B34F1	
Klemmkastenlage *terminal box position*	oben *top*	
Gewicht *weight*	40	[kg]
Gehäusematerial *frame material*	Aluminium *aluminum*	
Schutzart *degree of protection*	IP55	
Isolationsklasse *insulation class*	155(F) nach 130(B) *155(F) to 130(B)*	
Betriebsart *duty type*	S1=Dauerbetrieb *S1=continuous duty*	
Drehrichtung *direction of rotation*	bidirektional *bidirectional*	
Kühlart *method of cooling*	IC411 - Eigenbelüftet *IC411 - self ventilated*	

Zusatzoptionen / *additional options*

Hinweise / *Notes*

IA=Anzugsstrom, IN=Bemessungsstrom
II=Starting current, IN=Nominal current
MA=Anzugsmoment, MK=Kippmoment, MN=Bemessungsmoment
TI=Starting torque, TB=Breaking point torque, TN=Nominal Torque

Technische Änderungen vorbehalten. Es können Abweichungen von kalkulierten- und Leistungsschilddaten entstehen.
Technical and ordering data are subject to change. There may be discrepancies between calculated and rating plate data.

Version   092020

Appendix E

Guideline for DC Test

E.1   Objective

This test is performed in order to measure the resistance across windings of a single phase in a three phase induction machine. The measured resistance can then be used to determine the value of the parameter R_1, in the steady state model of a three phase induction machineseen in Figure 5.3.

E.2   Methodology

E.2.1   List of Materials

- Multimeter
- Measuring probes
- Three phase AC induction machine for measurements
- Thermostat

E.2.2   Procedure

1. Ensure the machine has been turned off for long enough to be at room temperature.

2. Use the thermostat to measure the room temperature, hence the machine temperature assuming it has reached room temperature, and note it.

3. Measure the resistance in your equipment, by connecting the two measuring probes, as illustrated in Figure E.1.

Figure E.1: Measuring of resistance in equipment

4. Ensure the AC machine is disconnected and is stationary.

5. Then measure the resistance across a phase by measuring at the shoe of the phase wire, as illustrated in Figure E.2.
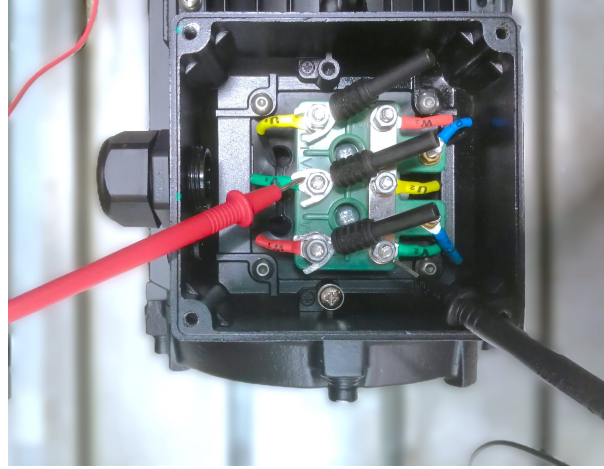
Figure E.2: Measuring of resistance in a phase

6. Remember to note both the equipment resistance and the per phase resistance

E.3 Data Analysis Methods

In order to find the exact measured per phase resistance, the measured per phase resistance has to be subtracted from the equipment resistance as shown in (E.1)

$$R_{DC\_phase\_exact} = R_{DC\_phase\_measured} - R_{DC\_equipment} \tag{E.1}$$

If there is a lot of noise around the equipment it would be a good idea to take multiple readings and average them out, by taking the mean value. This can be done over e.g. five readings and calculated as shown in (E.2) and (E.3)

$$R_{M\_DC\_phase\_exact} = \frac{\sum_{n=1}^{5} R_{DC\_phase\_exact_n}}{5} \tag{E.2}$$

$$t_{M\_DC} = \frac{\sum_{n=1}^{5} t_{DC_n}}{5} \tag{E.3}$$

Appendix F

Guideline for No Load Test

F.1 Objective

This test is performed in order to determine the machine parameters of a three phase AC machine. The measurements can be used to determine power, current, resistance and voltage at no load of the AC machine. This is primarily used for iron loss and mutual flux calculations.

F.2 Methodology

F.2.1 List of Materials

- Three phase AC induction machine for measurements
- Three phase variable voltage transformer (variotrafo)
- Three phase power analyzer
- Connection lead wires
- Cable shoes for connection lead wires
- Three phase AC power supply
- Mount for the AC induction machine

F.2.2 Procedure

1. Ensure the AC machine is disconnected from any mechanical load, is stationary, and firmly attached to the mount on the lab table.

2. Connect the cable shoes to each phase in the AC machine, as shown in Figure F.1. (In the picture it is done for a Y connection)
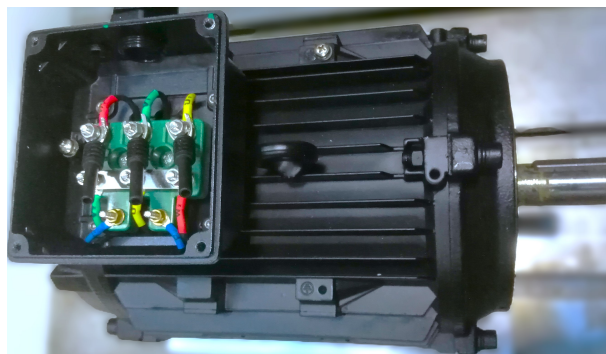
Figure F.1: Cable shoes mounted onto each phase in the AC machine

3. If the machine has no natural cooling e.g. a cooling fan, a separate fan should be used, since these machines often are made either for a ventilation fan or having another cooling system installed

later. This was done for the test with the FAB112M as seen in Figure F.2.

Figure F.2: External fan for cooling of FAB112M

4. Then connect each shoe to a connection lead wire, as shown in Figure F.3. (In the picture it is done for a Y connection)
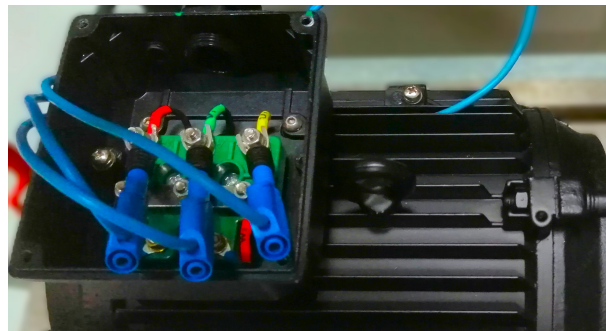
Figure F.3: Connection lead wires connected to the cable shoes

5. Connect the connection lead wires to the three phase power analyzer

6. connect the three phase power analyser to the variable voltage transformer (variotrafo). Hence the variotrafo is connected to the AC machine trough the three phase power analyzer. An example of the AC machine connected to the power analyser and variotrafo can be seen illustrated in Figure F.4.
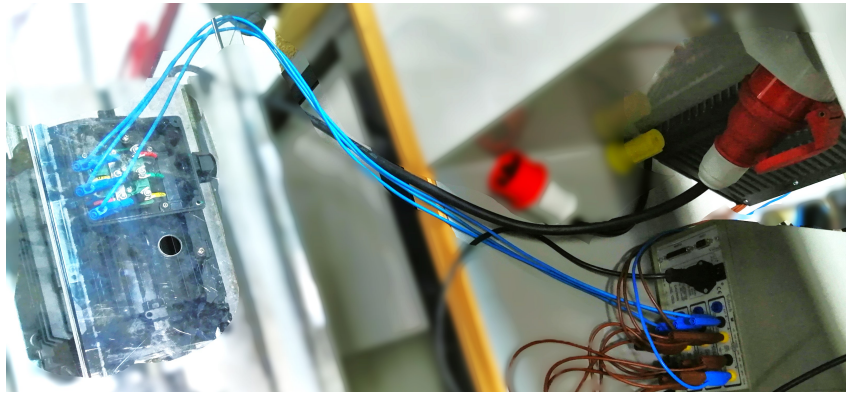
Figure F.4: Example of AC machine connected to power analyser and variotrafo

7. Setup enclosures such as acrylic enclosure for machine and fence. An example of this can be seen illustrated in Figure F.5.
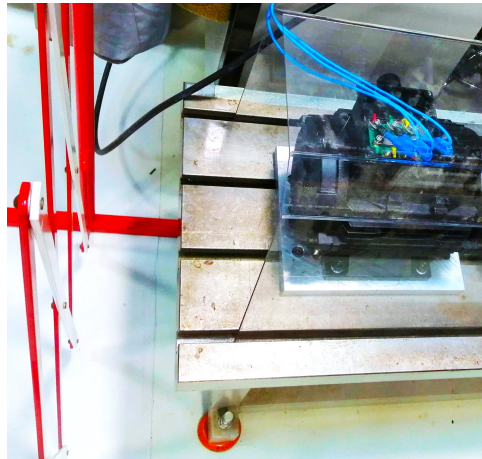
Figure F.5: Example of fence and acrylic enclosure for the AC machine during tests.

8. Start the three phase power analyzer and connect the variotrafo to the three phase AC power supply. An illustration of the power analyser and the variotrafo can be seen in Figure F.6 and Figure F.7.
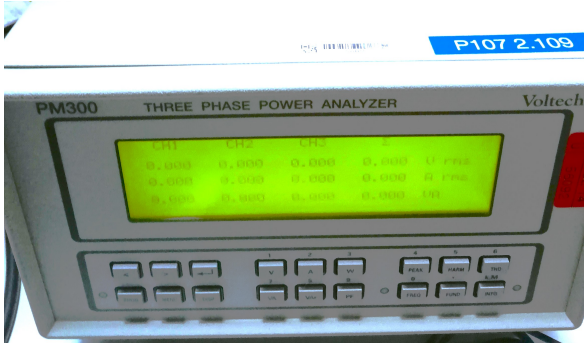
Figure F.6: Picture of power analyser at zero voltage input
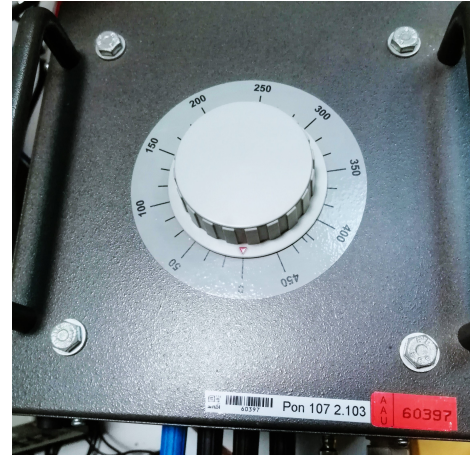
Figure F.7: Picture of variotrafo set to zero voltage

9. Measurements can now begin and will be done as follows: Test at three or more values of voltages between 125% and 75% of the nominal voltage, with a point near 100% rated voltage, and three or more values of voltage between 50% of rated voltage and 20% of rated voltage or to that point where further voltage reduction increases the current. This is based of IEEE std 112 - 2017 (2017), furthermore it is expected that the frequency applied during no load tests is equal to the rated frequency.

10. Start at the lowest voltage for measurements, hence set the variotrafo to this voltage. Sometimes the variotrafo is not that precises, so adjust according to the values on the power analyser instead.

11. Wait a couple of minutes until the numbers on the power analyzer has somewhat settled and note the measurements.

12. Then set the variotrafo to the next voltage range, wait a couple of minutes for the power analyzer numbers to settle and note the measurements.

13. Repeat the step above for the rest of the voltage ranges which needs to be tested at.

14. After taking the last voltage measurement turn off the variotrafo, and wait for the machine to stop spinning.

15. Then as quickly as possible perform a DC test as described in Appendix E, but skip step 1 and 2 in order to find the resistance during the no load tests.

F.3 Data Analysis Methods

In order to find the exact measured per phase resistance, the measured per phase resistance has to be subtracted from the equipment resistance as shown in (F.1)

$$R_{NL,LL} = R_{NL,LL\_measured} - R_{NL,LL\_equipment} \tag{F.1}$$

If there is a lot of noise around the equipment it would be a good idea to take multiple readings and average them out, by taking the mean value. This can be done over e.g. five readings and calculated as shown in (F.2), (F.3), (F.4), and (F.5).

$$\overline{U}_{NL,LL} = \frac{\sum_{n=1}^{5} U_{NL,LL_n}}{5} \tag{F.2}$$

$$\bar{I}_{NL,LL} = \frac{\sum_{n=1}^{5} I_{NL,LL_n}}{5} \tag{F.3}$$

$$\bar{P}_{NL} = \frac{\sum_{n=1}^{5} P_{NL_n}}{5} \tag{F.4}$$

$$\bar{R}_{NL,LL} = \frac{\sum_{n=1}^{5} R_{NL,LL_n}}{5} \tag{F.5}$$

Remember to correct the current and voltage to per phase depending on which configuration the machine had during the test:

For a Δ configured machine the voltage and current per phase is determined as seen in (F.6) and (F.7).

$$U_{NL} = \bar{U}_{NL,LL} \tag{F.6}$$

$$I_{NL} = \frac{\bar{I}_{NL,LL}}{\sqrt{3}} \tag{F.7}$$

For a Y configured machine the voltage and current per phase is determined as seen in (F.8) and (F.9)

$$U_{NL} = \frac{\bar{U}_{NL,LL}}{\sqrt{3}} \tag{F.8}$$

$$I_{NL} = \bar{I}_{NL,LL} \tag{F.9}$$

Appendix G

Guideline for Locked Rotor Test

G.1 Objective

The objective of this experiment is to conduct a locked rotor test on a three-phase AC machine to determine its key parameters, including locked rotor current, locked rotor torque, and locked rotor power factor, using two wattmeters to measure input power and line voltage. This experiment is applicable to both Δ and Y (star) configurations of three-phase AC machines.

G.2 Methodology

G.2.1 List of Materials

- Three phase AC induction machine for measurements
- Variable frequency and voltage drive (frequency converter)
- Three phase power analyzer
- Connection lead wires
- Cable shoes for connection lead wires
- Three phase AC power supply
- Mount for the AC induction machine
- Mount for locking the AC machines rotor in place

G.2.2 Procedure

1. Ensure the AC machine is disconnected from any mechanical load, is stationary, and firmly attached to the mount on the lab table.

2. Then lock the rotor in place using the mount, an example can be seen in Figure G.1.

Figure G.1: Cable shoes mounted onto each phase in the AC machine

3. Connect the cable shoes to each phase in the AC machine, as shown in Figure G.2 (In the picture it is done for a Y connection)
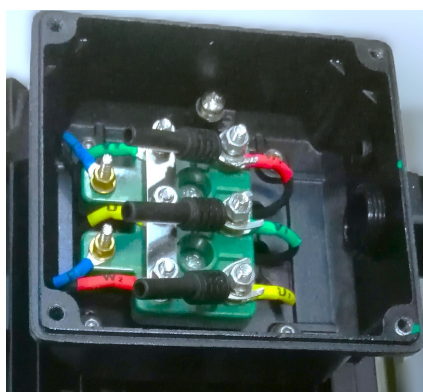
Figure G.2: Cable shoes mounted onto each phase in the AC machine

4. Connect each shoe to a connection lead wire, as shown in Figure G.3. (In the picture it is done for a Y connection)
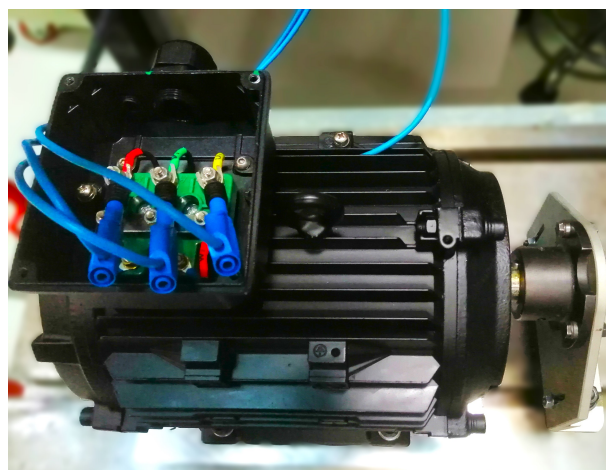
Figure G.3: Connection lead wires connected to the cable shoes

5. Connect the connection lead wires to the three phase power analyzer

6. Connect the power analyzer to the variable frequency and voltage drive (frequency converter), so the AC machine is connected to the frequency converter trough the power analyzer.

7. Setup enclosures such as acrylic enclosure for machine and fence. An example of this can be seen illustrated in Figure G.4.
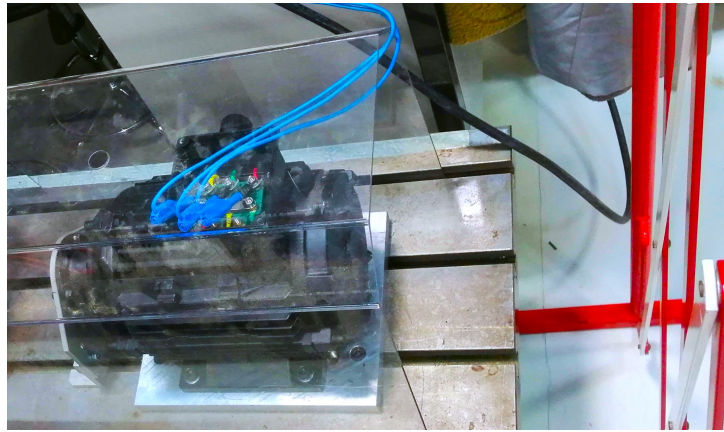
Figure G.4: Example of fence and acrylic enclosure for the AC machine during tests.

8. While the frequency converter is turned off, adjust the frequency settings. Based off the IEEE std 112 - 2017 (2017), the locked rotor tests should be run at a max of 25% rated frequency, however not all frequency converters can run at that low frequencies so get it as low as possible, but always lower than rated.

9. Turn on the power analyser and connect the frequency converter to the AC power supply. An illustration of the power analyser and the frequency converter can be seen in Figure G.5 and Figure G.6.
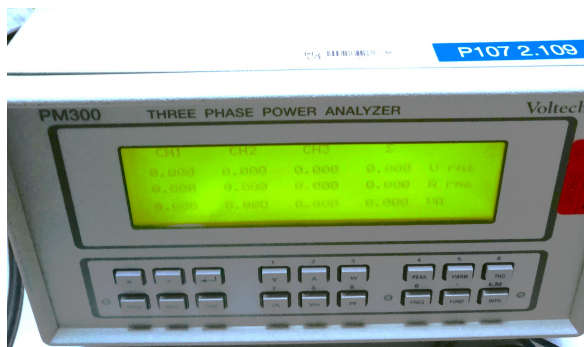
Figure G.5: Picture of power analyser at zero voltage input

Figure G.6: Picture of the frequency converter

10. Measurements can now begin and should be done as quickly as possible, using the adjustable voltage function in the frequency converter, adjust until the current is just below the rated current.

11. After this wait for a couple of seconds until the numbers on the power analyzer has somewhat stabilized and note the measurements.

12. After noting the measurements turn off the frequency converter.

13. Then as quickly as possible perform a DC test as described in Appendix E, but skip step 1 and 2 in order to find the resistance during the locked rotor test.

G.3 Data Analysis Methods

In order to find the exact measured per phase resistance, the measured per phase resistance has to be subtracted from the equipment resistance as shown in (G.1)

$$R_{LR,LL} = R_{LR,LL\_measured} - R_{LR,LL\_equipment} \tag{G.1}$$

If there is a lot of noise around the equipment it would be a good idea to take multiple readings and average them out, by taking the mean value. This can be done over e.g. five readings and calculated as shown in (G.2), (G.3), (G.4), and (G.5).

$$\overline{U}_{LR,LL} = \frac{\sum_{n=1}^{5} U_{LR,LL_n}}{5} \tag{G.2}$$

$$\overline{I}_{LR,LL} = \frac{\sum_{n=1}^{5} I_{LR,LL_n}}{5} \tag{G.3}$$

$$\overline{P}_{LR} = \frac{\sum_{n=1}^{5} P_{LR_n}}{5} \tag{G.4}$$

$$\overline{R}_{LR,LL} = \frac{\sum_{n=1}^{5} R_{LR,LL_n}}{5} \tag{G.5}$$

Remember to correct the current and voltage to per phase depending on which configuration the machine had during the test:

For a Δ configured machine the voltage and current per phase is determined as seen in (G.6) and (G.7).

$$U_{NL} = \overline{U}_{NL,LL} \tag{G.6}$$

$$I_{NL} = \frac{\overline{I}_{NL,LL}}{\sqrt{3}} \tag{G.7}$$

For a Y configured machine the voltage and current per phase is determined as seen in (G.8) and (G.9)

$$U_{NL} = \frac{\overline{U}_{NL,LL}}{\sqrt{3}} \tag{G.8}$$

$$I_{NL} = \overline{I}_{NL,LL} \tag{G.9}$$

Appendix H

Test data for Y3PE112M machine

H.1 Data From DC Test

Table H.1: DC test measurement for the Y3PE112M4 both line to line and per phase seen as Y configured

DC test data		
T_{DC} [°C]	$R_{1_{DC,LL}}$ [Ω]	$R_{1_{DC}}$ [Ω]
22	2.15	1.08

H.2 Data From No Load Test

Table H.2: No load test measurements for the Y3PE112M4 both line to line and per phase seen as Y configured

No-load data						
$R_{1_{NL,LL}}$ [Ω]	$R_{1_{NL}}$ [Ω]	$U_{NL,LL}$ [V]	U_{NL} [V]	$I_{NL,LL} = I_{NL}$ [A]	P_{NL} [W]	f_{NL} [Hz]
2.27	1.14	445	257	5.63	374	50
2.27	1.14	400	231	4.20	267	50
2.27	1.14	300	173	2.71	151	50
2.27	1.14	240	139	2.09	108	50
2.27	1.14	200	115	1.72	85.5	50
2.27	1.14	160	92.6	1.37	67.2	50
2.27	1.14	120	69.4	1.04	52.7	50
2.27	1.14	80.2	46.3	0.748	40.7	50
2.27	1.14	40.2	23.2	0.636	34.0	50

H.3 Data From Locked Rotor Test

Table H.3: Locked rotor test measurements for the Y3PE112M4 both line to line and per phase seen as Y configured

			Locked rotor data				
T_{LR}	$R_{1_{LR,LL}}$ [Ω]	$R_{1_{LR}}$ [Ω]	$U_{LR,LL}$ [V]	U_{LR} [V]	$I_{NL,LL} = I_{NL}$ [A]	P_{LR} [W]	f_{LR} [Hz]
25.8	2.18	1.09	15.7	9.07	3.84	85.5	15.0
27.5	2.20	1.10	17.8	10.3	3.77	88.6	20.0
29.6	2.21	1.11	19.8	11.4	3.82	88.6	25.0
29.2	2.21	1.11	22.1	12.7	3.81	90.4	30.0
30.6	2.22	1.11	24.5	14.1	3.82	93.0	35.0
33.0	2.24	1.12	55.2	31.9	7.96	415	40.0
36.1	2.27	1.13	57.3	33.1	7.55	384	45.0
40.6	2.31	1.15	62.0	35.8	7.50	392	50.0
42.8	2.32	1.16	67.6	39.0	7.57	410	55.0
44.7	2.34	1.17	71.7	41.4	7.50	410	60.0

H.4 Data from load test

			Load test data				
$U_{LT,LL}$ [V]	$I_{LT,LL}$ [A]	P_{LT} [W]	T_{LT} [°C]	$R_{LT,LL}$ [Ω]	τ_{LT} [Nm]	n_{LT} [rpm]	$P_{LT,mech}$ [W]
405	9.85	5902	67.9	2.53	33.66	1441	5079
401	9.08	5321	62.3	2.48	30.45	1447	4613
400	8.08	4613	65.5	2.51	26.41	1454	4022
400	6.62	3485	59.5	2.46	19.82	1466	3043
400	5.35	2383	56.7	2.43	13.17	1479	2040
400	4.46	1322	54.3	2.41	6.77	1490	1056

Table H.4: Results from load test on Y3PE112M4 at thermal settling

Appendix I

Test description load test

I.1 Objective

The objective of the load test is to evaluate the performance and reliability of induction machines under various load conditions.

I.2 Methodology

I.2.1 List of materials

- Three phase AC induction machine for testing
- Three phase variable voltage transformer (variotrafo)
- Three phase power analyzer
- Connection lead wires
- Cable shoes for connection lead wires
- Three phase AC power supply
- Mount for the AC induction machine
- Multimeter
- Dynamometer
- Load machine with a drive
- Coupling between load machine and machine for testing

I.2.2 Setup

The machine is mounted in a drive test bench, which includes a dynamometer and load machine as seen in I.1.
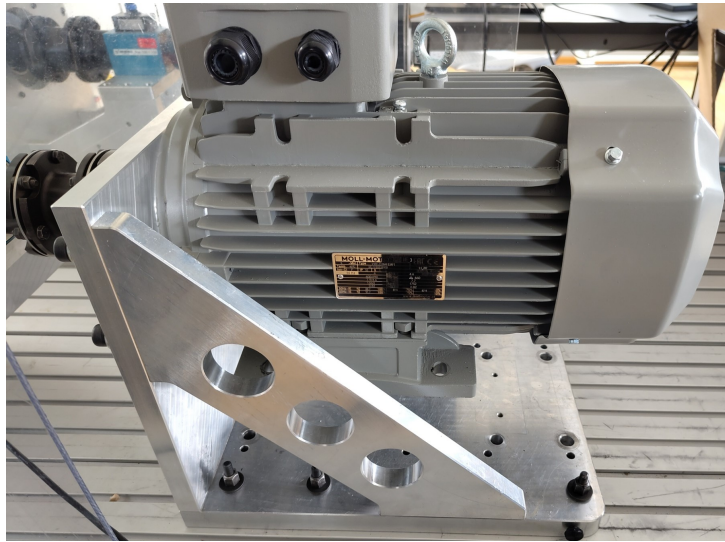
Figure I.1: Y3PE112M4 mounted in the drive test bench

The machine is then connected to a varotrafo through a three phase power analyser, as seen in Figure I.2.
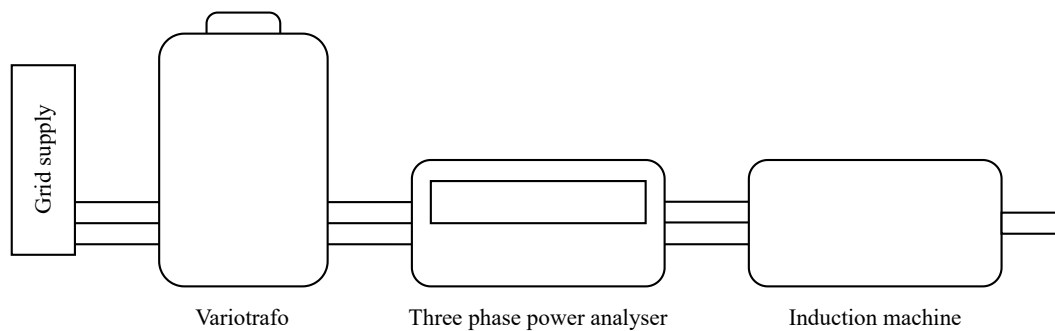
Figure I.2: Machine connection through variotrafo and three phase power analyser

I.2.3 Procedure

1. Ensure a DC resistance test has been made before this

2. Ensure the AC machine is aligned correctly in the test bench using an appropriate mount.

3. Turn on the drive of the load machine, without loading it.

4. Tare the dynamometer

5. Connect the machine for testing to the variotrafo through the three-phase power analyzer.

6. Turn the variotrafo on and adjust until the voltage at the load point is roughly obtained

7. Use the load machine drive to load the machines at the desired load point

8. Adjust the voltage on the variotrafo again until the desired voltage during load is obtained

9. Wait until the machine has settled at the desired thermal point

10. When thermal settling is done, measure by e.g. taking pictures of the 3-phase power analyzer and the dynamometer screens.

11. Right after measurements are taken, get ready for another DC resistance measurement test.

12. Stop loading the machines by turning off the load control in the drive of the load machine.

13. Turn off the variotrafo, hence stopping the test machine.

14. Both the load and test machine should be turned off at this point, so wait for the rotation to die out.

15. Measure the line-to-line DC resistance across the windings, do this as quickly as possible to not lose the thermal settling temperature.

16. Having performed the load tests, the dynamometer should be checked for drifting.

17. Set the load machine drive to speed control, without turning it on.

18. Do NOT tare the dynamometer but note what the tare value is.

19. Turn on the test machine by turning on the variotrafo.

20. Turn on the speed control and set it to 500 RPM.

21. Wait for the torque to settle, then note the torque measured at this speed point.

22. Then set the speed control to 750 RPM.

23. Wait for the torque to settle, then note the torque measured at this speed point.

24. Repeat the two steps above until the following speed points have been tested: 1500, 1250, 1000, 750, 500, -500, -750, -1000, -1250, -1500.

25. The measured torque at the different speeds can then be used to check for torque bias during measurements.

I.3   Data analysis Methods

First the DC bias of the torque sensor in the dynamometer, must be accounted for. To do this the torque measurements at different speeds, are used as seen in (I.1).

$$\tau_{bias} = \frac{\tau_{+1500} + \tau_{+1250} + \tau_{+1000} + \tau_{+750} + \tau_{+500} + \tau_{-1500} + \tau_{-1250} + \tau_{-1000} + \tau_{-750} + \tau_{-500}}{10} \qquad (I.1)$$

This torque bias must then be subtracted from all the torque measurement from the test, before calculating the exact load point values as seen in (I.2).

$$P_{mech} = (\tau_{measured} - \tau_{bias}) \cdot \frac{2 \cdot \pi}{60} \cdot n_{meaured} \qquad (I.2)$$

Appendix J

Test data for FAB112M-4

J.1   Data from load test

Load test data							
$U_{LT,LL}$ [V]	$I_{LT,LL}$ [A]	P_{LT} [W]	T_{LT} [°C]	$R_{LT,LL}$ [Ω]	τ_{LT} [Nm]	n_{LT} [rpm]	$P_{LT,mech}$ [W]
402	9.99	5945	76.8	2.53	33.60	1433	5042
401	9.19	5396	76.0	2.52	30.58	1439	4608
399	8.09	4630	76.4	2.53	26.29	1450	3992
402	6.49	3459	78.0	2.54	19.56	1463	2997
401	5.21	2377	73.5	2.50	13.11	1476	2026
402	4.25	1290	78.4	2.54	6.45	1487	1004

Table J.1: Results from load test on FAB112M-4 at 70-80 °C winding temperature

Load test data							
$U_{LT,LL}$ [V]	$I_{LT,LL}$ [A]	P_{LT} [W]	T_{LT} [°C]	$R_{LT,LL}$ [Ω]	τ_{LT} [Nm]	n_{LT} [rpm]	$P_{LT,mech}$ [W]
400	9.93	5871	56.5	2.37	33.21	1438	5001
399	9.20	5365	55.5	2.36	30.38	1445	4597
404	8.09	4629	55.5	2.36	26.22	1455	3995
401	6.57	2496	53.6	2.34	19.49	1467	2994
403	5.22	2352	56.7	2.37	12.81	1479	1984
400	4.26	1309	53.8	2.34	6.52	1490	1018

Table J.2: Results from load test on FAB112M-4 at 50-60 °C winding temperature

Load test data							
$U_{LT,LL}$ [V]	$I_{LT,LL}$ [A]	P_{LT} [W]	T_{LT} [°C]	$R_{LT,LL}$ [Ω]	τ_{LT} [Nm]	n_{LT} [rpm]	$P_{LT,mech}$ [W]
401	9.87	5825	38.3	2.25	32.82	1445	4967
402	9.19	5369	37.7	2.25	30.40	1450	4617
399	8.11	4604	38.9	2.26	26.02	1456	3968
400	6.57	3479	38.7	2.25	19.60	1468	3014
401	5.23	2356	37.7	2.25	12.80	1479	1983
401	4.32	1247	36.5	2.24	6.51	1488	1015

Table J.3: Results from load test on FAB112M-4 at 30-40 °C winding temperature

Appendix K

Test data for UMP-3C3-210-25-4

K.1 Data From DC Test

Table K.1: DC test measurement for the UMP-3C3-210-25-4 both line to line and per phase seen as Y configured

DC test data		
T_{DC} [°C]	$R_{1_{DC,LL}}$ [Ω]	$R_{1_{DC}}$ [Ω]
20.5	2.20	1.10

K.2 Data From No Load Test

Table K.2: No load test measurements for the UMP-3C3-210-25-4 both line to line and per phase seen as Y configured

No-load data						
$R_{1_{NL,LL}}$ [Ω]	$R_{1_{NL}}$ [Ω]	$U_{NL,LL}$ [V]	U_{NL} [V]	$I_{NL,LL} = I_{NL}$ [A]	P_{NL} [W]	f_{NL} [Hz]
2.29	1.15	71.8	41.5	0.710	59.0	50
2.32	1.16	80.2	46.3	0.738	62.2	50
2.33	1.17	120	69.4	0.899	65.5	50
2.35	1.18	160	92.6	1.16	84.5	50
2.38	1.19	201	116	1.44	94.4	50
2.41	1.21	240	139	1.75	120	50
2.49	1.25	302	174	2.27	153	50
2.66	1.33	401	232	3.64	245	50
2.77	1.39	439	253	4.82	318	50

K.3 Data From Locked Rotor Test

Table K.3: Locked rotor test measurements for the UMP-3C3-210-25-4 both line to line and per phase seen as Y configured

			Locked rotor data				
T_{LR}	$R_{1_{LR,LL}}$ [Ω]	$R_{1_{LR}}$ [Ω]	$U_{LR,LL}$ [V]	U_{LR} [V]	$I_{NL,LL} = I_{NL}$ [A]	P_{LR} [W]	f_{LR} [Hz]
24.1	2.24	1.12	86.3	49.8	7.49	438	60
25.0	2.26	1.13	80.5	46.5	7.50	428	55
27.8	2.26	1.13	74.8	43.2	7.51	420	50
26.9	2.28	1.14	68.9	39.8	7.52	410	45
28.4	2.29	1.15	63.1	36.5	7.53	402	40
27.0	2.27	1.14	29.0	16.8	3.79	98.1	35
27.3	2.26	1.13	25.9	14.9	3.77	94.4	30
27.5	2.28	1.14	22.9	13.2	3.77	91.6	25
27.5	2.28	1.14	19.9	11.5	3.77	88.6	20
27.5	2.28	1.14	17.3	10.0	3.76	86.0	15

K.4 Data from load test

			Load test data				
$U_{LT,LL}$ [V]	$I_{LT,LL}$ [A]	P_{LT} [W]	T_{LT} [°C]	$R_{LT,LL}$ [Ω]	τ_{LT} [Nm]	n_{LT} [rpm]	$P_{LT,mech}$ [W]
400	9.99	5945	78.9	2.72	33.31	1437	5013
400	9.15	5402	76.0	2.69	30.43	1443	4598
401	8.04	4661	78.1	2.71	26.34	1452	4005
400	6.38	3469	75.9	2.69	19.60	1465	3007
399	4.97	2333	74.3	2.68	12.93	1477	2000
401	4.00	1277	73.8	2.67	6.30	1488	982

Table K.4: Results from load test on UMP-3C3-210-25-4 at 70-80 °C winding temperature

			Load test data				
$U_{LT,LL}$ [V]	$I_{LT,LL}$ [A]	P_{LT} [W]	T_{LT} [°C]	$R_{LT,LL}$ [Ω]	τ_{LT} [Nm]	n_{LT} [rpm]	$P_{LT,mech}$ [W]
399	9.99	5924	53.7	2.50	33.15	1444	5013
400	9.13	5359	53.9	2.50	30.09	1449	4566
401	8.06	4647	56.3	2.52	26.33	1457	4017
402	6.40	3457	56.9	2.53	19.56	1468	3007
401	5.00	2325	56.6	2.52	12.71	1479	1969
401	4.01	1276	54.7	2.51	6.48	1488	1010

Table K.5: Results from load test on UMP-3C3-210-25-4 at 50-60 °C winding temperature

			Load test data				
$U_{LT,LL}$ [V]	$I_{LT,LL}$ [A]	P_{LT} [W]	T_{LT} [°C]	$R_{LT,LL}$ [Ω]	τ_{LT} [Nm]	n_{LT} [rpm]	$P_{LT,mech}$ [W]
402	9.80	5807	31.9	2.31	32.90	1450	4996
399	9.17	5363	35.5	2.34	30.30	1454	4614
400	8.12	4666	38.7	2.37	26.40	1461	4039
400	6.38	3426	39.4	2.37	19.30	1472	2975
401	5.09	2371	40.2	2.38	13.04	1481	2023
402	4.08	1292	39.1	2.37	6.41	1490	1000

Table K.6: Results from load test on UMP-3C3-210-25-4 at 30-40 °C winding temperature

K.5 Data from DC Thermal Test

Table K.7: Measured temperatures during DC thermal test of the UMP-3C3-210-25-4.

| Elapsed time [min] | Temperature [°C] | | | | | |
| | Ambient | Winding | Bearing | | Rear end bell | Housing |
			DE	NDE		
0	22.0	23.8	23.3	23.4	22.3	23.3
10	22.0	32.9	24.2	24.2	23.1	24.8
15	22.0	35.8	25.9	25.7	24.4	26.9
20	22.0	38.0	27.9	27.7	26.0	28.8
25	22.0	39.9	29.7	29.5	27.6	30.6
30	22.0	42.5	31.3	31.1	28.8	32.1
35	22.0	44.7	32.9	32.6	30.1	33.6
40	22.0	46.3	34.6	34.4	31.1	35.3
45	22.0	48.0	35.8	35.7	32.4	36.4
50	22.0	49.5	37.3	37.1	33.7	37.9
55	22.0	50.7	38.6	38.4	34.8	39.1
60	22.0	52.4	39.8	39.5	35.9	40.1
65	22.0	53.6	40.9	40.7	36.4	41.0
70	22.0	54.6	42.0	41.8	37.7	42.2
75	22.0	56.0	43.0	42.8	38.3	43.4
80	22.5	57.0	43.9	43.7	38.9	44.1
85	22.5	58.0	44.9	44.7	39.9	44.3
90	22.5	59.2	45.8	45.6	40.1	44.8
95	22.5	59.9	46.6	46.4	40.7	45.4
100	22.5	60.7	47.4	47.2	41.2	46.2
105	22.5	62.0	48.2	48.0	41.6	46.6
110	22.0	62.8	48.9	48.7	41.9	46.7
115	22.0	63.4	49.6	49.4	49.4	46.7
120	22.0	64.4	50.3	50.0	42.2	47.7
125	22.0	65.4	51.0	50.7	42.5	47.7
130	22.0	65.7	51.6	51.3	42.8	48.4
135	22.0	66.6	52.2	51.9	43.1	47.9
140	22.0	67.2	52.8	52.4	42.6	48.0
145	22.0	67.5	53.3	52.9	47.9	51.8
150	22.0	68.4	53.8	53.4	48.0	51.0
155	22.0	69.0	54.2	53.9	48.1	50.0
160	22.0	69.2	54.7	54.3	48.7	50.7
165	22.0	70.0	55.2	54.8	48.4	50.9
170	22.0	70.4	55.7	55.2	48.8	50.7
175	22.0	70.6	56.0	55.6	49.4	50.7
180	22.0	71.2	56.5	56.0	48.4	51.1
185	22.0	72.8	56.8	56.4	48.5	50.8
190	22.0	72.0	57.2	56.7	48.6	49.8
195	22.0	72.4	57.5	57.1	48.4	49.3
200	22.0	73.0	57.9	57.3	48.5	50.5

K.6 Data from fan speed profile

Table K.8: Average air speed readings, used to generate air speed profile across UMP-3C3-210-25-4

Axial distance from blower [mm]	Average air speed [m/s]	air speed [p.u]
30	14.4	1.00
40	14.2	0.99
50	14.2	0.99
70	14.0	0.97
90	13.3	0.92
110	13.2	0.92
130	13.0	0.91
150	12.4	0.86
170	12.0	0.83
190	11.6	0.80
210	10.9	0.76
230	11.2	0.78
250	10.6	0.74
270	10.2	0.71
290	9.9	0.69

K.7 Data from fan load test

Table K.9: Measured temperatures during fan load test for the UMP-3C3-210-25-4, including the measured fan speed.

Elapsed time	Temperature [°C]						Fan speed [rpm]
	Ambient	Winding	Bearing DE	NDE	Rear end bell	Housing	
00:00	21.2	20.7	20.0	20.0	21.6	21.5	1469
00:02	21.0	47.1	28.2	26.3	25.6	26.7	1468
00:17	21.4	45.3	33.9	33.2	30.5	29.7	1467
00:27	21.3	47.7	35.3	35.1	31.6	30.6	1467
00:37	21.5	49.4	36.3	36.3	32.6	31.2	1465
00:47	21.2	50.3	36.8	36.9	33.2	31.4	1466
00:57	21.4	50.9	37.2	37.4	33.6	31.7	1467
01:07	21.4	51.3	37.5	37.8	34.0	32.0	1465
01:17	21.5	51.6	37.7	38.0	34.1	32.1	1466
01:27	21.2	51.8	37.8	38.1	34.3	32.1	1466
01:37	21.5	52.0	38.0	38.2	34.4	32.1	1465
01:47	21.5	52.1	38.2	38.4	34.6	32.2	1466
01:57	21.5	52.2	38.2	38.4	34.6	32.3	1465

Table K.10: Readings from Three phase power analyser during fan load test of UMP-3C3-210-25-4

Elapsed time	Line to Line Voltage [V]	Line to Line Current [A]	Power [W]
00:00	0	0	0
00:02	381	6.48	3450
00:17	381	6.37	3390
00:27	382	6.38	3404
00:37	382	6.32	3359
00:47	381	6.31	3359
00:57	380	6.35	3374
01:07	380	6.35	3385
01:17	380	6.38	3405
01:27	380	6.33	3415
01:37	380	6.33	3375
01:47	380	6.35	3386
01:57	380	6.32	3368

Appendix L

Guideline for fan speed profile test

L.1 Objective

This test is used to determine the airflow profile of the fan given by Multi-Wing to emulate a customer-specific case.

L.2 Methodology

L.2.1 List of materials

- Fan pack from Multi-Wing
- Induction machine for testing
- Three phase variable voltage transformer (variotrafo)
- Three phase power analyzer
- Three phase AC power supply
- Digital anemometer
- 2x iron support trestles
- 4x Clamps
- Tachometer

L.2.2 Setup

To emulate a real world fan load scenario, the UMP-3C3-210-25-4 is mounted in a fan pack and placed in a vertical position as seen in Figure L.1.
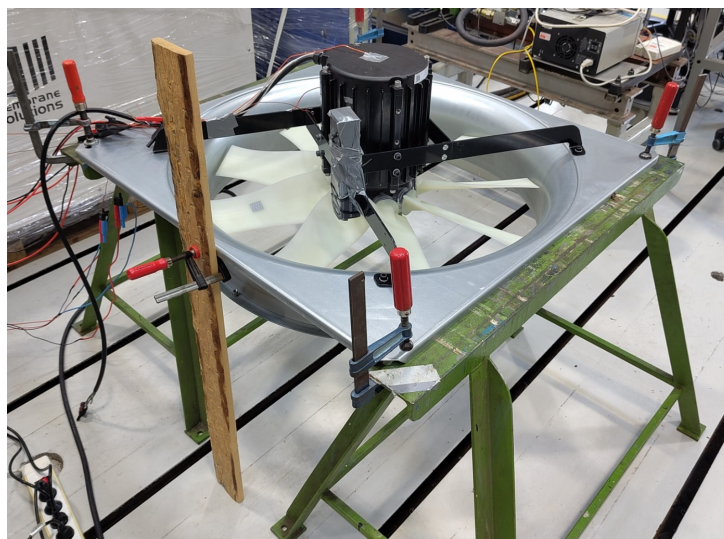
Figure L.1: Overview of setup used in fan speed profile test.

Measurement point are then marked on the housing of the machine, to determine the measurement points. The air speed can then be probed close to the housing as seen in Figure L.2.
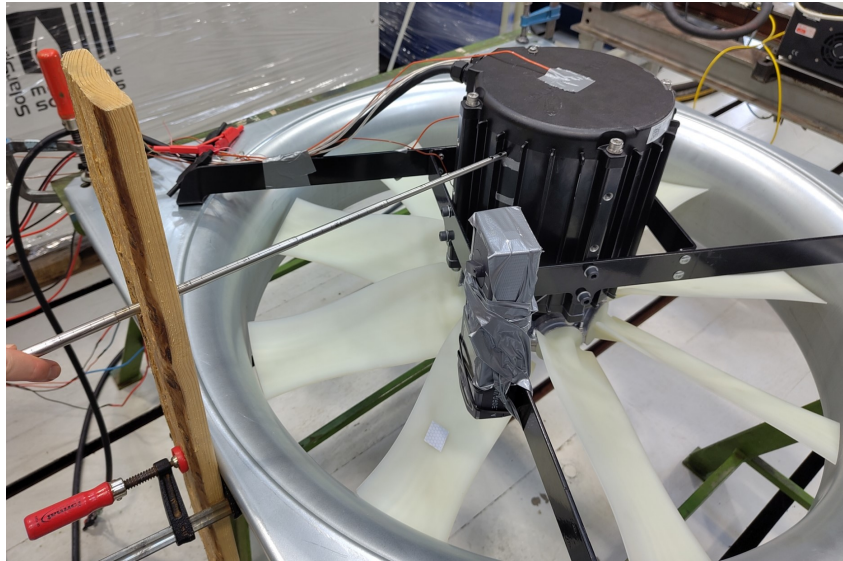
Figure L.2: Image showing, how to probe the air speed using an anemometer.

The machine is then connected to a varotrafo through a three phase power analyser, as seen in Figure L.3.

Figure L.3: Machine connection through variotrafo and three phase power analyser

L.2.3   Procedure

1. Assemble the fan pack with the induction machine for testing.

2. Place the assembled fan pack on the iron support trestles.

3. Connect the variotrafo the 3-phased AC power supply and the 3-phased power analyzer.

4. Connect the induction machine to the variotrafo through the 3-phased power analyzer.

5. Clear the area and ensure shielding is appropriate

6. Turn on the variotrafo and adjust the voltage until the load point is achieved

7. Wait for the machine to thermally settle, or ensure that the fan speed is approximately the same as at the thermal settling point.

8. Begin measuring the airflow with the anemometer held against the machine housing.

9. an airflow measurement should then be noted at the following points from the front end of the machine: 5 mm, 15 mm, 25 mm, 45, 65 mm, 85 mm, 105 mm, 125 mm, 145 mm, 165 mm, 185 mm, 205 mm, 225 mm, 245 mm, and 265 mm, Or until the back end has been reached.

10. Repeat the above 3 times so 3 tests have been measured to get the average.

11. Turn off the induction machine by turning off the variotrafo.

L.3 Data analysis Methods

To conclude the test, the average air speed at each distance is calculated, an example of how to calculate the average is seen in (L.1).

$$\bar{v}_{Avg} = \frac{\sum_{n=1}^{3} v_{measured,n}}{3} \tag{L.1}$$

Appendix M

Guideline for DC thermal test

M.1 Objective

This test is performed to measure the transient thermal response of the UMP-3C3-210-25-4 when subjected to an approximately constant DC current across all phases.

M.2 Methodology

M.2.1 List of material

- UMP-3C3-210-25-4 with 3 PT100 temperature sensors and 2 thermocouples of type K internally mounted
- DC power supply
- Connection lead wires
- 2x External Thermocouples of type K
- 7x Multimeters

M.2.2 Setup

Before the test can proceed, thermocouples are added to the outer housing, located as seen in Figure M.1.
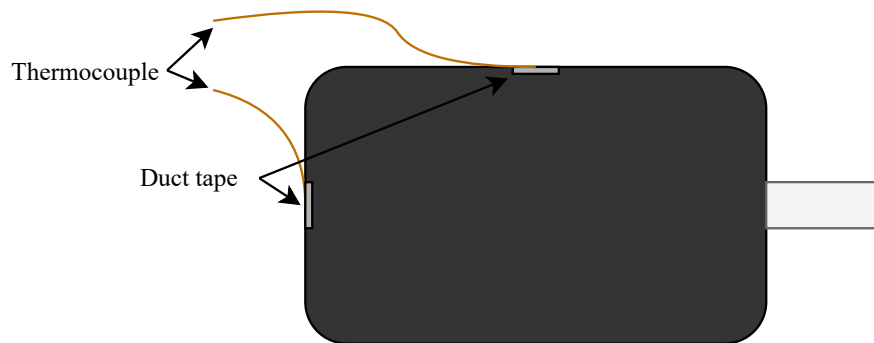
Figure M.1: Thermocouple placement on UMP-3C3-210-25-4

M.2.3 Procedure

1. Ensure the induction machine is at room temperature, and note the ambient temperature.

2. Note the starting time

3. Connect leads of DC power supply to two of UMP-3C3-210-25-4's phases.

4. Turn on the DC power supply, and keep adjusting the voltage to keep an approximately constant current of 7.5 A.

5. Continuously reconnect the DC supply every 30 seconds according to Figure M.2.
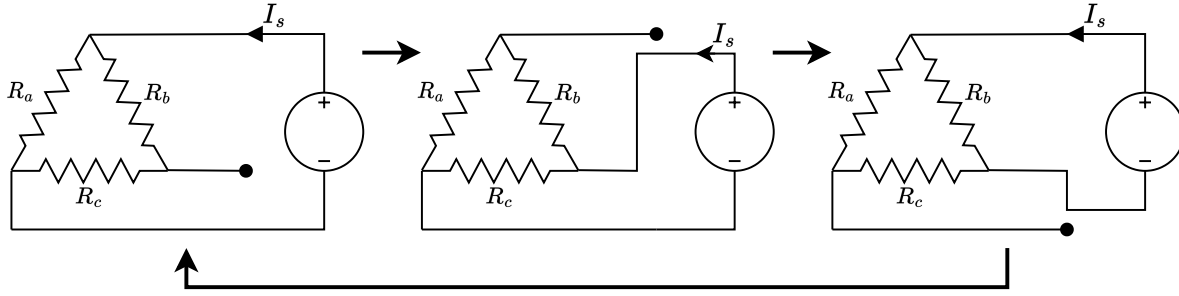
Figure M.2: Cycles of wiring configurations during DC-current thermal test

6. Continuously note the following every 5 minutes:

   - Time
   - Resistance of all three PT100's
   - DE bearing temperature
   - NDE bearing temperature
   - Housing temperature
   - Rear end bell temperature
   - Ambient temperature

7. End measurements after 41 measurements

M.3   Data Analysis

To determine the temperatures of the winding, the resistance measurements from the PT100's are used to calculate the average winding temperature.

First all PT 100 measurements are used to calculate a temperature measurement as seen in (M.1) to (M.3), where $A = 3.90830 \cdot 10^{-3}$ and $B = -5.77500 \cdot 10^{-7}$.

$$T_{A,n} = \frac{-A + \sqrt{A^2 - 4 \cdot B \cdot \left(1 - \frac{R_{PT100,A,n}}{R_0}\right)}}{2 \cdot B} \tag{M.1}$$

$$T_{B,n} = \frac{-A + \sqrt{A^2 - 4 \cdot B \cdot \left(1 - \frac{R_{PT100,B,n}}{R_0}\right)}}{2 \cdot B} \tag{M.2}$$

$$T_{C,n} = \frac{-A + \sqrt{A^2 - 4 \cdot B \cdot \left(1 - \frac{R_{PT100,C,n}}{R_0}\right)}}{2 \cdot B} \tag{M.3}$$

The average winding temperature is then determined for each measurement point as seen in (M.4).

$$T_{winding,n} = \frac{T_{A,n} + T_{B,n} + T_{C,n}}{3} \tag{M.4}$$

To calculate the input power, the average phase resistance of each measurement point is calculated as seen in (M.5).

$$R_{1,n} \approx R_{1,ambient} \cdot \frac{T_{winding,n} + 243.5}{T_{ambient,n} + 243.5} \tag{M.5}$$

The total power dissipated in each winding can then be calculated, as seen in (M.6).

$$P_{winding} = \frac{2}{9} \cdot (7.5\,\text{A})^2 \cdot R_{1,n} \tag{M.6}$$

Appendix N

Guideline for fan load test

N.1 Objective

The aim of this test, is to determine steady state temperatures of the motor under fan load conditions.

N.2 Methodology

N.2.1 List of Materials

- Fan pack from Multi-Wing
- Induction machine for testing, with internally mounted thermal detectors
- Three phase variable voltage transformer (variotrafo)
- Three phase power analyzer
- Three phase AC power supply
- Digital anemometer
- 2x iron support trestles
- 4x Clamps
- Tachometer with reflective tape
- 16 channel thermocouple monitor
- 2x external thermocouples of type K
- 3x Multimeters (If needed to measure the internally mounted thermal detectors)

N.2.2 Setup

before the test can be conducted, thermocouples have to be mounted to the machine. A thermocouple should be mounted to the central housing and rear end bell, as seen in Figure N.1. the Machine is then mounted in a fan pack and placed in a vertical position as seen in Figure N.2.
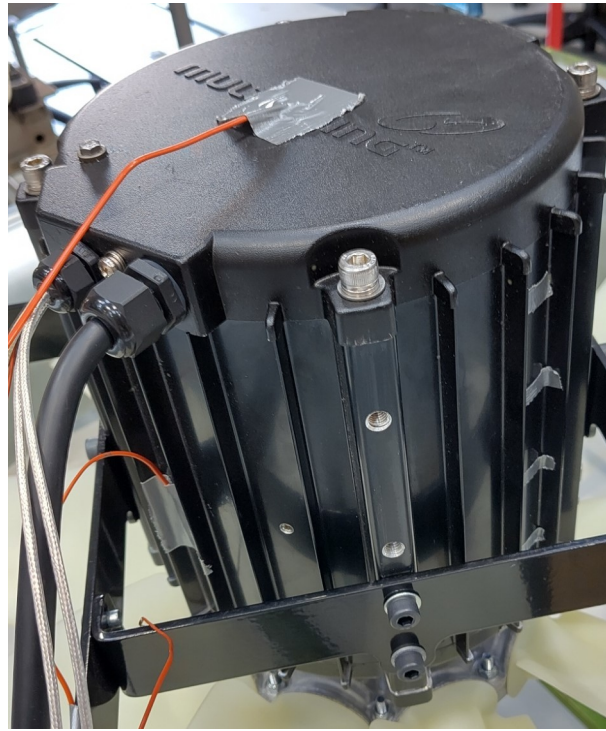
Figure N.1: Placement of thermocouples on machine before fan load test is run
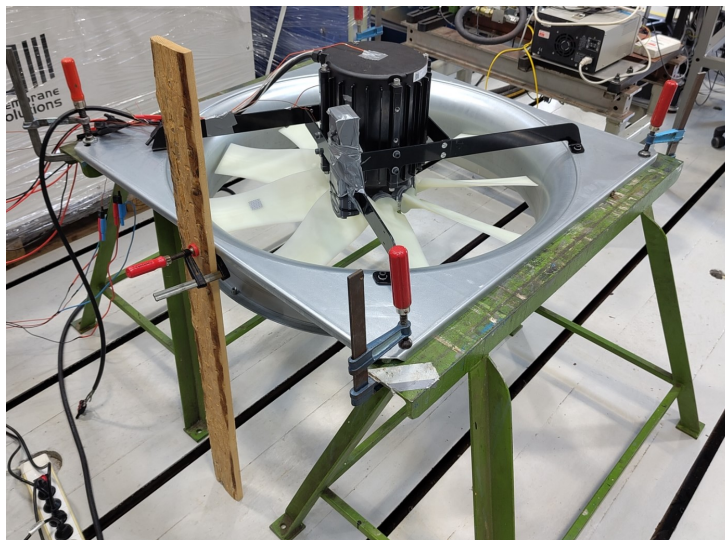
Figure N.2: Overview of setup used in fan speed profile test.

The machine is then connected to a varotrafo through a three phase power analyser, as seen in Figure N.3.

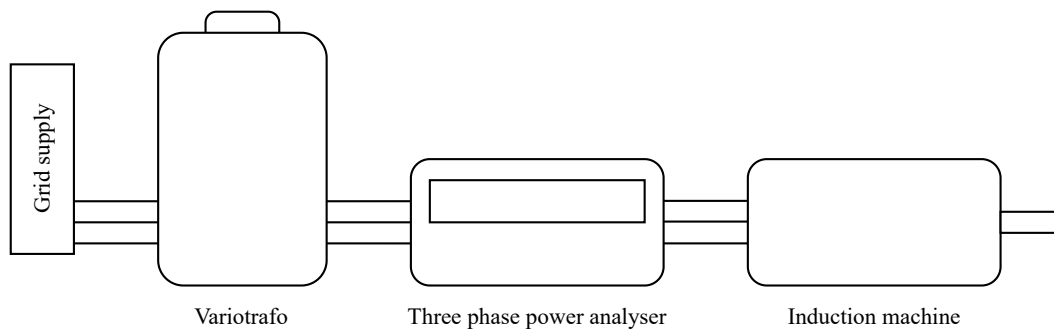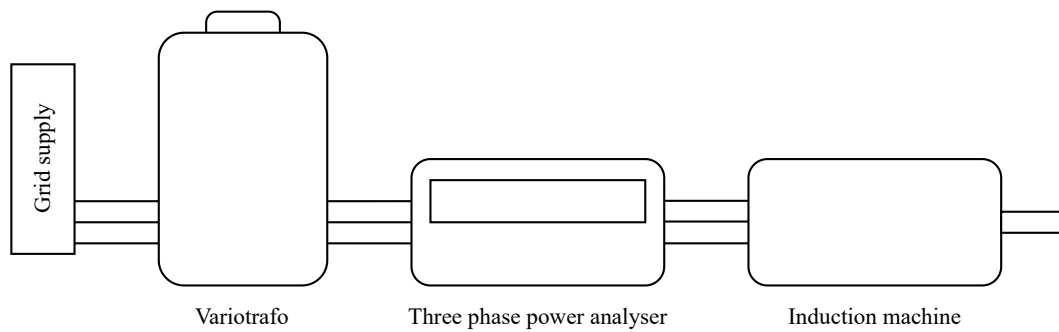**Figure N.3:** Machine connection through variotrafo and three phase power analyser

The thermocouples are connected to a 16 channel thermocouple monitor, while the PT100's are connected to a multimeter.

N.2.3 Procedure

1. Assemble the fan pack with the induction machine for testing.

2. Place the assembled fan pack on the iron support trestles.

3. Secure the Tachometer to the fan setup, and place the reflective tape on a fan wing below it

4. Make sure the tachometer can be turned on from afar and is readable.

5. Connect the variotrafo the 3-phased AC power supply and the 3-phased power analyzer.

6. Connect the induction machine to the variotrafo through the 3-phased power analyzer.

7. Clear the area and ensure shielding is appropriate

8. Note the starting temperatures of the parts being measured, including the ambient temperature.

9. Turn on The variotrafo and adjust the voltage until the load point is achieved.

10. Then take a secondary reading of temperature and an initial reading of the 3 phased power analyzer, flow using the anemometer, and speed using the tachometer.

11. then every 10 minutes take a reading of temperature, the 3 phased power analyzer, the airflow using the anemometer, and the fan speed using the tachometer.

12. Continue taking readings every 10 minutes until it is determined that the machine has hit thermal equilibrium.

13. Having performed the necessary readings, the variotrafo can be turned off, stopping the induction machine and fan.

N.3 Data Analysis

If PT100 thermal sensors were used as internally mounted thermal detectors, please use the manual to convert the measured resistance into temperature measurements.

A machine has thermally settled if it follows the thermal equilibrium defined in IEC 60034-2-1:2014 (2014) stated as the state reached when the temperature rises of several parts of the machine do not vary by more than a gradient of 2 K per hour.

Appendix O

Python scripts

O.1 MotorCAD length sweep script

```python
# need to import win32com.client to use MotorCAD.AppAutomation
import win32com.client
import csv
import time

mcApp = win32com.client.Dispatch("MotorCAD.AppAutomation") # create Motor-CAD
    ActiveX connection
mcApp.SetVariable("MessageDisplayState",2) # Set messages to display in message
    window

# Initialisation of varaiables
lengths = [90,88,86,84,82,80,78,76,74,72,70,68,66,64,62,60,58,56,54] # Rotor stack
    lengths
Temp_res = 0 # Temporary result variable
Results = [] # Result variable
P = 0 # Temporary power variable used to prevent geometry fail
cs = 1 # Variable to keep track of progress

start_time = time.time()  # Start recording time

print("Sweep initiated")

for length in lengths:
    mcApp.SetVariable("Stator_Lam_Length", length+0.75) # Set stator length
    mcApp.SetVariable("Rotor_Lam_Length", length) # Set rotor length


    completion = cs/(len(lengths))*100 # Calculate completion progress
    mcApp.DoMagneticCalculation() # Perform calculations in MotorCAD
    ex, P = mcApp.GetVariable("OutputPower_Mechanical") # Read resulting power
    output

    # If power = 0, run simulation again as it is likely due to a geometry fail
    if P == 0:
        print("Geometry fail encountered, trying again...")
        mcApp.DoMagneticCalculation()

    ex, EffRes = mcApp.GetVariable("SystemEfficiency") # Extract efficiency result
    print("Calculation progress: %.1f%%" % completion) # Display completion progress

    cs += 1

    # Ensure output is 4 kW, otherwise report efficiency of 0.
    if P <= 3990:
        Temp_res = 0
    else:
        Temp_res = round(EffRes,2)

```

```
45       Results.append(Temp_res) # Save temporary results in results array
46
47 # Export results to a csv file
48 rows = []
49 k = 0
50 for length in lengths:
51       rows.append([str(length), str(Results[k])])
52       k += 1
53 with open('Saved_results_sweep.csv', 'w', newline='') as savefile:
54       writer = csv.writer(savefile)
55       writer.writerows(rows)
56
57 print("Solving completed.") # Print message that the solving is completed
58 elapsed_time = time.time() - start_time  # Record elapsed time
59 minutes = int(elapsed_time // 60) # Calculate minutes
60 seconds = int(elapsed_time % 60) # Calculate seconds
61 print(f"Total completion time: {minutes} minutes {seconds} seconds") # Print final
      calculation time
```

O.2   MotorCAD run all wire options

```
1 # need to import win32com.client to use MotorCAD.AppAutomation
2 import win32com.client
3 import csv
4 import time
5
6 mcApp = win32com.client.Dispatch("MotorCAD.AppAutomation") # create Motor-CAD
      ActiveX connection
7 mcApp.SetVariable("MessageDisplayState",2) # Set messages to display in message
      window
8
9 # Initialisation of varaiables
10 StatorStackLength = 90.75 # Initial stator stack length
11 RotorStackLength = 90 # Initial rotor stack length
12 Wire_options = [] # Array to store wire options in
13 Temp_res = [0,0] # Temperary results array
14 Results = [] # Results array to store final results
15 P = 0 # Temporary variable used to prevent geometry fail
16
17 start_time = time.time()  # Start recording time
18
19 # Load csv file with wire options
20 with open('Wire_sizes_test.csv') as csv_file:
21     csv_reader = csv.reader(csv_file, delimiter='\t')
22     line_count = 0
23     for row in csv_reader:
24         Wire_options.append([float(row[0]), float(row[1]), int(row[2]), int(row[3])
      ])
25         line_count += 1
26     combinations = 2*line_count
27     print(f'{combinations} wire combinations loaded.') # Display how many wire
      combinations have been loaded
28
29 option_count = 0
30 for option in Wire_options:
31     dCu = option[0]
32     dWire = option[1]
33     turns = option[2]
34     strands = option[3]
35     mcApp.SetVariable("Wire_Diameter", dWire) # Set new wire diameter in MotorCAD
36     mcApp.SetVariable("Copper_Diameter", dCu) # Set new conductor diameter in
```

A 48

```python
         MotorCAD
37       mcApp.SetVariable("NumberStrandsHand", strands) # Set new strands in hand in
         MotorCAD
38       mcApp.SetVariable("MagTurnsConductor", turns) # Set new amount of turns in
         MotorCAD
39
40       # Run a wire combination in both Delta and Star configuration
41       for connection in range(2):
42           mcApp.SetVariable("WindingConnection", connection) # Sets the winding
         connection to Delta(0) or Star(1)
43           completion = (option_count*2 + 1 + connection)/(line_count*2)*100 #
         Calculate completion progress
44           mcApp.DoMagneticCalculation() # Perform electro magnetic calculation in
         MotorCAD
45           ex, P = mcApp.GetVariable("OutputPower_Mechanical") # Extract mechanical
         power from MotorCAD
46
47           #Check if the power = 0 to ensure geometry fail has not occured.
48           if P == 0:
49               print("Geometry fail encountered, trying again...")
50               mcApp.DoMagneticCalculation()
51           ex, EffRes = mcApp.GetVariable("SystemEfficiency") # Extract efficiency
         result
52           print("Calculation progress: %.1f%%" % completion) # Display completion
         progress
53
54           # Ensure the output power is correct
55           if P <= 3990:
56               Temp_res[connection] = 0
57           else:
58               Temp_res[connection] = round(EffRes,2) # Save efficiency result in
         temporary array
59
60       Results.append([Temp_res[0],Temp_res[1]]) # Save results in array
61       option_count += 1 # Proceed to next wire option
62
63  # Export results to csv file
64  rows = []
65  k = 0
66  for option in Wire_options:
67      rows.append([str(option[0]),str(option[1]),str(option[2]),str(option[3]),str(
         Results[k][0]),str(Results[k][1])])
68      k += 1
69  with open('Saved_results.csv', 'w', newline='') as savefile:
70      writer = csv.writer(savefile)
71      #writer.writerow(fields)
72      writer.writerows(rows)
73  print("Solving completed.")
74  elapsed_time = time.time() - start_time  # record elapsed time
75  minutes = int(elapsed_time // 60)
76  seconds = int(elapsed_time % 60)
77  print(f"Total completion time: {minutes} minutes {seconds} seconds") # Displayy
         final run-time
```

Appendix P

Wire combination simulatation results

P.1   List of combinations with 67.3% slot fill factor

Table P.1: List of examined wire combinations using 67.3% slot fill factor.

Option	Diameter [mm] Conductor	Wire	Number of turns	Strands in hand	Slot fill	Copper fill	Connection
1	0.457	0.519	149	1	67.3%	45.2%	Star
2	0.457	0.519	149	1	67.3%	45.2%	Delta
3	0.457	0.519	74	2	66.9%	45.1%	Star
4	0.457	0.519	74	2	66.9%	45.1%	Delta
5	0.457	0.519	49	3	66.6%	44.8%	Star
6	0.457	0.519	49	3	66.6%	44.8%	Delta
7	0.457	0.519	37	4	66.9%	45.1%	Star
8	0.457	0.519	37	4	66.9%	45.1%	Delta
9	0.457	0.519	29	5	65.9%	44.1%	Star
10	0.457	0.519	29	5	65.9%	44.1%	Delta
11	0.540	0.576	121	1	67.3%	47.6%	Star
12	0.540	0.576	121	1	67.3%	47.6%	Delta
13	0.540	0.576	60	2	66.9%	47.2%	Star
14	0.540	0.576	60	2	66.9%	47.2%	Delta
15	0.540	0.576	40	3	66.9%	47.2%	Star
16	0.540	0.576	40	3	66.9%	47.2%	Delta
17	0.540	0.576	30	4	66.9%	47.2%	Star
18	0.540	0.576	30	4	66.9%	47.2%	Delta
19	0.540	0.576	24	5	66.9%	47.2%	Star
20	0.540	0.576	24	5	66.9%	47.2%	Delta
21	0.560	0.606	109	1	67.2%	46.1%	Star
22	0.560	0.606	109	1	67.2%	46.1%	Delta
23	0.560	0.606	54	2	66.7%	45.7%	Star
24	0.560	0.606	54	2	66.7%	45.7%	Delta
25	0.560	0.606	36	3	66.7%	45.7%	Star
26	0.560	0.606	36	3	66.7%	45.7%	Delta
27	0.560	0.606	27	4	66.7%	45.7%	Star
28	0.560	0.606	27	4	66.7%	45.7%	Delta
29	0.560	0.606	21	5	65.2%	44.4%	Star
30	0.560	0.606	21	5	65.2%	44.4%	Delta
31	0.600	0.649	95	1	67.1%	46.2%	Star
32	0.600	0.649	95	1	67.1%	46.2%	Delta
33	0.600	0.649	47	2	66.6%	45.7%	Star
34	0.600	0.649	47	2	66.6%	45.7%	Delta
35	0.600	0.649	31	3	66.0%	45.2%	Star

36	0.600	0.649	31	3	66.0%	45.2%	Delta
37	0.600	0.649	23	4	65.4%	44.7%	Star
38	0.600	0.649	23	4	65.4%	44.7%	Delta
39	0.600	0.649	19	5	67.1%	46.6%	Star
40	0.600	0.649	19	5	67.1%	46.2%	Delta
41	0.670	0.722	77	1	67.3%	46.6%	Star
42	0.670	0.722	77	1	67.3%	46.6%	Delta
43	0.670	0.722	38	2	66.6%	46.0%	Star
44	0.670	0.722	38	2	66.6%	46.0%	Delta
45	0.670	0.722	25	3	65.9%	45.4%	Star
46	0.670	0.722	25	3	65.9%	45.4%	Delta
47	0.670	0.722	19	4	66.6%	46.0%	Star
48	0.670	0.722	19	4	66.6%	46.0%	Delta
49	0.670	0.722	15	5	65.9%	45.4%	Star
50	0.670	0.722	15	5	65.9%	45.4%	Delta
51	0.710	0.762	69	1	67.2%	46.9%	Star
52	0.710	0.762	69	1	67.2%	46.9%	Delta
53	0.710	0.762	34	2	66.4%	46.3%	Star
54	0.710	0.762	34	2	66.4%	46.3%	Delta
55	0.710	0.762	23	3	67.2%	46.9%	Star
56	0.710	0.762	23	3	67.2%	46.9%	Delta
57	0.710	0.762	17	4	66.4%	46.3%	Star
58	0.710	0.762	17	4	66.4%	46.3%	Delta
59	0.710	0.762	13	5	64.1%	44.2%	Star
60	0.710	0.762	13	5	50.9%	44.2%	Delta
61	0.800	0.855	54	1	66.4%	46.6%	Star
62	0.800	0.855	54	1	66.4%	46.6%	Delta
63	0.800	0.855	27	2	66.4%	46.6%	Star
64	0.800	0.855	27	2	66.4%	46.6%	Delta
65	0.800	0.855	18	3	66.4%	46.6%	Star
66	0.800	0.855	18	3	66.4%	46.6%	Delta
67	0.800	0.855	13	4	64.4%	44.9%	Star
68	0.800	0.855	13	4	64.4%	44.9%	Delta
69	0.800	0.855	10	5	62.5%	43.3%	Star
70	0.800	0.855	10	5	62.5%	43.3%	Delta
71	0.850	0.909	48	1	66.7%	46.8%	Star
72	0.850	0.909	48	1	66.7%	46.8%	Delta
73	0.850	0.909	24	2	66.7%	46.8%	Star
74	0.850	0.909	24	2	66.7%	46.8%	Delta
75	0.850	0.909	16	3	66.7%	46.8%	Star
76	0.850	0.909	16	3	66.7%	46.8%	Delta
77	0.850	0.909	12	4	66.7%	46.8%	Star
78	0.850	0.909	12	4	66.7%	46.8%	Delta
79	0.850	0.909	9	5	63.3%	43.9%	Star
80	0.850	0.909	9	5	63.3%	43.9%	Delta
81	0.900	0.959	43	1	66.5%	47.0%	Star
82	0.900	0.959	43	1	66.5%	47.0%	Delta
83	0.900	0.959	21	2	65.3%	45.9%	Star
84	0.900	0.959	21	2	65.3%	45.9%	Delta
85	0.900	0.959	14	3	65.3%	45.9%	Star

86	0.900	0.959	14	3	65.3%	45.9%	Delta
87	0.900	0.959	10	4	62.8%	43.7%	Star
88	0.900	0.959	10	4	62.8%	43.7%	Delta
89	0.950	1.012	39	1	67.0%	47.5%	Star
90	0.950	1.012	39	1	67.0%	47.5%	Delta
91	0.950	1.012	19	2	65.7%	46.3%	Star
92	0.950	1.012	19	2	65.7%	46.3%	Delta
93	1.000	1.062	35	1	66.4%	47.2%	Star
94	1.000	1.062	35	1	66.4%	47.2%	Delta
95	1.000	1.062	17	2	64.9%	45.9%	Star
96	1.000	1.062	17	2	64.9%	45.9%	Delta
97	1.060	1.124	31	1	66.0%	47.0%	Star
98	1.060	1.124	31	1	66.0%	47.0%	Delta
99	1.060	1.124	15	2	64.3%	45.5%	Star
100	1.060	1.124	15	2	64.3%	45.5%	Delta
101	1.120	1.184	28	1	66.1%	47.4%	Star
102	1.120	1.184	28	1	66.1%	47.4%	Delta
103	1.120	1.184	14	2	66.1%	47.4%	Start
104	1.120	1.184	14	2	66.1%	47.4%	Delta
105	0.750	0.832	58	1	67.3%	44.0%	Star
106	0.750	0.832	58	1	67.3%	44.0%	Delta
107	0.750	0.832	29	2	67.3%	44.0%	Star
108	0.750	0.832	29	2	67.3%	44.0%	Delta
109	0.750	0.832	19	3	66.4%	43.3%	Star
110	0.750	0.832	19	3	66.4%	43.3%	Delta
111	0.750	0.832	14	4	65.5%	42.5%	Star
112	0.750	0.832	14	4	65.5%	42.5%	Delta
113	0.750	0.832	11	5	64.5%	41.7%	Star
114	0.750	0.832	11	5	64.5%	41.7%	Delta

P.2 List of combinations with 73.1% slot fill factor

Table P.2: List of examined wire combinations using 73.1% slot fill factor.

Option	Diameter [mm]		Number of turns	Strands in hand	Slot fill	Copper fill	Connection
	Conductor	Wire					
115	0.457	0.519	165	1	73.1%	50.2%	Star
116	0.457	0.519	165	1	73.1%	50.2%	Delta
117	0.457	0.519	82	2	72.8%	49.9%	Star
118	0.457	0.519	82	2	72.8%	49.9%	Delta
119	0.457	0.519	55	3	73.1%	50.2%	Star
120	0.457	0.519	55	3	73.1%	50.2%	Delta
121	0.457	0.519	41	4	72.8%	49.9%	Star
122	0.457	0.519	41	4	72.8%	49.9%	Delta
123	0.457	0.519	33	5	73.1%	50.2%	Star
124	0.457	0.519	33	5	73.1%	50.2%	Delta
125	0.540	0.576	134	1	73.1%	52.7%	Star
126	0.540	0.576	134	1	73.1%	52.7%	Delta
127	0.540	0.576	67	2	73.1%	52.7%	Star
128	0.540	0.576	67	2	73.1%	52.7%	Delta

129	0.540	0.576	44	3	72.2%	51.9%	Star
130	0.540	0.576	44	3	72.2%	51.9%	Delta
131	0.540	0.576	33	4	72.2%	51.9%	Star
132	0.540	0.576	33	4	72.2%	51.9%	Delta
133	0.540	0.576	26	5	71.3%	51.2%	Star
134	0.540	0.576	26	5	71.3%	51.2%	Delta
135	0.560	0.606	21	1	73.1%	51.2%	Star
136	0.560	0.606	21	1	73.1%	51.2%	Delta
137	0.560	0.606	60	2	72.6%	50.8%	Star
138	0.560	0.606	60	2	72.6%	50.8%	Delta
139	0.560	0.606	40	3	72.6%	50.8%	Star
140	0.560	0.606	40	3	72.6%	50.8%	Delta
141	0.560	0.606	30	4	72.6%	50.8%	Star
142	0.560	0.606	30	4	72.6%	50.8%	Delta
143	0.560	0.606	24	5	72.6%	50.8%	Star
144	0.560	0.606	24	5	72.6%	50.8%	Delta
145	0.600	0.649	105	1	72.8%	51.0%	Star
146	0.600	0.649	105	1	72.8%	51.0%	Delta
147	0.600	0.649	52	2	72.2%	50.5%	Star
148	0.600	0.649	52	2	72.2%	50.5%	Delta
149	0.600	0.649	35	3	72.8%	51.0%	Star
150	0.600	0.649	35	3	72.8%	51.0%	Delta
151	0.600	0.649	26	4	72.2%	50.5%	Star
152	0.600	0.649	26	4	72.2%	50.5%	Delta
153	0.600	0.649	21	5	72.8%	51.0%	Star
154	0.600	0.649	21	5	72.8%	51.0%	Delta
155	0.670	0.722	85	1	72.9%	51.5%	Star
156	0.670	0.722	85	1	72.9%	51.5%	Delta
157	0.670	0.722	42	2	72.2%	50.9%	Star
158	0.670	0.722	42	2	72.2%	50.9%	Delta
159	0.670	0.722	28	3	72.2%	50.9%	Star
160	0.670	0.722	28	3	72.2%	50.9%	Delta
161	0.670	0.722	21	4	72.2%	50.9%	Star
162	0.670	0.722	21	4	72.2%	50.9%	Delta
163	0.670	0.722	17	5	72.9%	51.5%	Star
164	0.670	0.722	17	5	72.9%	51.5%	Delta
165	0.710	0.762	76	1	72.8%	51.7%	Star
166	0.710	0.762	76	1	72.8%	51.7%	Delta
167	0.710	0.762	38	2	72.8%	51.7%	Star
168	0.710	0.762	38	2	72.8%	51.7%	Delta
169	0.710	0.762	25	3	71.9%	51.0%	Star
170	0.710	0.762	25	3	71.9%	51.0%	Delta
171	0.710	0.762	19	4	72.8%	51.7%	Star
172	0.710	0.762	19	4	72.8%	51.7%	Delta
173	0.710	0.762	15	5	71.9%	51.0%	Star
174	0.710	0.762	15	5	71.9%	51.0%	Delta
175	0.800	0.855	60	1	72.3%	51.8%	Star
176	0.800	0.855	60	1	72.3%	51.8%	Delta
177	0.800	0.855	30	2	72.3%	51.8%	Star
178	0.800	0.855	30	2	72.3%	51.8%	Delta

179	0.800	0.855	20	3	72.3%	51.8%	Star
180	0.800	0.855	20	3	72.3%	51.8%	Delta
181	0.800	0.855	15	4	72.3%	51.8%	Star
182	0.800	0.855	15	4	72.3%	51.8%	Delta
183	0.800	0.855	12	5	72.3%	51.8%	Star
184	0.800	0.855	12	5	72.3%	51.8%	Delta
185	0.850	0.909	53	1	72.2%	51.7%	Star
186	0.850	0.909	53	1	72.2%	51.7%	Delta
187	0.850	0.909	26	2	71.1%	50.7%	Star
188	0.850	0.909	26	2	71.1%	50.7%	Delta
189	0.850	0.909	17	3	70.0%	49.7%	Star
190	0.850	0.909	17	3	70.0%	49.7%	Delta
191	0.850	0.909	13	4	71.1%	50.7%	Star
192	0.850	0.909	13	4	71.1%	50.7%	Delta
193	0.850	0.909	10	5	68.9%	48.8%	Star
194	0.850	0.909	10	5	68.9%	48.8%	Delta
195	0.900	0.959	48	1	72.8%	52.5%	Star
196	0.900	0.959	48	1	72.8%	52.5%	Delta
197	0.900	0.959	24	2	72.8%	52.5%	Star
198	0.900	0.959	24	2	72.8%	52.5%	Delta
199	0.900	0.959	16	3	72.8%	52.5%	Star
200	0.900	0.959	16	3	72.8%	52.5%	Delta
201	0.900	0.959	12	4	72.8%	52.5%	Star
202	0.900	0.959	12	4	72.8%	52.5%	Delta
203	0.950	1.012	43	1	72.6%	52.4%	Star
204	0.950	1.012	43	1	72.6%	52.4%	Delta
205	0.950	1.012	21	2	71.1%	51.2%	Star
206	0.950	1.012	21	2	71.1%	51.2%	Delta
207	1.000	1.062	39	1	72.6%	52.6%	Star
208	1.000	1.062	39	1	72.6%	52.6%	Delta
209	1.000	1.062	19	2	71.0%	51.3%	Star
210	1.000	1.062	19	2	71.0%	51.3%	Delta
211	1.060	1.124	35	1	72.8%	53.1%	Star
212	1.060	1.124	35	1	72.8%	53.1%	Delta
213	1.060	1.124	17	2	71.1%	51.6%	Star
214	1.060	1.124	17	2	71.1%	51.6%	Delta
215	1.120	1.184	31	1	71.8%	52.5%	Star
216	1.120	1.184	31	1	71.8%	52.5%	Delta
217	1.120	1.184	15	1	69.9%	50.8%	Star
218	1.120	1.184	15	1	69.9%	50.8%	Delta
219	0.750	0.832	64	1	72.9%	59.8%	Star
220	0.750	0.832	64	1	72.9%	59.8%	Delta
221	0.750	0.832	32	2	72.9%	59.8%	Star
222	0.750	0.832	32	2	72.9%	59.8%	Delta
223	0.750	0.832	21	3	72.0%	58.9%	Star
224	0.750	0.832	21	3	72.0%	58.9%	Delta
225	0.750	0.832	16	4	72.9%	59.8%	Star
226	0.750	0.832	16	4	72.9%	59.8%	Delta
227	0.750	0.832	12	5	69.2%	56.0%	Star
228	0.750	0.832	12	5	69.2%	56.0%	Delta

P.3   List of simulation results with 67.3% slot fill factor

Table P.3: INDSÆT CAPTION

Option	Efficiency (%)	Above 87.45%
1	N/A	No
2	N/A	No
3	N/A	No
4	N/A	No
5	N/A	No
6	N/A	No
7	N/A	No
8	84.75	No
9	N/A	No
10	87.42	No
11	N/A	No
12	N/A	No
13	N/A	No
14	N/A	No
15	N/A	No
16	82.91	No
17	N/A	No
18	87.60	Yes
19	81.34	No
20	79.08	No
21	N/A	No
22	N/A	No
23	N/A	No
24	N/A	No
25	N/A	No
26	85.42	No
27	N/A	No
28	86.98	No
29	85.03	No
30	49.55	No
31	N/A	No
32	N/A	No
33	N/A	No
34	N/A	No
35	N/A	No
36	87.23	No
37	82.55	No
38	71.08	No
39	86.82	No
40	28.92	No
41	N/A	No
42	N/A	No
43	N/A	No
44	84.23	No
45	78.27	No

46	83.23	No
47	86.81	No
48	28.89	No
49	86.23	No
50	N/A	No
51	N/A	No
52	N/A	No
53	N/A	No
54	86.43	No
55	83.01	No
56	71.55	No
57	87.59	Yes
58	16.61	No
59	N/A	No
60	N/A	No
61	N/A	No
62	N/A	No
63	N/A	No
64	87.06	No
65	87.35	No
66	21.74	No
67	65.75	No
68	5.12	No
69	N/A	No
70	1.97	No
71	N/A	No
72	N/A	No
73	81.23	No
74	79.01	No
75	87.59	Yes
76	12.57	No
77	48.03	No
78	3.80	No
79	N/A	No
80	N/A	No
81	N/A	No
82	79.31	No
83	85.25	No
84	49.97	No
85	80.08	No
86	6.93	No
87	N/A	No
88	1.99	No
89	N/A	No
90	83.78	No
91	86.84	No
92	29.00	No
93	N/A	No
94	86.12	No
95	87.55	Yes

96	16.57	No
97	N/A	No
98	87.41	No
99	86.24	No
100	N/A	No
101	N/A	No
102	87.69	Yes
103	80.30	No
104	7.04	No
105	N/A	No
106	N/A	No
107	N/A	No
108	87.41	No
109	86.48	No
110	28.11	No
111	N/A	No
112	6.65	No
113	28.10	No
114	N/A	No

P.4   List of simulation results with 73.1% slot fill factor

Table P.4: INDSÆT CAPTION

Option	Efficiency (%)	Above 87.45%
115	N/A	No
116	N/A	No
117	N/A	No
118	N/A	No
119	N/A	No
120	N/A	No
121	N/A	No
122	82.51	No
123	N/A	No
124	87.21	No
125	N/A	No
126	N/A	No
127	N/A	No
128	N/A	No
129	N/A	No
130	78.96	No
131	N/A	No
132	87.36	No
133	75.83	No
134	86.74	No
135	N/A	No
136	N/A	No
137	N/A	No
138	N/A	No
139	N/A	No

140	83.55	No
141	N/A	No
142	87.90	Yes
143	82.10	No
144	79.93	No
145	N/A	No
146	N/A	No
147	N/A	No
148	N/A	No
149	N/A	No
150	86.56	No
151	75.52	No
152	86.69	No
153	85.93	No
154	51.37	No
155	N/A	No
156	N/A	No
157	N/A	No
158	81.64	No
159	N/A	No
160	87.95	Yes
161	85.91	No
162	51.36	No
163	88.01	Yes
164	17.55	No
165	N/A	No
166	N/A	No
167	N/A	No
168	85.09	No
169	79.94	No
170	83.62	No
171	87.72	Yes
172	30.41	No
173	86.72	No
174	N/A	No
175	N/A	No
176	N/A	No
177	N/A	No
178	87.98	Yes
179	86.79	No
180	39.55	No
181	86.78	No
182	N/A	No
183	49.48	No
184	3.98	No
185	N/A	No
186	N/A	No
187	75.58	No
188	86.70	No
189	87.88	Yes

190	17.21	No
191	67.10	No
192	5.44	No
193	18.71	No
194	2.06	No
195	N/A	No
196	N/A	No
197	82.41	No
198	80.17	No
199	87.99	Yes
200	13.37	No
201	49.70	No
202	4.01	No
203	N/A	No
204	80.70	No
205	85.94	No
206	51.46	No
207	N/A	No
208	84.57	No
209	87.33	No
210	30.27	No
211	N/A	No
212	86.76	No
213	88.02	Yes
214	17.55	No
215	N/A	No
216	87.88	Yes
217	86.70	No
218	N/A	No
219	N/A	No
220	N/A	No
221	N/A	No
222	87.33	No
223	85.53	No
224	50.45	No
225	87.73	Yes
226	12.80	No
227	62.30	No
228	3.75	No

Appendix Q

Test data for prototype machine

Q.1   Data From DC Test

Table Q.1: DC test measurement for the prototype machine both line to line and per phase seen as Y configured

DC test data		
T_{DC} [°C]	$R_{1_{DC,LL}}$ [Ω]	$R_{1_{DC}}$ [Ω]
23.5	2.20	1.10

Q.2   Data From No Load Test

Table Q.2: No load test measurements for the prototype machine both line to line and per phase seen as Y configured

No-load data						
$R_{1_{NL,LL}}$ [Ω]	$R_{1_{NL}}$ [Ω]	$U_{NL,LL}$ [V]	U_{NL} [V]	$I_{NL,LL} = I_{NL}$ [A]	P_{NL} [W]	f_{NL} [Hz]
2.20	1.10	72.1	41.6	0.717	60.3	50
2.23	1.12	80.7	46.6	0.732	62.4	50
2.26	1.13	120	69.2	0.878	63.7	50
2.28	1.14	160	92.5	1.15	84.6	50
2.28	1.14	200	116	1.42	95.5	50
2.30	1.15	240	139	1.73	115	50
2.30	1.15	301	174	2.27	149	50
2.35	1.17	401	231	3.80	241	50
2.40	1.20	441	255	5.39	334	50

Q.3   Data from fan load test

Table Q.3: Measured temperatures during fan load test for the prototype machine, including the measured fan speed.

Elapsed time	Temperature [°C]					Fan speed [rpm]
	Ambient	Winding	DE	Rear end bell	Housing	
00:00	23.4	46.6	30.1	31.0	31.6	1468
00:07	23.6	45.0	34.0	32.9	32.8	1467
00:13	23.6	47.2	36.0	33.4	32.9	-
00:23	23.7	49.7	37.7	34.1	33.3	1466
00:33	23.7	51.1	39.0	34.9	33.6	1466
00:43	23.7	52.0	39.6	35.2	33.9	1466
00:53	23.9	52.5	40.0	35.4	34.2	1466
01:03	23.9	53.0	40.2	35.9	34.9	1466
01:14	23.9	53.0	40.2	35.9	35.1	1465
01:23	23.9	53.2	40.4	36.1	35.5	1466
01:33	23.9	53.1	40.4	36.3	35.7	1465
01:43	23.9	53.2	40.4	36.7	35.8	1466
01:53	24.0	53.2	40.6	37.0	36.0	1466

Table Q.4: Readings from Three phase power analyser during fan load test of prototype machine

Elapsed time	Line to Line Voltage [V]	Line to Line Current [A]	Power [W]
00:00	379	6.46	3413
00:07	380	6.44	3406
00:13	380	6.43	3408
00:23	379	6.43	3405
00:33	378	6.43	3402
00:43	380	6.37	3373
00:53	378	6.38	3376
01:03	380	6.36	3368
01:14	381	6.36	3365
01:23	380	6.33	3344
01:33	379	6.38	3380
01:43	380	6.40	3398
01:53	380	6.42	3407